Philipp Frühwirt, BSc

Magnetic Switching Followed By NMR Spectroscopy

MASTER'S THESIS

to achieve the university degree of

Master of Science

Master's degree programme: Chemistry

submitted to

Graz University of Technology

Supervisor

Univ.-Prof. Mag. rer. nat. Dr. phil. Georg Gescheidt-Demner

Institute of Physical and Theoretical Chemistry

Second Supervisor: Eduard Stadler, MSc BSc

Graz, May 2017

AFFIDAVIT

I declare that I have authored this thesis independently, that I have not used other than the declared sources/resources, and that I have explicitly indicated all material which has been quoted either literally or by content from the sources used. The text document uploaded to TUGRAZonline is identical to the present master‘s thesis.

Date

Signature

Acknowledgement

First of all, I cordially want to thank Georg, who gave me the opportunity to work on this project and to write my master thesis in his working group. Furthermore, I want to say that I appreciated the offer from Georg to work as student assistant during the master thesis.

I owe special thanks to Eduard, who showed to me how to work with the NMR spectrometers and taught me all the things I need to know about NMR theory, relaxation and pulse programs. Without his help and some of his data, this work would not be finished. Also thank you for proofreading parts of this thesis.

Furthermore, I want to thank Anna, Max, Dimi, David and also Yasmin and Roman for the good time in the working group and all the fruitful and interesting discussions and the critical questions (especially from Dimi) during our group meetings.

I am also very grateful for the help with the vacuum line and the chemicals from Hilde, the technical support I got from Christian and all kinds of organizational things done by Marion.

Sincere thanks are given to the whole Institute of Physical and Theoretical Chemistry.

The last five years of studying chemistry would not have been as amusing and informative, if I had not met my colleagues and friends Maria, Katharina, Stefanie, Sebastian and Thomas. I want to thank them for all the fun we had during our lab courses, doing our homework and learning together.

I would like to thank my family and particularly my parents, Sonja and Ernst, and my sister Sandra for their support over the last five years of my studies. Times were not always easy, especially in stressful situations, but they always backed me and confirmed me in my decisions. Without them, I would not be where I am now.

Abstract

In a typical NMR experiment, most of the instrumental time is consumed by the relaxation delay. To accelerate NMR experiments, a reduction of the longitudinal relaxation time, which determines the length of the relaxation delay, is required. A possibility to achieve this goal is the addition of paramagnetic substances to the NMR sample. This method named *paramagnetic relaxation enhancement* (PRE) is often accompanied by line broadening of the peaks in the NMR spectrum.

To bypass this drawback, a recently developed switchable Ni(II) complex (MeO-RP) can be used. The spin state of this Ni(II)-porphyrin complex can be altered by illuminating it with light. It can be cycled between a diamagnetic and paramagnetic state. While the FID is acquired, the complex resides in the diamagnetic state and is “silent”. During the relaxation delay it is then switched to the paramagnetic state (“active”) with a green high-power LED. Before the next scan is recorded, the complex is switched back to its diamagnetic state with a blue high-power LED.

The properties of this photo-switchable complex were employed in different NMR experiments. In a theoretical model based on the experimental data of the model compound Ni-$TPPF_{20}$, another Ni(II)-porphyrin complex, the optimal concentration of MeO-RP for the experiments was determined to be 1.5 mM in toluene-d_8 and $CHCl_3$ (10% (v/v)).

First, the kinetics of the switching processes were studied by monitoring the longitudinal relaxation rate of the $CHCl_3$ peak or the shift differences of this peak due to susceptibility changes. It was found that the switching process from the diamagnetic to the paramagnetic state is usually four to five times slower than the reverse process, which is usually completed within 6 seconds.

A modified saturation recovery experiment, in which the magnetic state was switched during the variable delay, demonstrates how the re-establishment of the z-magnetization can be influenced by the spin switch. In the so-called DARE (*dynamically accelerated relaxation enhancement*) experiment a gain in signal intensity of 10% was observed for the $CHCl_3$ peak. This is due to the faster

relaxation in the recycle delay between two scans, which increases the amount of recovered z-magnetization and hence the signal intensity.

Another benefit of the used system is its reversibility. In a long-term switching experiment, where the complex is repeatedly cycled between both magnetic states, it could be shown that the complex remains photo-switchable even after 225 cycles.

Finally, control experiments with Ni-TPPF$_{20}$, which is not photo-switchable, showed that all the effects described above arose from the light-induced generation of paramagnetic species and not from the temperature gradients in the sample.

Zusammenfassung

Der größte Teil der Messzeit eines NMR-Experiments wird von Wartezeiten zwischen Scans in Anspruch genommen. Um NMR-Experimente zu beschleunigen, muss die longitudinale Relaxationszeit, welche die Länge des Relaxationsdelays bestimmt, verkürzt werden. Eine Möglichkeit, dies zu erreichen, ist die Zugabe von paramagnetischen Substanzen zur Probe. Diese Methode, die *Paramagnetic Relaxation Enhancement* (PRE) genannt wird, geht oftmals mit einer Verbreiterung der Linien im NMR-Spektrum einher.

Um diesen Nachteil zu vermeiden, kann ein kürzlich entwickelter schaltbarer Ni(II)-Komplex (MeO-RP) eingesetzt werden. Der Spin-Zustand dieses Ni(II)-Porphyrin-Komplexes kann verändert werden, wenn der Komplex mit Licht bestrahlt wird. Er kann zwischen einem diamagnetischen und paramagnetischen Zustand hin und her geschaltet werden. Während der Datenaufnahme bleibt der Komplex im diamagnetischen Zustand und ist inaktiv. Dann wird er während des Relaxationsdelays mit einer grünen LED in den paramagnetischen Zustand versetzt. Bevor der nächste Scan aufgenommen wird, schaltet man den Komplex mit einer blauen LED zurück in den diamagnetischen Zustand.

Diese Eigenschaft des mit Licht schaltbaren Komplexes wurde in verschiedenen NMR-Experimenten ausgenutzt. In einem theoretischen Modell, das auf den experimentellen Daten der Modell-Verbindung Ni-$TPPF_{20}$, eines anderen Ni(II)-Porphyrin-Komplexes, basiert, wurde die optimale Konzentration für die Experimente – 1.5 mM in Toluol-d_8 und $CHCl_3$ (10% (v/v)) – bestimmt.

Zuerst wurde die Kinetik der Schaltprozesse untersucht, wobei die longitudinale Relaxationsrate oder die Shift-Differenz des $CHCl_3$-Peaks (bedingt durch die Änderung der Suszeptibilität) verfolgt wurde. Es zeigte sich, dass der Schaltprozess vom diamagnetischen zum paramagnetischen Zustand üblicherweise fünf- bis sechsmal langsamer vonstatten geht als der umgekehrte Prozess.

Ein modifiziertes Saturation Recovery-Experiment, bei dem der magnetische Zustand innerhalb des variablen Delays umgeschaltet wurde, zeigt, wie die Wiederherstellung der z-Magnetisierung vom Spin-Schalter beeinflusst wird. Im

sogenannten DARE-Experiment (*dynamically accelerated relaxation enhancement*) wurde ein Zuwachs in der Signal-Intensität des $CHCl_3$-Peaks beobachtet. Das ist durch die schnellere Relaxation im Relaxationsdelay zwischen zwei Scans bedingt, welche den Anteil der relaxierten z-Magnetisierung und somit die Signal-Intensität erhöht.

Ein anderer Vorteil des verwendeten Systems ist seine Reversibilität. Ein Langzeit-Schalt-Experiment, in dem der Komplex wiederholt zwischen den beiden magnetischen Zuständen hin und her geschaltet wurde, zeigt, dass Komplex auch nach 225 Zyklen schaltbar bleibt.

Zum Schluss wurde mittels Kontroll-Experimente mit Ni-$TPPF_{20}$ (nicht durch Licht schaltbar) gezeigt, dass all jene zuvor beschriebenen Effekte auf die lichtinduzierte Bildung von paramagnetischer Spezies und nicht auf die Temperatur-Gradienten in der Probe zurückzuführen sind.

Contents

1. Introduction

Compared to many spectroscopic methods, nuclear magnetic resonance (NMR) spectroscopy suffers from its low sensitivity due to the small difference in population of the excited and the ground state. The poor sensitivity is accompanied by a small signal to noise (S/N) ratio. The energy gap between the different magnetic states is determined by the gyromagnetic ratio γ (depending on nucleus, ^{1}H has the highest value) and the strength of the magnetic field. The higher both quantities, the higher the energy gap and thus the higher the sensitivity. Furthermore, the sensitivity is also governed by the natural abundance of the NMR-active isotope. In case of ^{13}C-NMR spectroscopy only 1% of all carbon atoms are NMR-active, which makes ^{13}C-NMR substantially less efficient ^{1}H-NMR spectroscopy.[1]

Owing to pulse NMR, which became available in the 1970s, the problem of low sensitivity can be circumvented by recording numerous scans or transients.[1] This method, which is known as *time averaging*, improves the S/N ratio and thus the sensitivity.[2] Long relaxation times, especially those of certain nuclei (^{13}C, ^{31}P, ^{15}N), are still an issue in pulsed NMR spectroscopy.[3] The longitudinal relaxation time describes the amount of time needed to establish or re-establish about 63% of the equilibrium magnetization (i.e. the z-magnetization).[1] If the spins are not in thermal equilibrium and the next scan is recorded, the signal intensity, which is proportional to the established z-magnetization, will be diminished. Hence, the S/N ratio also suffers from long relaxation times.[2]

When waiting for the spins to return to equilibrium after excitation, recording NMR spectra can become a very time-consuming business. It is estimated, that at least 80% of the instrumental time is made up by recycle or relaxation delays, in which the equilibrium magnetization has to be re-established.[4]

In presence of paramagnetic additives such as transition metal ions or their complexes, the spins (re-)establish thermal equilibrium faster than without these additives. This phenomenon is known as *paramagnetic relaxation enhancement* (PRE).[5] Actually, this form of enhancement is present in a typical NMR sample due to the molecular oxygen dissolved in the NMR solvents, unless the sample is degassed.[2] Paramagnetic agents based on lanthanide complexes are also applied in magnetic resonance imaging (MRI) in medicine, where they are known as *contrast agents*.[6,7]

Not only the longitudinal relaxation rate, but also the transverse relaxation rate is influenced by paramagnetic additives. Depending on the metal ion, these agents can also cause severe line broadening[8], as the linewidth is connected to the transverse relaxation rate.[2]

A recent development are photo-switchable contrast agents (or relaxation enhancement agents) based on a Ni(II)-porphyrin complex. Due to their molecular structure and functionality this class of compounds was named *record players* by their developers. By illuminating the agent named MeO-RP (see Figure 1) with green light, an azo-group isomerizes and facilitates an intramolecular coordination of a tethered pyridine ligand to the central Ni^{2+} ion. This causes the metal ion to undergo a spin state switch and the complex becomes paramagnetic. The benefit of this system is its reversibility, so the diamagnetic state of the complex can be restored, when it is irradiated with blue light.[9–11]

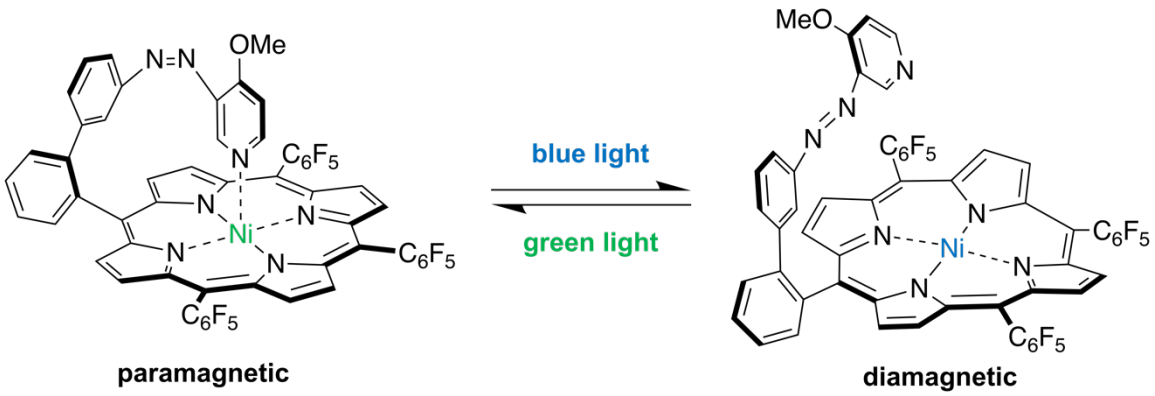

Figure 1. *Structures of the paramagnetic and diamagnetic isomer of the methoxy-substituted record player (MeO-RP).*[11]

With this new switchable PRE agent, it should be possible to overcome the disadvantage of traditional relaxation enhancement agents – their line broadening effect. When the FID is acquired, the agent is switched “off” (diamagnetic). During the relaxation delay the agent is switched “on” (paramagnetic) and leads to a faster relaxation and before the next scan is recorded, the agent is rendered diamagnetic again. This application utilizes the enhancement of the longitudinal relaxation rate, while suppressing the drawback, which is increasing the transverse relaxation rate and thus leading to undesirable line broadening.

In the theoretical part of this thesis, a concise introduction into NMR spectroscopy is given. It is explained, how NMR spectroscopy in principle works and how a basic NMR experiment is performed.

The second section of the theoretical part is dedicated to relaxation, one of the most important processes in NMR spectroscopy. Relaxation is characterized by two quantities, the longitudinal and the transverse relaxation time or the corresponding rates, which are outlined in the theoretical part. Based on the local magnetic field experienced by the spins in a sample, different relaxation mechanisms are discussed briefly. Furthermore, both relaxation processes are going to be connected to the motion of molecules in the sample.

Another section is devoted to the use of paramagnetic substances in NMR spectroscopy (as shift and relaxation agents) and MRI (as contrast agents). At first glance, these applications may just have the fact in common, that paramagnetic substances are required to evoke these effects. Actually, two types of interactions – the *dipolar* and the *contact interaction* – play a prevailing role in these applications.

The last section of the theoretical part focusses on spin state switches represented by the used Ni(II)-porphyrin-based relaxation or contrast agents.

In the experimental part of this thesis, investigations of the magnetic switching behavior of MeO-RP, which might also be used as contrast agent in the future[11], are presented. The magnetic switching process (from paramagnetic to diamagnetic or the reverse process) is monitored by measuring the longitudinal relaxation rate of residual protons in toluene-d_8 and later the protons of added $CHCl_3$. Furthermore, the switching process is also followed by detecting the shift difference induced by

the paramagnetic species. Additionally, an experiment named DARE is described, in which the influence of longitudinal relaxation on the signal intensity is observed. To prove that the observed effects are caused by MeO-RP and not by temperature gradients in the sample, control experiments with the model compound Ni-$TPPF_{20}$ (see Figure 2) were conducted.

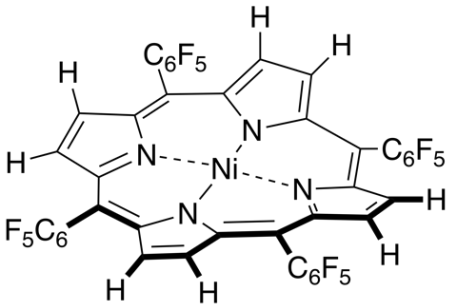

Figure 2. *Structure of diamagnetic Ni-$TPPF_{20}$.*[12]

To provide an overview over the experimental results and how the individual subsections are associated, an additional chapter of this thesis named *Experimental Design* presents the aims of this thesis, a flow chart and short description of the experiments. In addition, a model is presented, which helped to determine the optimal concentration for the switching experiments.

At the end, a conclusion and an outlook to future developments and applications of spin state switches is given.

2. Theoretical Background

2.1. Basic Principles of Nuclear Magnetic Resonance (NMR)

2.1.1. The Magnetic Resonance

Nuclear magnetic resonance (NMR) spectroscopy is a spectroscopic method, which is based on the magnetic properties of the nuclei of atoms. Nuclei are characterized by the *spin quantum number* I, which has non-negative integer or half-integer values[1]:

$$I = 0, \frac{1}{2}, 1, \frac{3}{2}, 2, \ldots \quad (1)$$

If the value of I is 0, the nucleus does not possess a spin and therefore cannot be observed in NMR spectroscopy. Unfortunately, this is the case for ^{12}C, which is one of the elements of special interest in organic chemistry. However, for ^{1}H or the proton, which is the second most important contributor to organic compounds, $I = \frac{1}{2}$ rendering the proton accessible for NMR spectroscopic investigations. The value of I is dependent on the number of protons and neutrons in the nucleus.[1]

I is closely related to the *spin angular momentum*, which can be represented as vector $\boldsymbol{I}$**.** Both the magnitude and the direction of this vector are quantized. The most important feature of the vector, however is its projection on the z-axis. Of course, the projection is also quantized and can be written as product of the magnetic quantum number, which has $2I + 1$ values, and the reduced Planck constant[1]:

$$I_z = m\hbar \text{ with } m = -I, -I+1, \ldots, 0, \ldots, I-1, I \quad (2)$$

All these projections correspond to energy levels, which are degenerate, when no magnetic field is present. If a magnetic nucleus experiences a magnetic field $\boldsymbol{B}$, its magnetic moment $\boldsymbol{\mu}$ interacts with $\boldsymbol{B}$ leading to a splitting of the energy levels. The energy of the interaction can be written as the scalar product of these vectors[1]:

$$E = -\boldsymbol{\mu} \cdot \boldsymbol{B} = -\mu_z B \tag{3}$$

When the magnetic field is applied in the direction of the z-axis, only the z-component of the magnetic moment has to be taken into account. Furthermore, the magnetic moment is directly proportional to the z-component of the angular momentum I – the proportionality constant is named *magnetogyric ratio* or *gyromagnetic ratio* γ, which is characteristic for a certain nucleus. Together with Equation (2) this can be rewritten as[1]:

$$\mu_z = \gamma I_z = m\hbar\gamma \tag{4}$$

Substituting μ_z in Equation (3) with the expression obtained in (4) the energy can be written as[1]:

$$E = -m\hbar\gamma B \tag{5}$$

With the selection rule $\Delta m = \pm 1$ in mind the energy difference can be expressed as[1]:

$$\Delta E = \hbar|\gamma|B \tag{6}$$

Finally, the frequency, at which a transition can be observed, can be calculated using Equation (7)[1]:

$$\nu = \frac{|\gamma|B}{2\pi} \tag{7}$$

The energy gap ΔE between the $2I + 1$ energy levels is dependent on the magnetogyric ratio and the strength of the magnetic field B. NMR spectrometers are usually operated with magnetic field strengths of 2.35 to 23.5 T (Tesla), which means that radiofrequencies (ν ranging from 100 to 1,000 MHz) have to be used to induce transitions (referred to ^{1}H).[1]

However, the protons in a compound are resonating at individual frequencies. This phenomenon, which is known as the *chemical shift* is the one of the most powerful benefits of NMR spectroscopy, as it allows distinguishing different functional groups. This chemical shift δ (given in ppm = *parts per million*) is defined as follows[1]:

$$\delta = 10^6 \frac{\nu_0 - \nu_{ref}}{\nu_{ref}} \tag{8}$$

ν_0 is the frequency of a certain nucleus and ν_{ref} is the frequency of a reference nucleus. In proton NMR spectroscopy tetramethylsilane (TMS) is used as reference substance. With a 400 MHz spectrometer, the proton resonances (aliphatic, aromatic and aldehyde groups) stretch over a frequency range of 4 kHz, which corresponds to a chemical shift range of 10 ppm.[1]

Another phenomenon which occurs in NMR spectroscopy and provides structural information is based on the interaction of magnetic nuclei within a molecule and is known under the terms *spin-spin coupling*, *scalar coupling* or *J-coupling*.[1]

2.1.2. The NMR Experiment

Before modern *pulse methods* were introduced to the field of NMR spectroscopy in the 1970s, *continuous wave methods* were used to record NMR spectra. In contrast to pulsed methods a radiofrequency field was present during the whole acquisition process – either it was changed in a fixed magnetic field or the magnetic field was constant and the frequency of the radio waves was varied.[1]

In modern pulsed NMR a liquid sample, which is filled into a cylindrical glass tube, is surrounded by a transmitter/receiver coil of wire in a strong and static magnetic field (2.35 to 23.5 T) produced by a superconducting magnet.[1]

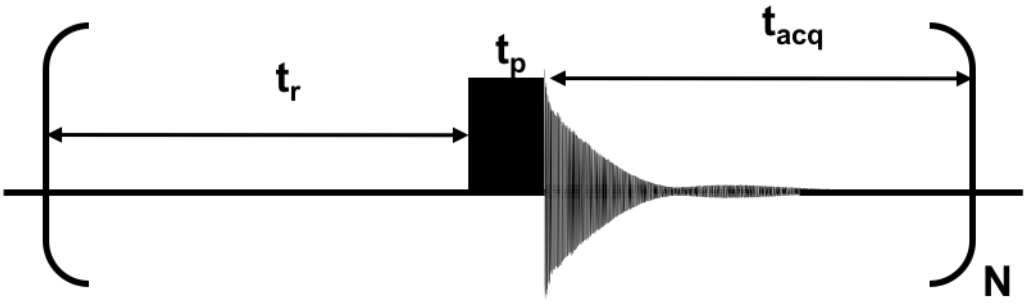

Figure 3. *A basic NMR experiment consisting of a relaxation delay (length t_r), a radiofrequency (RF) pulse (length t_p) and the acquisition time (length t_{acq}). The sequence is repeated N times (N = number of scans). [Figure adapted from [2]]*

Prior to the excitation with the radiofrequency pulse (indicated by the black rectangle in Figure 3) the spins can equilibrate in the relaxation delay (t_r lasts a few seconds). The RF pulse is then applied (usually, t_p < 20 μs) via the coil. This causes a decaying oscillating magnetization in the sample, which induces a current in the coil. In the acquisition time (t_{acq} = a few seconds), the *FID* (*free induction decay*) of this magnetization is recorded. The NMR spectrum is obtained by Fourier transformation of the FID.[1,2]

Often, the acquisition of one FID is not sufficient to meet the criteria of a useful and interpretable spectrum because of the low signal-to-noise (S/N) ratio.[2] The solution of the problem is very simple – by repeating the acquisition (see Figure 3) N times, the S/N ratio is improved by the factor of $\sqrt{N}$. This method is known as *time averaging* and illustrates the power of the pulsed NMR compared to the "ancient" continuous wave methods – which is increasing the sensitivity by recording numerous scans or transients.[1,2]

The intent of the previous paragraphs is giving a short explanation of how a basic pulsed NMR experiment works. Of course, the matter is much more complicated than presented here. In order to get a deeper understanding of the NMR experiments, two models are suitable – the first one is the *vector model*, where the motion of the total magnetization is described using classical mechanics.[1] A more sophisticated approach is the *product operator model* based on quantum mechanics.[2]

The processes, which occur in the time after the excitation with the RF pulse and lead to the decay of the FID, are going to be elucidated in Chapter 2.2.

2.1.3. Linewidths and Lineshapes

The line shape occurring in a typical NMR spectrum is shown in Figure 4. Every peak or line observed in an NMR spectrum has a characteristic width W at half of the peak height ($h/2$), which is 2 Hz in Figure 4. This *absorption mode Lorentzian line shape* is obtained when an exponentially decaying time-domain signal (the FID) is subjected to a Fourier transformation.[2]

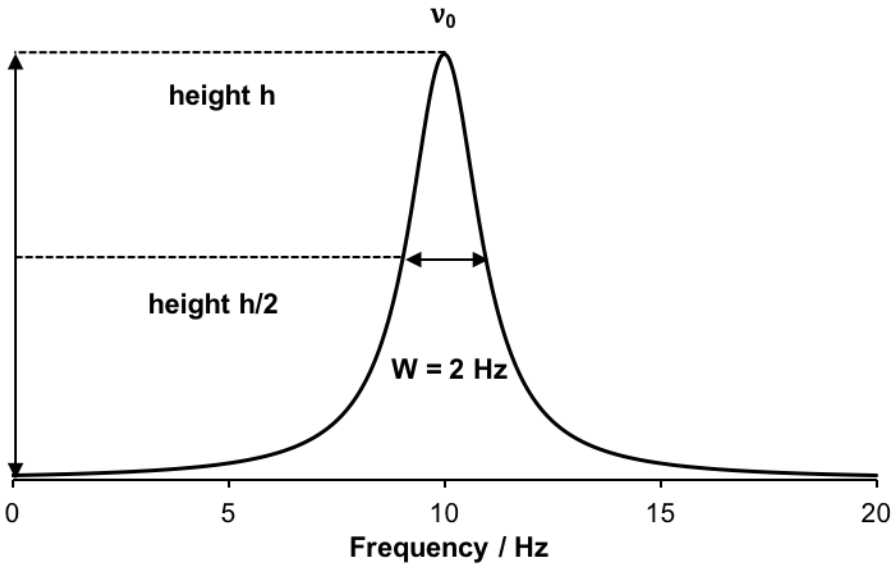

Figure 4. *Absorption mode line shape. The maximum of the peak ν_0 is at 10 Hz, the width at half maximum W is 2 Hz. [Figure adapted from [2]]*

The lines, which constitute an NMR spectrum are usually very narrow (W is in the range of a few Hz), when comparing it with the frequency of the NMR spectrometer (several hundred MHz).[2] If the width of certain peak is increased (*line broadening*), the following factors might be responsible[1]:

- An inhomogeneous magnetic field leads to line broadening, as equal molecules experience a different strength of $\boldsymbol{B}$ leading to slightly different resonance frequencies.
- Chemical and conformational equilibria can also cause line broadening (*life-time broadening*).
- NMR-active nuclei with I > ½ often show broad signals (due to the quadrupolar relaxation, see Section 2.2.7.).

Other effects are closely related to the relaxation and are discussed in the following chapter.

2.2. Relaxation and Relaxation Mechanisms

2.2.1. The Longitudinal Relaxation

In the previous chapter the interaction of a nuclear magnetic moment with the surrounding magnetic field was taken as a starting point to introduce the splitting of the energy levels.

The population n of these energy states (α = lower level ($m = +\frac{1}{2}$) and β = upper level ($m = -\frac{1}{2}$) in the case of ^{1}H) at thermal equilibrium is described by the Boltzmann distribution[1]:

$$\frac{n_\beta}{n_\alpha} = e^{-\frac{\Delta E}{kT}} \tag{9}$$

For a proton at a field of 9.4 T (400 MHz spectrometer) and at 300 K, the thermal energy (expressed as product of the Boltzmann constant and the temperature, kT) is much bigger than the energy difference ΔE between those two levels. As a result,

only a small difference in the population (e.g. 15,625 spins in the lower level and 15,624 in the upper level) is observed. This almost equal population of both energy levels is the reason for the small sensitivity of the NMR spectroscopy compared to e.g. electronic spectroscopy where $\Delta E \gg kT$. At higher magnetic fields the energy difference is bigger resulting in a higher *polarization* (= difference in relative population).[1]

Another approach to the description of the population of the energy levels is the concept of bulk magnetization $\boldsymbol{M}$, which is a sum of the individual magnetic moments of the nuclei present in the sample. As a vector quantity, it is aligned with the direction of the magnetic field (the principal axis) to minimize the energy of the interaction. The preference of alignment however is very slight, only one out of 10^5 spins is actually aligned with the principal axis.[2]

If a sample is placed in a magnetic field for the first time, it takes some time for the bulk magnetization to build up. After some time, a constant value, the *equilibrium magnetization,* is reached. The time, which it takes for spins to establish the equilibrium magnetization, is called *relaxation time*.[2]

When the magnetization vector $\boldsymbol{M}$ is tilted away from the z-axis, it starts to rotate about this axis, which is called *Larmor precession* and is depicted in Figure 5. The precession frequency (*Larmor frequency*) has the same magnitude as the frequency in Equation (7), though the algebraic sign of the Larmor frequency depends on γ. For positive values of γ a negative Larmor frequency is obtained. If a nucleus has a negative γ value, the Larmor frequency is positive.[2]

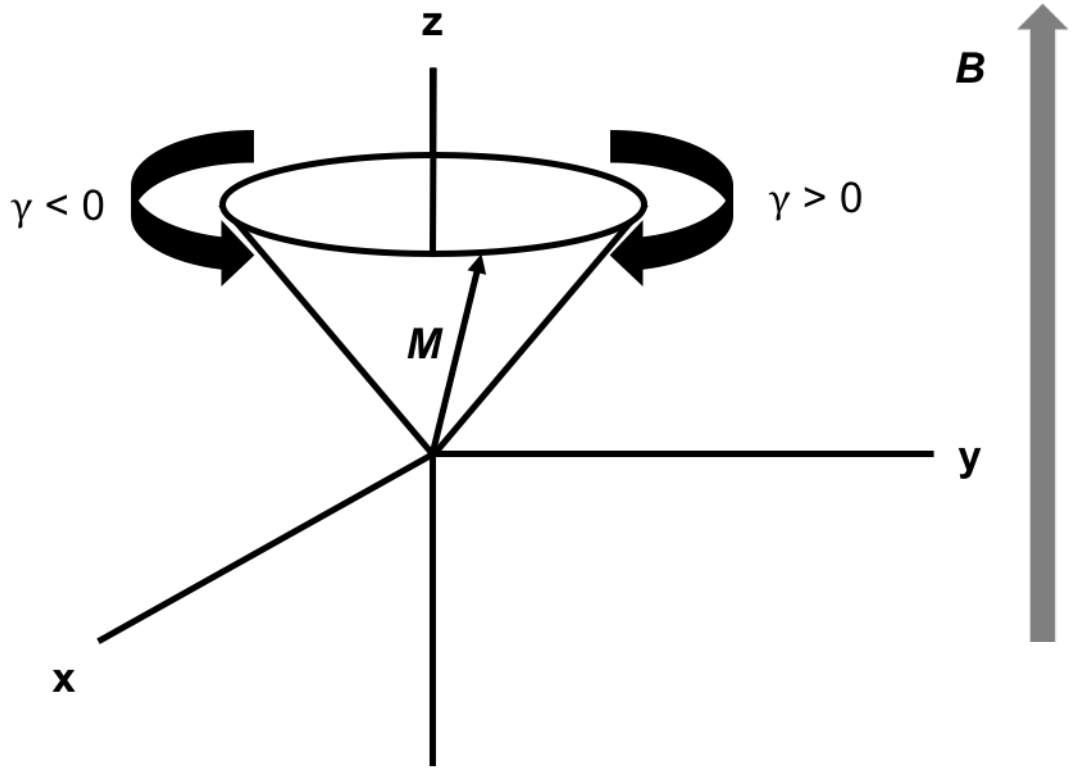

Figure 5. *Depending on the algebraic sign of γ the magnetization $\boldsymbol{M}$ rotates about the axis of the magnetic field $\boldsymbol{B}$ (= z-axis) clockwise (when viewed from the +z direction, for $\gamma > 0$) or counter-clockwise (for $\gamma < 0$). [Figure adapted from [2]]*

At equilibrium, the magnetization is aligned with the direction of the magnetic field. When a radiofrequency pulse hits the sample the magnetization is tilted away from the axis towards the xy-plane. Simultaneously, the magnetization starts rotating about the direction of the magnetic field. Depending on the length of a radiofrequency pulse, the angle, which is enclosed by the positive z-axis and the vector $\boldsymbol{M}$, can be controlled.[13]

By applying a 90° pulse, the magnetization is tilted away from its equilibrium position (aligned with the z-axis) toward the xy-plane, where it rotates about the z-axis. This new "position" of $\boldsymbol{M}$ corresponds to equal populations of the energy levels, as the z-component of $\boldsymbol{M}$ is zero. The process, in which the magnetization returns to its thermal equilibrium characterized by the Boltzmann distribution is called *spin-lattice* or *longitudinal relaxation*.[13]

Equation (10) shows a mathematical expression for the relaxation process based on the population difference Δn. The characteristic quantity of this equation is the

spin-lattice relaxation time or *longitudinal relaxation time* T_1. Δn_{eq} corresponds to the population difference at thermal equilibrium. For $t = T_1$ the population difference has reached about 63% of the equilibrium value.[1]

$$\Delta n(t) = \Delta n_{eq}(1 - e^{-\frac{t}{T_1}}) \tag{10}$$

The determination of T_1 is usually accomplished by the *inversion recovery* (IR) experiment. A 180° pulse inverts ***M*** to the –z axis and after a variable delay τ, a 90° pulse rotates the z-magnetization, which was recovered during the delay, onto the xy-plane. The FID is recorded and after Fourier transformation an NMR spectrum is obtained, where the signal intensity is directly proportional to the z-magnetization.[1]

In 1946, Bloch[14] presented an expression for the (re)-establishment of the z-magnetization M_z:

$$\frac{dM_z}{dt} = \frac{M_0 - M_z}{T_1} \tag{11}$$

Solving this differential equation yields an equation for the z-magnetization as a function of time[2]:

$$M_z(t) = (M_z(0) - M_0)e^{-\frac{t}{T_1}} + M_0 \tag{12}$$

When the initial z-magnetization $M_z(0)$ corresponds to the negative equilibrium magnetization M_0 (or M_{eq}) and $t = \tau$, Equation (12) can be simplified to give[2]:

$$M_z(\tau) = M_0(1 - 2e^{-\frac{\tau}{T_1}}) \tag{13}$$

In Figure 6 the pulse sequence of the inversion recovery as well as the plot of the z-magnetization as a function of τ is shown. The signal intensity is directly proportional to M_z.[1]

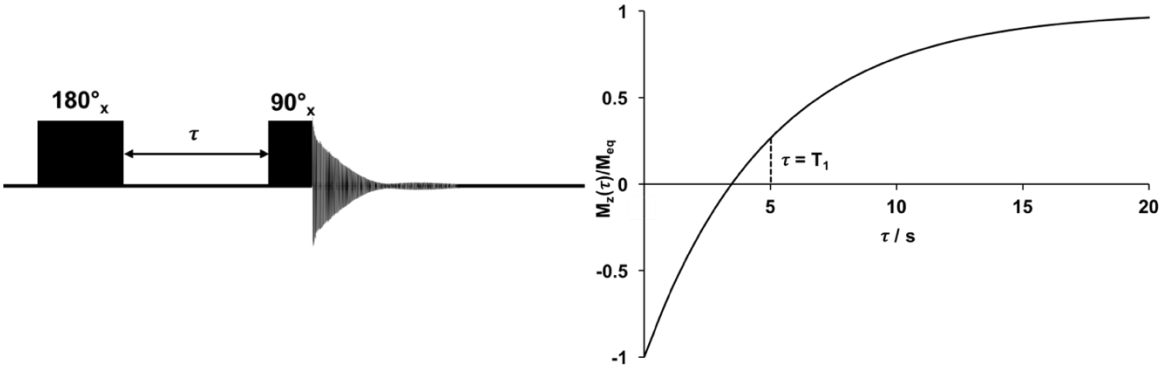

Figure 6. *Left: Pulse scheme for an inversion recovery experiment consisting of a 180°$_x$ pulse, a variable delay τ, a 90°$_x$ pulse and the acquisition of the FID. Right: M_z normalized to M_{eq} is plotted as a function of the delay time for T_1 = 5 s. [Figure adapted from [1]]*

For nuclei with long T_1 values (^{13}C, ^{31}P, ^{15}N) this method is rather time-consuming.[3] A much faster method for determining T_1 is the *saturation recovery* (SR) experiment.[15] The initial 180° pulse of the IR experiment is replaced by a sequence of 90° pulses followed by a dephasing field gradient pulse in the SR experiment. This saturation block causes the magnetization to vanish completely. After the delay time τ, a 90° pulse is applied to record the transverse magnetization in the FID.[16]

By setting $M_z(0) = 0$ and $t = \tau$ in Equation (12) the re-establishment of the z-magnetization after the saturation is given by[16]:

$$M_z(\tau) = M_0(1 - e^{-\frac{\tau}{T_1}}) \tag{14}$$

The z-magnetization as function of the delay time is plotted in the right part of Figure 7 next to the pulse sequence of the SR experiment.

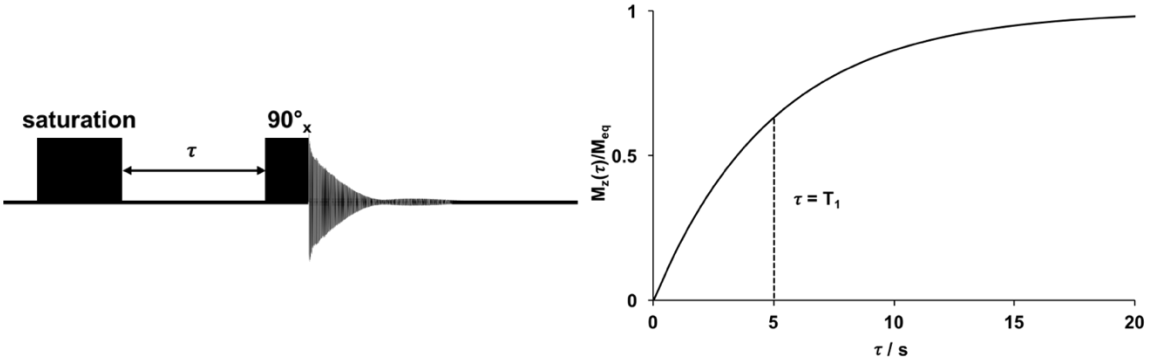

Figure 7. *Left: Pulse scheme for a SR experiment consisting of a saturation pulse train, a variable delay τ, a 90°$_x$ pulse and the acquisition of the FID. Right: M_z normalized to M_{eq} is plotted as a function of the delay time for T_1 = 5 s.*

Compared to other forms of spectroscopy the relaxation process in NMR spectroscopy is very slow. It can take minutes to establish the equilibrium magnetization. What appears to be a drawback of NMR spectroscopy, actually allows us to conduct multi-pulse NMR experiments and obtain high resolution NMR spectra, as it is possible to observe and manipulate the transverse magnetization.[2]

Slow relaxation can also be disadvantageous when it comes to the repeating of NMR experiments to improve the S/N ratio. To ensure the re-establishment of the equilibrium magnetization, enough time has to be incorporated between two scans or transients. Otherwise the signal intensity will be diminished.[2]

2.2.2. The Transverse Relaxation

The longitudinal relaxation describes only the process which leads to a re-establishment of the z-magnetization after an excitation with a 90° pulse. Another relaxation process causes the magnetization in the xy-plane – the transverse magnetization – to vanish over time. This process is named *transverse relaxation* or *spin-spin relaxation*, which is characterized by the time constant T_2.[13]

Furthermore, T_2 is also linked to the linewidth W of the Lorentzian lineshape of the NMR signal shown in Chapter 2.1.3.[2]:

$$W = \frac{1}{\pi T_2} \tag{15}$$

Despite the information given in Equation (15) it is not possible to determine T_2 from the linewidth of a certain resonance, as the inhomogeneity of the applied field also has an influence on the linewidth. To obtain T_2 values, an experiment called *spin-echo experiment* is conducted. It comprises the following sequence: $90°_x - \tau - 180°_y - \tau$. The latter pulse corrects the dephasing caused by an inhomogeneous magnetic field, but the effects of the spin-spin relaxation are not refocused by the 180° pulse. Ultimately the transverse magnetization completely vanishes, when the equilibrium is reached, due to the effects of transverse relaxation.[1]

2.2.3. The Local Field

The spins in the sample do not only feel the presence of the strong magnetic field of the NMR magnet, but also the oscillating fields of the nearby magnetic moments, which are known under the term *local field* ($\boldsymbol{B}_{\mathrm{loc}}$). This much weaker magnetic field is far from steady. As it is generated by moving molecules, its magnitude and direction vary permanently.[2]

These local fields can have the same effect on a single spin as a radiofrequency pulse has on the whole spins of the sample. Under good circumstances, the transverse component of the local field oscillates in a frequency similar to the Larmor frequency and rotates the neighboring magnetic moment into a new direction.[2]

In the end these intermolecular magnetic interactions, which are modulated by the molecular motion, cause the spins to return to thermal equilibrium.[1]

2.2.4. The Influence of Rotational Motion on Relaxation

In liquids, it is a very difficult task for molecules to rotate freely, as they often collide with other molecules, which influences the speed of the rotation or leads to a change in the rotation axis. To distinguish these processes from unhindered rotation, these phenomena are described as *tumbling*.[1]

Characteristic for molecules in liquids is the *rotational correlation time* τ_c. It is the average time which it takes for molecules to rotate about an angle of one radian (ca. 57°).[1] Depending on the size of the molecules, τ_c ranges from the picosecond (small molecules) to the nanosecond range (small proteins), which corresponds to frequencies ranging from 10^7 to 10^{10} Hz.[2]

To connect the rotational diffusion occurring in liquids to the relaxation, another quantity has to be introduced - the *spectral density* $J(\omega)$. It is a function of the angular frequency ω (in rad s^{-1})[1]:

$$J(\omega) = \frac{2\tau_c}{1 + \omega^2\tau_c^2} \tag{16}$$

$J(\omega)$ can be considered as a measure for the amount of random motion that occurs with an angular frequency ω (with a known value of τ_c).[1,2]

Longitudinal relaxation occurs when the fluctuating local fields have components oscillating at the Larmor frequency ω_0 ($= 2\pi\nu_0$). For that reason, the longitudinal relaxation rate $R_1 = T_1^{-1}$ depends on the gyromagnetic ratio γ, the mean-square value of the local magnetic field $\langle B_{loc}^2 \rangle$ and on the spectral density $J(\omega_0)$[1,2]:

$$\frac{1}{T_1} = \gamma^2 \langle B_{loc}^2 \rangle J(\omega_0) = \gamma^2 \langle B_{loc}^2 \rangle \frac{2\tau_c}{1 + \omega_0^2\tau_c^2} \tag{17}$$

In Figure 8 the dependence of the longitudinal relaxation time T_1 on the rotational correlation time τ_c for three Larmor frequencies of ^{1}H (200, 500 and 1,000 MHz) is shown.

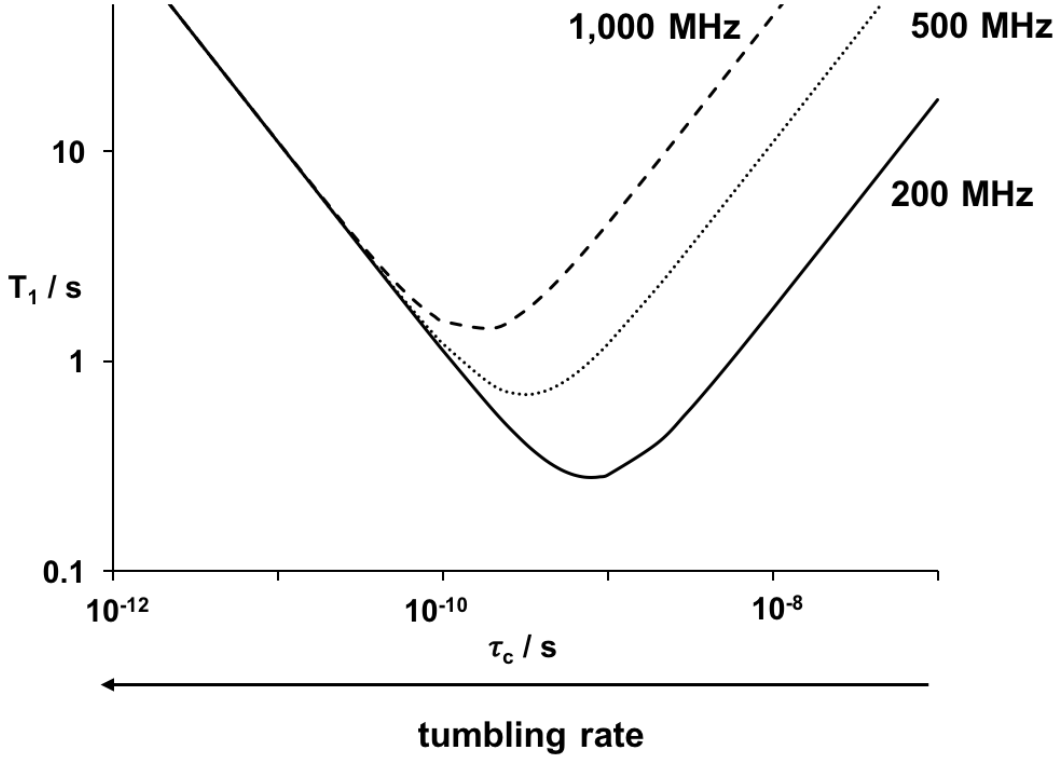

Figure 8. *T_1 as a function of τ_c (note the logarithmic scales on both axes) for $\omega_0/2\pi$ = 200 MHz (solid line), 500 MHz (dotted line) and 1,000 MHz (dashed line). The pre-factor ($\gamma^2\langle B_{loc}^2\rangle$ = 4.5·10^9 rad^2 s^{-2}) was kept constant for all cases and corresponds to the dipolar coupling of two protons (distance 2 Å).*[1] *[Figure adapted from [1]]*

As can be seen in Figure 8, the longitudinal relaxation rate is also a function of the applied magnetic field (expressed as the frequency of the spectrometer). At higher field strengths the minimum is shifted to smaller τ_c values. Furthermore, in the case of increasing field strength the longitudinal relaxation becomes slower at smaller tumbling rates (higher τ_c values).

According to the curves shown above two cases can be distinguished: In the *fast motion regime* or *extreme narrowing*[2], where $\omega_0\tau_c \ll 1$, the statements $J(\omega_0) \approx 2\tau_c$ and $T_1 \propto 1/\tau_c$ are valid. Additionally, the dependency on the magnetic field also vanishes, as the spectral density J becomes independent of the Larmor frequency ω_0.[1]

In the second case, the *slow motion regime* or *spin diffusion regime*[2], for which $\omega_0\tau_c \gg 1$, the statements $J(\omega_0) \approx \frac{2}{\omega_0^2\tau_c}$ and $T_1 \propto \tau_c$ are true. Furthermore, the

longitudinal relaxation time is dependent on the field strength in this regime, which explains the different curves in the right part of Figure 8. At all events, the fastest relaxation time is obtained when $\tau_c = 1/\omega_0$.[1]

The following conclusions related to T_1 can be drawn[1]:

- The rotational correlation time τ_c is dependent on the temperature, the viscosity and the size of the molecules, which therefore influence T_1.
- Smaller molecules (relative molecular mass $M_r < 1{,}000$) are found in the left part of the curves (faster tumbling), whereas slowly tumbling molecules (e.g. proteins, $M_r > 1{,}000$) fall to the right of the minima.
- How the relaxation rate R_1 is influenced by a change in temperature solely depends on the size of the molecule. For molecules on the left side in Figure 8, the relaxation is accelerated when decreasing the temperature. Larger molecules (on the right side) have a higher rate at elevated temperatures.
- In more viscous solvents τ_c is longer.
- As the gyromagnetic ratio is also included in Equation (17), it can be concluded that other nuclei have higher T_1 values than ^{1}H nuclei.

A similar equation[1,2] as Equation (17), which is also based on the random field relaxation model[17], can be attributed to the transverse relaxation rate $R_2 = T_2^{-1}$, too:

$$\frac{1}{T_2} = \frac{1}{2}\gamma^2\langle B_{loc}^2\rangle J(\omega_0) + \frac{1}{2}\gamma^2\langle B_{loc}^2\rangle J(0) = \frac{1}{2}\gamma^2\langle B_{loc}^2\rangle\left(\frac{2\tau_c}{1+\omega_0^2\tau_c^2} + 2\tau_c\right) \qquad (18)$$

The first term in the equation can also be written as $\frac{1}{2}T_1^{-1}$ (contribution of longitudinal relaxation). As with T_1, a distinction of cases makes sense at this point: in the fast motion regime, where $\omega_0\tau_c \ll 1, J(\omega_0) \approx 2\tau_c = J(0)$ and finally, $T_2 = T_1$ is obtained.[1] In this regime, both rates or times are independent on the applied magnetic field.

As τ_c becomes bigger, the slow motion regime is reached, where $\omega_0\tau_c \gg 1$, and it is found that $J(\omega_0) \ll J(0)$ and $T_2 \propto 1/\tau_c$.[1]

The dependence of both relaxation times on τ_c for two ^{1}H Larmor frequencies (200 and 1,000 MHz) is displayed in Figure 9.

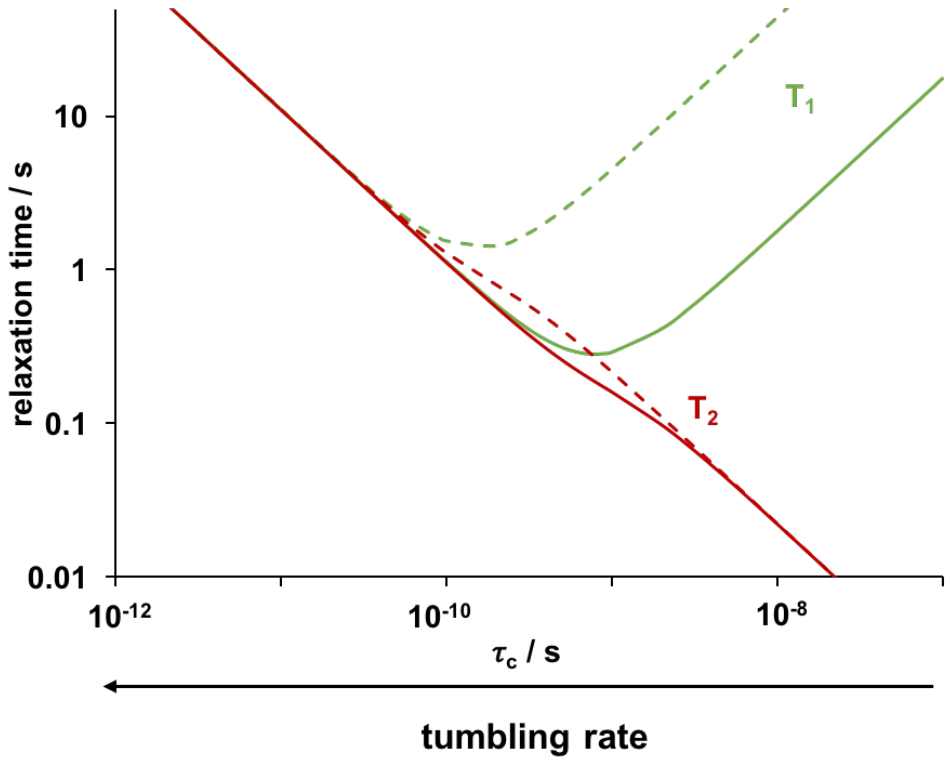

Figure 9. *Plot of T_1 (green curves) and T_2 (red curves) as a function of τ_c (note the logarithmic scales on both axes) for $\omega_0/2\pi$ = 200 MHz (solid lines) and 1,000 MHz (dashed lines). The pre-factor ($\gamma^2\langle B_{loc}^2\rangle$ = 4.5·10^9 rad^2 s^{-2}, obtained from [1]) is the same as used in Figure 8 and was kept constant for both frequencies. [Figure adapted from [1]]*

In contrast to the longitudinal relaxation time, which is field-dependent in the slow motion regime, the dependency of the transverse relaxation time on the magnetic field strength is less pronounced. Moreover, for both motional regimes the following relation exists: $T_2 \propto 1/\tau_c$.

Ultimately, it can be concluded that bigger molecules ($M_r > 1{,}000$) such as proteins have high T_1 values (i.e. slow re-establishment of z-magnetization), but their transverse relaxation is quite fast leading to broad peaks, as the linewidth depends on T_2.[1]

2.2.5. The Dipolar Mechanism

In the previous chapters the concept of relaxation was introduced and it was stated that local fields are responsible for the return of the spins to the thermal equilibrium. A closer look at the mechanisms is going to be provided in this and the two subsequent small chapters.

As the name of this chapter, *dipolar mechanism*, implies, the interaction of two spins (dipoles) is responsible for the relaxation of a certain nucleus, which experiences the local field of a neighboring spin. The strength of this field is a function of the distance (dependence on r^{-3}) and the gyromagnetic ratio of the spin (the larger γ the larger B_{loc}). Moreover, the orientation of the vector connecting those two spins or nuclei relative to the direction of the static magnetic field is also of importance.[2]

The same interaction, which has also an impact on the chemical shifts in presence of paramagnetic substances, is going to be discussed in Chapter 2.3.1. in more detail.

2.2.6. The Chemical Shift Anisotropy

The chemical shift is a result of the magnetic field experienced by a certain nucleus, which consists of the static magnetic field and a smaller local field induced by the electrons around the nucleus. As the electrons are not distributed equally over the whole molecule, the size of the induced field depends on the orientation of the molecule relative to the applied field. In liquid samples this anisotropy of the chemical shift cannot be observed, as the nuclei experience an average field due to the fast tumbling of the molecules – the shift is *isotropic*.[2]

This tumbling of the molecules in solution causes changes in the magnitude and direction of the local field, which then induces relaxation of the nuclei.[2]

2.2.7. The Quadrupolar Relaxation

Characteristic for nuclei with $I > \frac{1}{2}$ (e.g. $^{14}\mathrm{N}$, $^{17}\mathrm{O}$, $^{35}\mathrm{Cl}$, $^{37}\mathrm{Cl}$) is their *electric quadrupole moment*, which is associated with an ellipsoidal charge distribution in the nucleus. Quadrupole moments interact with electrical field gradients, that are usually present in low symmetry environments. In environments of higher symmetry (e.g. octahedral or tetrahedral), non-uniform charge distributions of electrons are cancelled out and no electrical field gradient can be observed.[1]

An example illustrates the effect of quadrupole moments on NMR spectra. Consider the following compounds $^{14}\mathrm{NMe_3}$ and $^{14}\mathrm{NMe_4^+}$. The signal of the first compound in the ^{14}N-NMR spectrum is about 100 Hz broad, whereas the tetramethylammonium ion has a 1 Hz wide signal. As a result of its tetrahedral symmetry, no electrical field gradient is present at the nitrogen and therefore no line-broadening is observed.[1]

As described in Chapter 2.2.2., the linewidth is connected to the transverse relaxation time T_2 (see Equation (15)), therefore a broad signal is an indication of fast transverse relaxation e.g. due to the quadrupolar interaction.[1]

2.3. Paramagnetic Substances in NMR and MRI

Paramagnetic substances such as certain transition metal complexes (d-block elements) and lanthanide complexes (f-block elements) are very useful reagents in NMR spectroscopy.[18] Two effects related to paramagnetic species are of special interest – the isotropic shift[18] and the relaxation effects[19], which are described and discussed in this chapter. Furthermore, a method to determine the magnetic susceptibility of paramagnetic complexes is presented in the framework of this chapter. The chapter is closed with a non-chemical application of paramagnetic relaxation agents as contrast agents in *magnetic resonance imaging* (MRI).

2.3.1. The Isotropic Shift

The chemical shift (in ppm), at which a certain signal of a paramagnetic molecule in solution is observed in NMR spectroscopy, depends on the diamagnetic and paramagnetic contributions (expressed in ppm), as shown in Equation (19)[18]:

$$\delta_{obs} = \delta_{diam.} + \delta_{param.} \tag{19}$$

The second term on the right side in Equation (19) is also known as isotropic shift δ_{iso} and can further be written as a sum of two interactions or contributions[18]:

$$\delta_{iso} = \delta_{contact} + \delta_{dipolar} \tag{20}$$

$\delta_{contact}$ represents the so-called *Fermi hyperfine contact interaction* (also named *scalar interaction*), whereas the second term, $\delta_{dipolar}$, describes the *dipolar* or *pseudocontact interaction* between electron and nucleus.[20]

In the following pages equations for both terms are presented and discussed based on a ferric porphyrin complex with two axially coordinated 3-methylpyridine ligands, which is very similar to the Ni-$TPPF_{20}$ · 2 py complex shown in Figure 13.[18]

The contact shift can be calculated using Equation (21)[18]:

$$\delta_{contact} = A_{con}^{i} \frac{\bar{g}\beta S(S+1)}{3g_n \hbar kT} \tag{21}$$

In the numerator of the fraction the average g-factor of the electron $\bar{g}$, the Bohr magneton β and the spin angular momentum quantum number S can be found, whereas in the denominator the g-factor of the nucleus g_n, the reduced Planck constant $\hbar$ and the Boltzmann constant k as well as the temperature T are displayed.[18]

The first factor in front of the fraction on the right side of Equation (21), A_{con}^{i}, is called the *hyperfine coupling constant* of the nucleus *i*. It is referred to the coupling of the electron and a certain nucleus (similar to the *J*-coupling constant).[18]

In quantum mechanical terms this contact interaction can be expressed using a Hamiltonian ($\widehat{H}_{con}$)[18]:

$$\widehat{H}_{con} = A_{con}^{i} \boldsymbol{I} \cdot \boldsymbol{S} \tag{22}$$

$\boldsymbol{I}$ is the nuclear angular momentum vector and $\boldsymbol{S}$ is electron angular momentum vector. The hyperfine coupling constant however can be written as[18]:

$$A_{con}^{i} = \frac{8\pi}{3} g\beta g_n \beta_n \left|\psi^i(0)\right|^2 \tag{23}$$

The g-factors g and g_n found in Equation (23) belong to the electron and nucleus, respectively. For the Bohr magneton (β, β_n) the same holds true. Most important however is the last factor, the square of the wave function (belonging to nucleus *i*) at the nucleus[18], which is a measure for the unpaired electron spin density found at the nucleus.[20]

Only for s-orbitals $\left|\psi^i(0)\right|^2$ is non-zero, which means that is possible to find unpaired electron spin density at the nucleus. As the unpaired electrons in transition metals are located in the d-orbitals and not the s-orbitals, they have to be transferred or delocalized to the s-orbitals of the ligands[18,20] as suggested by McConnell[21,22] and also Bloembergen[23].

Spin density can only be transferred from the metal ion to the ligand orbitals, when metal-ligand bonds are available. Otherwise, A_{con}^{i} becomes zero, which causes the contact interaction or shift to vanish.[18] In lanthanide complexes, where the unpaired electrons are found in 4f orbitals deep inside the metal ion, the delocalization of spin density is negligible and the contact shift is very small.[20]

If the contact shift is zero, the only term that can principally contribute to the isotropic shift is the dipolar or pseudocontact shift.[18] In contrast to the contact mechanism,

the dipolar mechanism relies on a through-space coupling of the nuclei of the ligands and the unpaired electrons of the metal ion. Furthermore, this mechanism only occurs in complexes showing magnetic anisotropy. Transition metals complexes such as octahedral Ni(II) complexes are magnetically isotropic, which means that no dipolar shift is observed.[20] This coupling can be considered as an interaction between two point dipoles and can also be formulated as a Hamiltonian ($\widehat{H}_{dipolar}$)[18]:

$$\widehat{H}_{dipolar} = -g\beta g_n\beta_n\left(\frac{\boldsymbol{I}\cdot\boldsymbol{S}}{\boldsymbol{r}^3}-\frac{3(\boldsymbol{S}\cdot\boldsymbol{r})(\boldsymbol{I}\cdot\boldsymbol{r})}{\boldsymbol{r}^5}\right) \tag{24}$$

The symbols found on the right side are the same as found in equations (22) and (23) except for $\boldsymbol{r}$, which represents distance between the metal and the nucleus. Classically the nuclear and the electron magnetic moments can be considered as bar magnets. From the Hamiltonian displayed in Equation (24) the dipolar or pseudocontact shift can be derived[18]:

$$\delta_{dipolar} = \frac{\beta^2 S(S+1)}{9kT}(g_{\parallel}^2 - g_{\perp}^2)\frac{1-3cos^2\theta^i}{r_i^3} \tag{25}$$

Compared to the contact shift shown in Equation (21) the expression on the right side of Equation (25) is much more sophisticated. The second factor describes the anisotropy in the electron distribution of the molecule as result of the spatial arrangements of the orbitals. In the iron porphyrin model system showing a D_{4h} symmetry two different g-factors can be observed ($g_{\parallel}$ and $g_{\perp}$) – one is lying along the z-axis and the other is found in the xy-plane of the porphyrin system. In general, the g-factor can be represented as scalar for isotropic electron distributions, whereas a tensor is necessary for the proper description of anisotropic electron distributions.[18]

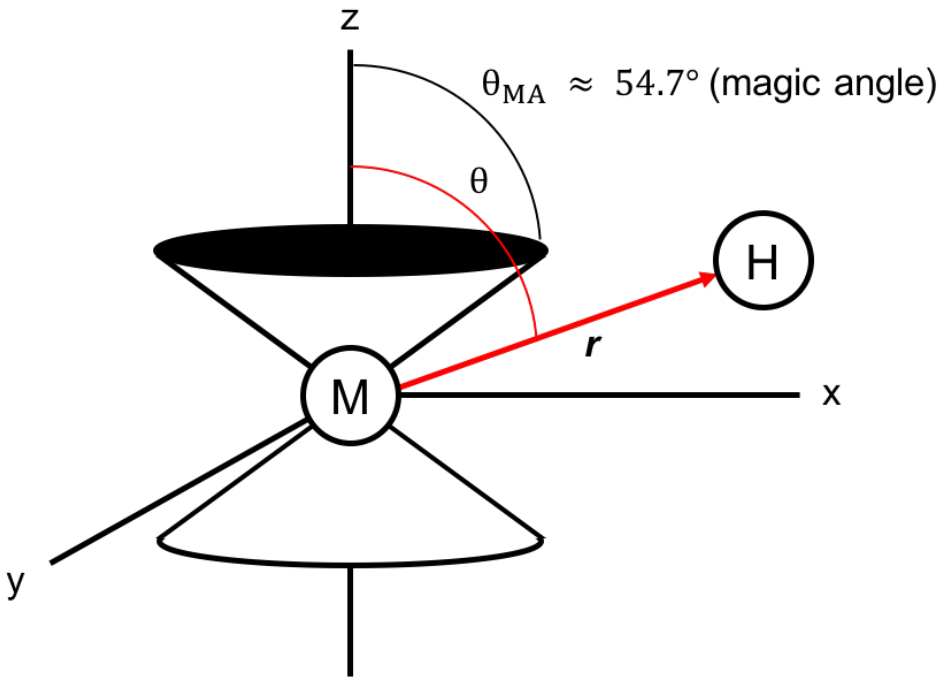

Figure 10. *Cartesian coordinate system, where the metal ion M is located at the origin. The vector (marked in red) between the metal ion and a proton H (e.g. of the ligand) is called* $\boldsymbol{r}$*.* θ *is the angle (marked in red) which is confined by the vector* $\boldsymbol{r}$ *and the z-axis. The double cone indicates the area where* $\theta = \theta_{MA}$*, which is the magic angle (≈ 54.7°). In this picture, the proton is located outside the cones (*$\theta > \theta_{MA}$*). [Figure adapted from* [18]*]*

Figure 10 shows the two variables found in the "geometric factor" of Equation (22). For an angle of about 54.7° (the *magic angle*), the term $1 - 3cos^2\theta^i$ becomes zero and thus the dipolar shift. Nuclei which are located on the cones, are not subjected to a dipolar shift.[18]

What kind of dipolar shift (shielding or deshielding) is sensed by a nucleus is dependent on the location of the nucleus (inside or outside the cones) as well as the magnetic anisotropy (expressed as $(g_{\parallel}^2 - g_{\perp}^2)$). If e.g. a nucleus located in the cone is subjected to a deshielding dipolar shift, a nucleus on the outside senses a shielding dipolar shift.[18]

As both contact and dipolar shift are functions of the spin angular quantum number S, it can be concluded that for a higher number of unpaired electrons a higher isotropic shift should be observable. Additionally, both are also dependent on the temperature, or to be more precise, linearly dependent on the inverse of the temperature. This is the case, when the molecules obey the Curie Law.[18]

A practical application of the dipolar coupling mechanism is the use of lanthanide shift reagents (LSRs) in NMR spectroscopy. The addition of lanthanide complexes such as Eu(III) complexes leads to a simplification of the NMR spectra.[24]

An example taken from literature[25] shall demonstrate the effects of lanthanide complexes on the observed shift. The experimental LIS (lanthanide-induced shift) is obtained by performing measurements of the shift for different concentrations of LSR and then extrapolating to a molar ratio of 1:1 (reagent : substrate).[25]

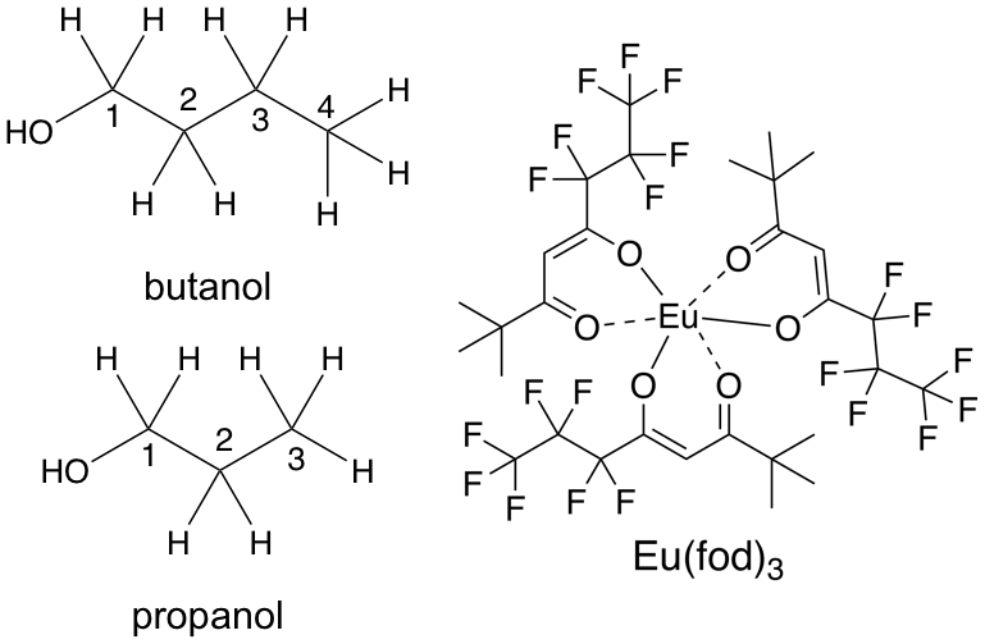

Figure 11. *Left: Structures of the primary alcohols butanol and propanol with numbered C-atoms. Right: Structure of the LSR Eu(fod)$_3$.*[25]

Table 1. *Experimental values for LIS (Δδ) in ppm (to lower field) for the hydrogen peaks of the substrates at 1:1 ratio (substrate : Eu(fod)$_3$). The spectra were recorded at 200 MHz spectrometer and the substrates (displayed in Figure 11 with numbered carbons) were dissolved in $CDCl_3$. [Data taken from* [25]*]*

substrate	Δδ(-OH)	Δδ(H-1)	Δδ(H-2)	Δδ(H-3)	Δδ(H-4)
butanol	90.33	20.90	12.82	8.98	4.38
propanol	107.73	25.65	15.65	10.05	-

The values given in Table 1 show that the hydroxyl group, which coordinates to the Eu(III) ion[26], experiences a very huge shift to lower field (up to 108 ppm for

propanol). More interestingly, the resonances of the smaller molecule propanol are not shifted that much to lower field compared to those of butanol. The further away the methylene groups are from the complex center, the smaller is the observed dipolar shift, as the magnitude of the shift is proportional to r^{-3} (see Equation (25)).

The dipolar shift introduced by LSRs is very well described by the McConnell-Robertson equation[22], which resembles Equation (25) and is only applicable in case of axial symmetry[26]:

$$\Delta\delta = K\frac{3cos^2\theta - 1}{r^3} \tag{26}$$

r and θ are defined in the same way as depicted in Figure 10. The constant K describes the magnetic properties of the species. This equation is only valid, if the isotropic shift originates just from dipolar interactions.[26] Indeed, contact interactions can be neglected for lanthanide complexes, as the unpaired electrons are located in the shielded 4f-orbitals.[20]

2.3.2. Determination of Magnetic Susceptibility via NMR Spectroscopy

In the last chapter, it was stated that paramagnetic transition metal and lanthanide complexes influence the position of signals assigned to ligands and substrate molecules, which coordinate to the complexes. This topic can also be approached from a somehow different side – the (bulk) susceptibility of the medium is responsible where a signal occurs e.g. in the ^{1}H-NMR spectrum.[27]

The following formula describes the shift of a proton signal in presence of paramagnetic ions or complexes[27,28]:

$$\frac{\delta\nu}{\nu_0} = \frac{2\pi}{3}(\chi_V - \chi_V') \tag{27}$$

$\delta\nu$ is the observed shift in frequency (in Hz), ν_0 is the frequency of the spectrometer (in Hz), χ_V represents the volume susceptibility in presence of paramagnetic substances and χ_V' the volume susceptibility of a reference solution.[28]

Based on Equation (27) the magnetic susceptibility of a paramagnetic compound can be determined by measuring the shift in frequency of a proton signal in presence of paramagnetic ions or complexes. This method, which was published by Evans[27] in 1959, features a coaxial NMR tube setup. The outer tube is filled with a solution of a paramagnetic substance such as a transition-metal complex and an inert reference substance (e.g. *tert*-butanol) in a standard NMR solvent, whereas the inner tube (capillary) contains just the solvent and the same amount of reference substance. In the NMR spectrum the methyl protons of *tert*-butanol resonate at two different frequencies.[27]

The paramagnetic susceptibility χ_M^P (in $cm^3\ mol^{-1}$) is calculated using[29]

$$\chi_M^P = \frac{\delta\nu^P M^P}{\nu_0 S_f m^P} + \chi_0 M^P + \chi_0 M^P \frac{(d_0 - d_s^P)}{m^P} - \chi_M^{dia} \tag{28}$$

where $\delta\nu^P$ is the observed shift in frequency (in Hz), M^P the molar mass of the paramagnetic substance (in $g\ mol^{-1}$), ν_0 the frequency of the NMR spectrometer (in Hz), S_f the shape factor of the magnet ($S_f = \frac{4\pi}{3}$ for a modern superconducting magnet), $\mathrm{m^P}$ the mass concentration of the paramagnetic substance (in $g\ cm^{-3}$), χ_0 the mass susceptibility of the solvent (in $cm^3\ g^{-1}$), d_0 the density of the solvent (in $g\ cm^{-3}$), d_s^P the density of the solution (in $g\ cm^{-3}$) and χ_M^{dia} the diamagnetic contribution of the compound (in $cm^3\ mol^{-1}$).[29]

In the end of this chapter it should be mentioned that the paramagnetic susceptibility is directly proportional to the inverse of the temperature. This relation is known as the Curie Law.[28]

2.3.3. Paramagnetic Relaxation Enhancement (PRE)

In Chapter 2.2. the different mechanisms giving rise to the relaxation processes in NMR spectroscopy were described and discussed briefly. What was neither mentioned nor discussed is the influence on the relaxation processes exerted by paramagnetic substances such as transition metal or lanthanide complexes.

How the concentration of a paramagnetic substance such as a Gd(III) complex (with its seven unpaired electrons) influences the longitudinal or transverse relaxation rate R_i of a certain nucleus, can be expressed using the following equation[6]:

$$R_i = \frac{1}{T_i} = \frac{1}{T_i^0} + c \cdot r_i \text{ with } i = 1,2 \tag{29}$$

T_i is the longitudinal ($i = 1$) or transverse ($i = 2$) relaxation time in presence of paramagnetic additives and T_i^0 the corresponding time without. c is the concentration of the paramagnetic species and r_i the *relaxivity*, which quantifies the change in the relaxation rate for a concentration of 1 mM paramagnetic species.[6]

In Equation (29) only a description of the impact on the relaxation due to the presence of paramagnetic species is provided, the mechanism behind this relaxation acceleration or enhancement is not given. What makes paramagnetic substances unique compared to diamagnetic substances are the unpaired electrons and that is where the explanation of the mechanism starts.

A magnetic moment cannot only be assigned to a magnetic nucleus (e.g. $I = \frac{1}{2}$), but also to an unpaired electron ($s = \frac{1}{2}$) found in paramagnetic substances. The only difference between those two moments is that the electron magnetic moment is 658 times bigger and therefore produces stronger local fields giving rise to an altered relaxation of neighboring nuclei (similar due to the dipolar mechanism in 2.2.5.).[19]

For the further discussion of the topic it is inevitable to introduce the electronic counterparts of T_1 and T_2 – the electron longitudinal relaxation time T_{1e} and electron transverse relaxation time T_{2e}. T_{1e} has values in the range of 10^{-8} to 10^{-12} s depending on the type of the paramagnetic metal ion and effects such as zero-field splitting (ZFS), magnetic anisotropy and spin-orbit coupling.[19]

A theoretical approach to the paramagnetic relaxation enhancement (PRE) observed in NMR spectroscopy is provided by the Solomon-Bloembergen-Morgan (SBM) theory.[15,23,30] As with the isotropic shifts, both the dipolar and the contact mechanism contribute to the relaxation.[19]

For that reason, the theory is quite complex and difficult to grasp. Thus, the effects of paramagnetic ions in terms of relaxation and line-broadening are illustrated using a simplified model based on the SBM theory.

Oktaviani et al.[8] presented a methodology, in which the paramagnetic contributions to the relaxation are regarded as a function of T_{1e}. Furthermore, it was shown that the presented model is suitable for the description of a high-spin Fe(III) based PRE agent (Fe(DO3A)), which was used to shorten the ^{1}H T_1 values in the protein α-synuclein.[8]

Additionally, a few assumptions are made in this model in order to reduce the complexity of the equations even further:

- The relaxation is only based on the dipolar mechanism neglecting the contact mechanism.[4,8]
- The “inner-sphere” model is applied[8], where a solvent molecule coordinates to the paramagnetic ion (in the “outer-sphere” model the solvent would reside in the second coordination sphere or in the bulk).[7]

The relaxation contributions caused by dipolar interactions in the inner-sphere model can be expressed by the following two equations[8,31]:

$$R_{1p} = \frac{2S(S+1)\gamma_I^2 g^2 \beta^2}{15r^6}\left(\frac{\mu_0}{4\pi}\right)^2\left[\frac{3\tau_{c1}}{1+\omega_I^2\tau_{c1}^2}+\frac{7\tau_{c2}}{1+\omega_S^2\tau_{c2}^2}\right] \tag{30}$$

$$R_{2p} = \frac{S(S+1)\gamma_I^2 g^2 \beta^2}{15r^6}\left(\frac{\mu_0}{4\pi}\right)^2\left[4\tau_{c1}+\frac{3\tau_{c1}}{1+\omega_I^2\tau_{c1}^2}+\frac{13\tau_{c2}}{1+\omega_S^2\tau_{c2}^2}\right] \tag{31}$$

R_{1p} and R_{2p} correspond to the relaxivities of Equation (29), *S* is the spin quantum number, γ_I the gyromagnetic ratio of the nucleus I, β the Bohr magneton, g the electron g-factor, r the distance between nuclear and electron spin, μ_0 the vacuum

permeability, ω_I and ω_S the Larmor frequencies of the nucleus and the electron, respectively.[8]

The effective longitudinal and transverse nuclear correlation times (τ_{c1} and τ_{c2}) are dependent on T_{1e} and T_{2e}, respectively, and the rotational correlation time τ_c[8]:

$$\frac{1}{\tau_{c1}} = \frac{1}{T_{1e}} + \frac{1}{\tau_c} \tag{32}$$

$$\frac{1}{\tau_{c2}} = \frac{1}{T_{2e}} + \frac{1}{\tau_c} \tag{33}$$

In Figure 12 the relaxation rates (= product of concentration and $\mathrm{R_{1p}}$ or $\mathrm{R_{2p}}$, see Equation (29)) are plotted for two different Larmor frequencies (200 and 1,000 MHz). Below the diagram, examples for metal ions are given, whose T_{1e} values lie in this range (e.g. Gd(III) has a T_{1e} value of 10^{-8} s [32]).

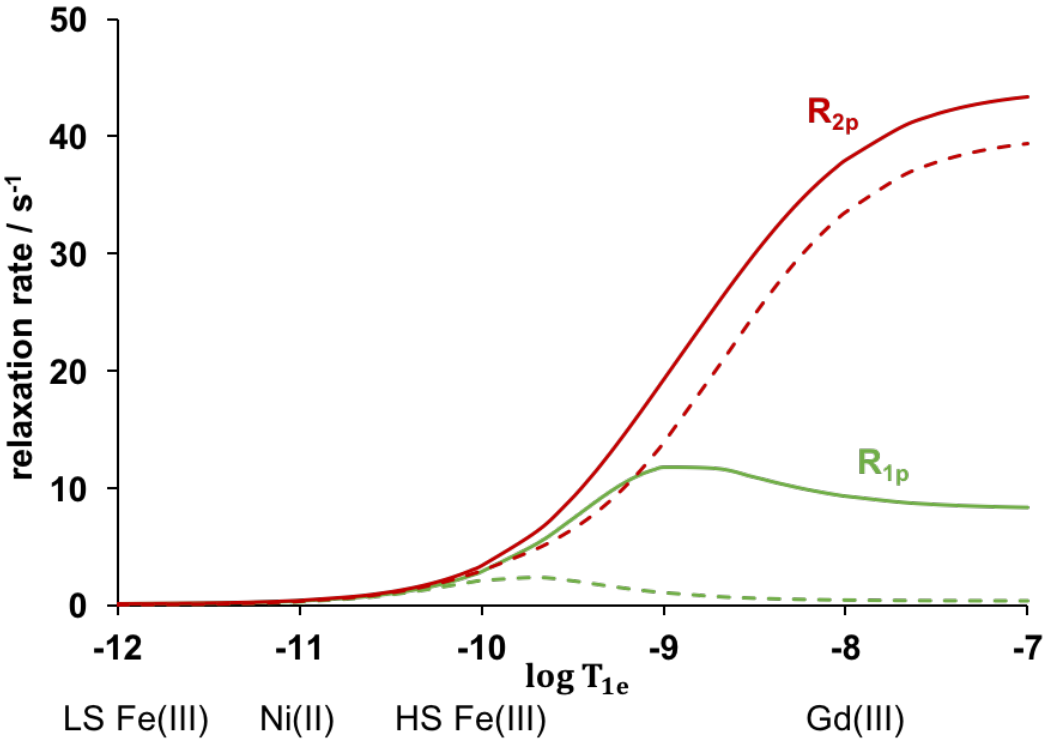

Figure 12. *Plot of $c \cdot R_{1p}$ and $c \cdot R_{2p}$ as functions of the decadic logarithm electron relaxation times T_{1e}. The prefactors containing first two factors in equations (30) and (31) and the concentrations were set to 10^{10}. τ_c was assumed as 2 ns and $T_{1e} \approx T_{2e}$.[8] The solid lines correspond to a frequency of 200 MHz (4.7 T) and the dashed lines to 1,000 MHz (23.5 T). Below the graph examples for metal ions with T_{1e} values in this magnitude are given (LS = low-spin, HS = high-spin). [Figure adapted from [8]]*

LS Fe(III) ($S = \frac{1}{2}$) and Ni(II) ($S = 1$) are located in the left part of Figure 12, which corresponds to the picosecond range. In this range $\tau_c > T_{1e}, T_{2e}$, the effective correlation times become approximately equal to the electron relaxation times – $\tau_{c1} \approx T_{1e}$ and $\tau_{c2} \approx T_{2e}$. Additionally, it is assumed that $T_{1e} \approx T_{2e}$, $\omega_I \tau_{c1} \ll 1$ and $\omega_S \tau_{c2} \ll 1$, so R_{1p} and R_{2p} can be written as[8]:

$$R_{1p} \approx R_{2p} = \frac{20S(S+1)\gamma_I^2 g^2 \beta^2}{15r^6} \left(\frac{\mu_0}{4\pi}\right)^2 T_{1e} \tag{34}$$

It is clearly visible that both rates are linearly dependent on T_{1e}. In this regime, the enhancement of the longitudinal relaxation is only slight. For that reason, a higher concentration of Ni(II) PRE (> 30 mM) is needed to exhibit a significant reduction of ^{1}H T_1 values. As the transverse relaxation rate is as small as the longitudinal relaxation rate, the effect on the line-width is very limited.[8]

In contrast to LS Fe(III) its high-spin counterpart ($S = \frac{5}{2}$) is characterized by a higher T_{1e} value (≈ 100 ps [32]). For the range of HS Fe(III) the following statements are true: $\omega_I \tau_{c1} < 1$ and $\omega_S \tau_{c2} > 1$. R_{1p} and R_{2p} are still linearly dependent on T_{1e}, however they are not "equal" anymore[8]:

$$R_{1p} = \frac{6S(S+1)\gamma_I^2 g^2 \beta^2}{15r^6} \left(\frac{\mu_0}{4\pi}\right)^2 T_{1e} \tag{35}$$

$$R_{2p} = \frac{7S(S+1)\gamma_I^2 g^2 \beta^2}{15r^6} \left(\frac{\mu_0}{4\pi}\right)^2 T_{1e} \tag{36}$$

PREs based on HS Fe(III) accelerate the longitudinal relaxation much more than Ni(II) or LS Fe(III) PREs do. Moreover, in presence of HS Fe(III) the lines are more broadened (i.e. higher R_{2p} value).[8]

If the T_{1e} values are increased even further, the effective correlation times $\tau_{c1} \approx \tau_c$, $\tau_{c2} \approx \tau_c$ and $\omega_I \tau_c > 1$, equations (30) and (31) become[8]:

$$R_{1p} = \frac{2S(S+1)\gamma_I^2 g^2 \beta^2}{15r^6} \left(\frac{\mu_0}{4\pi}\right)^2 \frac{3\tau_c}{1+\omega_I^2 \tau_c^2} \tag{37}$$

$$R_{2p} = \frac{S(S+1)\gamma_I^2 g^2 \beta^2}{15r^6} \left(\frac{\mu_0}{4\pi}\right)^2 \left[4\tau_c + \frac{3\tau_c}{1+\omega_I^2 \tau_c^2}\right] \tag{38}$$

As can easily be seen, both quantities are not linearly dependent on T_{1e} anymore. These last two equations are valid for e.g. Gd(III) ($S = \frac{7}{2}$; $T_{1e} \approx 10^{-8}$ s [32]), for which $T_{1e} > \tau_c$. $R_{2p} > R_{1p}$ means that severe line broadening can be expected from Gd(III).[8]

In the last two pages only the T_{1e} values of the different paramagnetic ions were considered. The different number of unpaired electrons was disregarded in the calculation of the curves in Figure 12, as the pre-factor was kept constant for all curves. It is quite clear, that the relaxation rates are higher, if more unpaired electrons are present in a PRE agent.

The field strength of the NMR equipment plays an important role, as going to lower fields or Larmor frequencies (e.g. 200 MHz) significantly increases both rates. The effect on the transverse component is not as big as the impact on the longitudinal component, whose maximum is shifted to higher electron relaxation times by one magnitude.

To speed up the longitudinal relaxation a suitable PRE agent should have a high r_1 value (high impact on T_1) and a low r_2 value (small impact on T_2). With a high transverse relaxivity r_2, the agent would cause severe line broadening. These requirements are met e.g. by the PRE agent Fe(DO3A).[8]

As mentioned in Chapter 2.2.4, the longitudinal relaxation rate depends on the gyromagnetic ratio (to be more precisely its square). Therefore it can be concluded that nuclei with smaller gyromagnetic ratios (than ^{1}H) should have smaller rates or longer T_1 values.[1]

Especially ^{13}C-NMR spectroscopy can be very tedious due to the long relaxation times (even up to 100 s).[33] To make things worse, ^{13}C has a very low natural abundance of about 1 %[1], therefore usually more than one scan is required to get a considerable S/N ratio in the spectrum.[34] Each scan is followed by a relaxation delay, which should be longer than T_1, otherwise the signal intensity decreases with each additional scan. Hence, recording several scans is a time-consuming business. Most of the time, the instrument is idle and waiting for the spins in the sample to re-establish equilibrium magnetization. An elegant method to accomplish the reduction of the longitudinal relaxation times and thus decreasing the experiment time is the addition of paramagnetic metal complexes such as $Cr(acac)_3$.[33–36]

2.3.4. Paramagnetic Relaxation Enhancement in MRI

A “non-chemical” application of paramagnetic relaxation enhancement agents is the use of Gd(III) complexes ($S = \frac{7}{2}$) as contrast agents in magnetic resonance imaging (MRI).[7]

This technique used in medicine is quite similar to NMR spectroscopy except the fact, that a patient is “inserted” into a superconducting magnet instead of a sample. In MRI, the water molecules incorporated in the body tissue, or to be more specific their protons, are monitored by pulsing them with radio waves.[7] The spatial resolution is achieved by applying field gradient pulses in the MRI sequences.[37] Gd^{3+} ions are in principle toxic, therefore they have to be applied in chelated form prior to a MRI examination.[7]

The signal intensity obtained in MRI has its origin in local variations of the longitudinal as well as the transverse relaxation rate of water protons. Pulse sequences applied in MRI can be T_1-weighted or T_2-weighted. In the first type Gd(III) based relaxation agents (T_1 agents with a ratio r_2/r_1 of 1 to 2) are favoured. T_2 agents (e.g. iron oxide particles) are used in the second type and have ratios of 10 or higher.[7]

2.4. Spin Switches based on Porphyrin Complexes

2.4.1. Spin Crossover and CISCO

Spin crossover (SCO), also known as *spin transition* (ST), is a phenomenon observed in certain transition metal complexes. When conditions such as temperature or pressure are changed, the metal ion in the center of the complex switches its spin state. A variation in the surrounding magnetic field or even illumination with light can also change the spin state of a transition metal ion. This transition of the spin state has a notable effect on the physical (e.g. color, magnetic behavior) or chemical properties of the substance.[38]

Additionally, the change in the spin state of a sample can also have "chemical" reasons. *Coordination-induced spin crossover* (CISCO) is typical for quadratic planar transition metal complexes like Ni(II)-porphyrins, which are usually diamagnetic ($S = 0$, low-spin). If one or two axial ligands coordinate to the Ni^{2+} ion, the newly formed complex undergoes a spin crossover and becomes paramagnetic ($S = 1$, high-spin). Ni-$TPPF_{20}$ (Ni(II)-tetrakis(pentafluorophenyl)porphyrin), an example for a nickel complex showing this phenomenon, is depicted in Figure 13.[12]

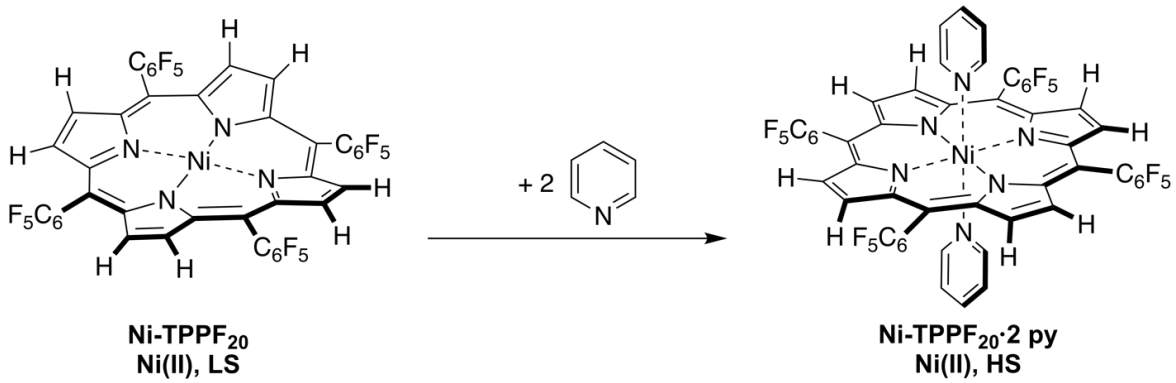

Figure 13. *Coordination of two pyridine molecules to diamagnetic Ni-$TPPF_{20}$ gives the paramagnetic Ni-$TPPF_{20}$ · 2 py complex (LS = low-spin, HS = high-spin).*[12]

A molecular orbital scheme showing the population of the d-orbitals (Figure 14) can provide an explanation for the CISCO observed for Ni(II)-porphyrin complexes.[39]

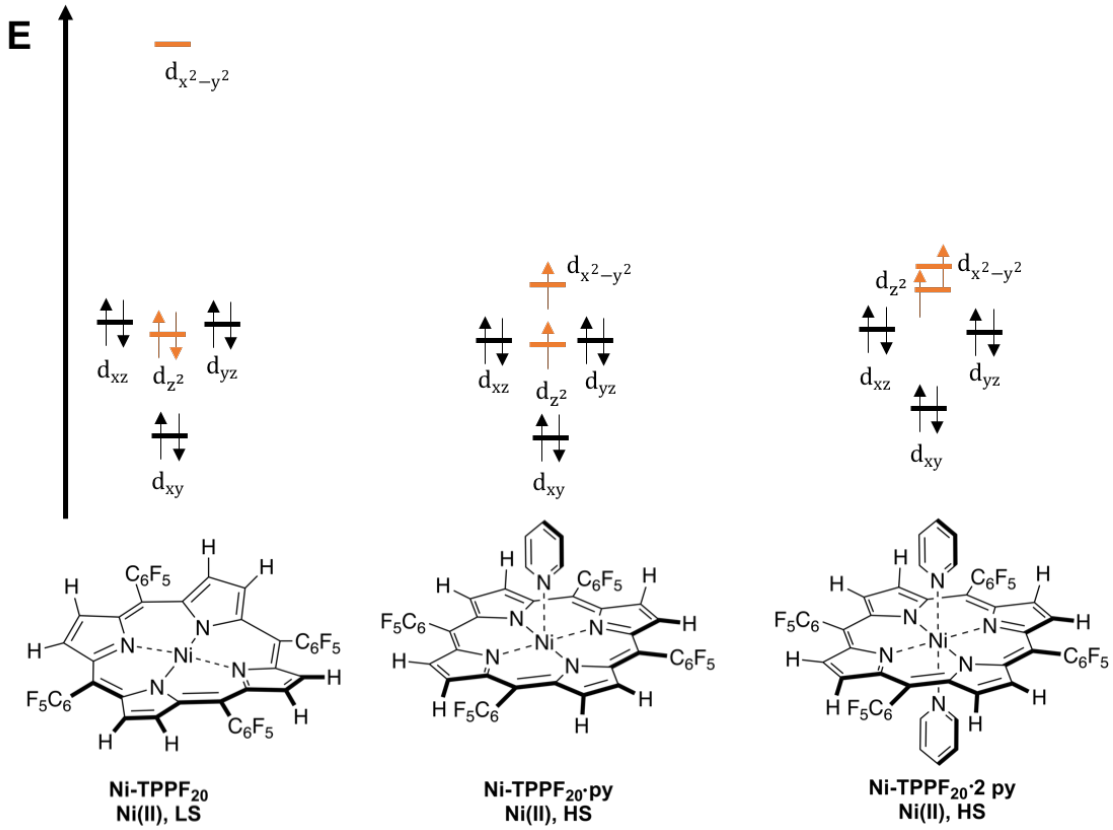

Figure 14. *Molecular orbital scheme showing the d-orbitals of the central Ni^{2+} ion. Left: square-planar Ni(II) complex ($S = 0$, low-spin). Middle: square-pyramidal Ni(II) complex ($S = 1$, high-spin). Right: square-bipyramidal Ni(II) complex ($S = 1$, high-spin). The orbital energies E were calculated for Ni-$TPPF_{20}$ and pyridine using DFT (B3LYP/6-31G* level).*[39] *[Figure adapted from* [39]*]*

Upon coordination of a pyridine molecule to one of the axial positions of square-planar Ni-$TPPF_{20}$ the orbital energy of the doubly occupied d_{z^2} orbital (marked in orange in Figure 14) is shifted to the level of the $d_{x^2-y^2}$ orbital (also marked in orange). After the spin-crossover a triplet ($S = 1$) is formed, in which both singly occupied orbitals are decreased in energy giving the configuration shown in the middle. The coordination of another pyridine leads to stabilization of both orbitals.[39]

The coordination of axial ligands does not only change the spin state of the central ion but also causes a flattening of the porphyrin plane.[39] For sterical reasons the phenyl rings are not in the plane of the porphyrin core.[40]

The spin switch discussed so far in this chapter only performs a CISCO when axial ligands are added to a solution of it. Indeed, this system is far away from reversibility

– the association constants for the reactions shown in Figure 15 are both > 1 [12] indicating the position of the equilibrium being shifted to the right.

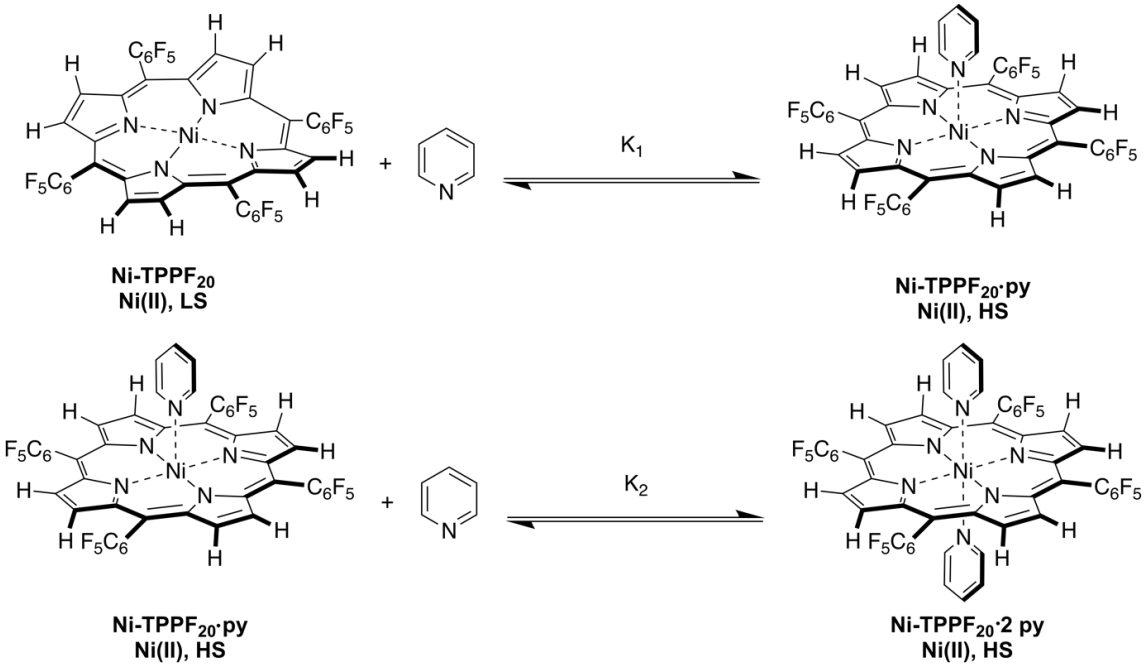

Figure 15. *Association constants (K_1 = 8.20 and K_2 = 22.40) for the coordination of a single pyridine molecule (first line) and coordination of a second pyridine molecule (second line). The association constants were measured at 298 K.*[12]

2.4.2. The *Record Player* Design

The disadvantage of the approach discussed in the previous chapter is the scarce control over the coordination of axial ligands, which is determined by the association constants of the complexation reactions. Actually, the only possibility to influence these equilibrium reactions apart from changing the temperature is the adaption of the electronic properties of the axial ligand (e.g. by electron-donating or -withdrawing substituents on the pyridine).[12]

Control over the coordination number can be achieved by attaching the ligand pyridine to a Ni(II)-porphyrin complex via a tether, which comprises a photo-switchable phenylazopyridine group.[9] By illuminating the complex with blue light (wavelength 435 nm) the azo group is isomerized to the (*E*)-configuration. The reverse process is induced with green light (500 nm). The attached pyridine can only coordinate, when the azo group in (*Z*)-configuration. Figure 16 illustrates the *light-driven, coordination-induced spin state switch* (LD-CISSS).[11]

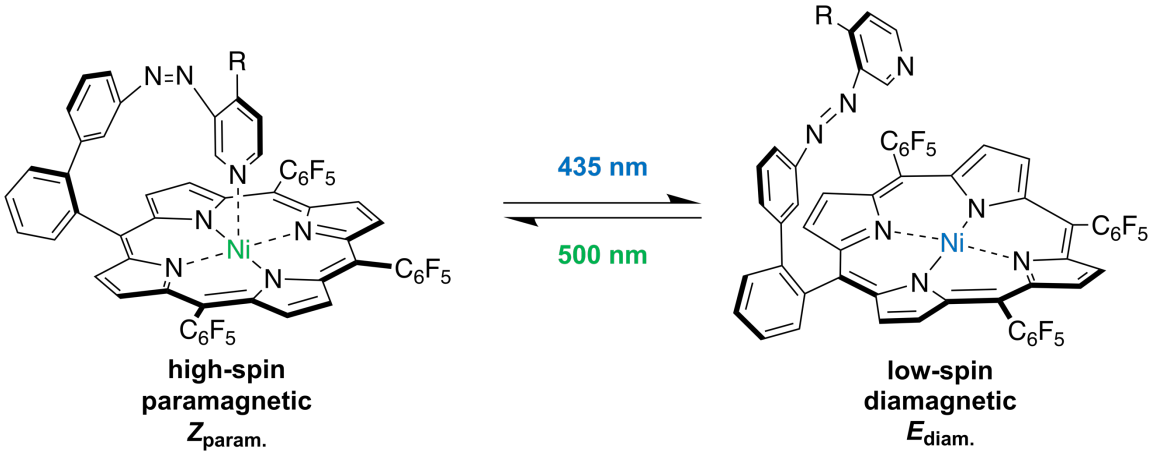

Figure 16. *The photoisomerization of the azopyridine group induces the spin state switch in the nickel porphyrin complex. The isomer on the left side ($Z_{param.}$, coordination number (CN) = 5, $S = 1$, high-spin) is paramagnetic and the other isomer ($E_{diam.}$, CN = 4, $S = 0$, low-spin) is diamagnetic. The type and influence of substituent R on the switching process are outlined in the paragraphs below.*[11]

Furthermore it also becomes clear why the complex is named *record player* - the phenylazopyridine moiety corresponds to a tone arm, the lone pair on the pyridine-N is the needle and the turntable housing is represented by the porphyrin plane.[9]

Figure 16 produces the illusion that only one isomer is abundant after longer irradiation with light of the corresponding wavelength (i.e. reaching the photostationary state (PSS)). Actually, both isomers (and also several rotamers) are present in both PSSs. Additionally, there is also another equilibrium between the coordinated and non-coordinated form of the (*Z*)-isomer, which is shown in Figure 17.[11]

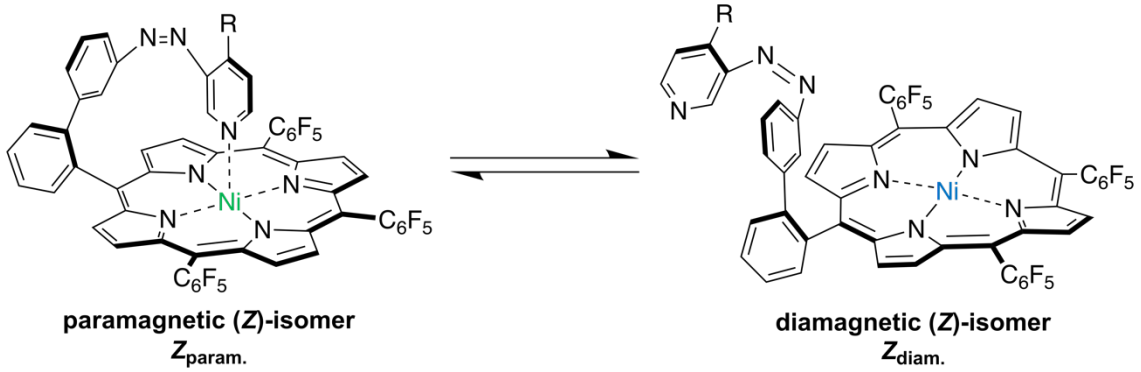

Figure 17. *Equilibrium between the coordinated (left hand) and the non-coordinated form (right hand) of the (Z)-isomer. The type and influence of the substituent R on this equilibrium are outlined in the paragraphs below.*[11]

Both equilibria can be characterized by ^{1}H-NMR spectroscopy, which is going to be discussed in Chapter 5.3. The percentages of the isomers in the PSS, which is reached after prolonged irradiation with 500 nm light, are shown in Table 2.[11]

Table 2. *Percentage of the different isomers ($Z_{param.}$, $Z_{diam.}$ and $E_{diam.}$) in solutions of the "record player" derivatives measured in acetone-d_6 at 20 °C after irradiating with 500 nm light (i.e. reaching the PSS 500 nm). [Data taken from [11]]*

R	percentage of $Z_{param.}$	percentage of $Z_{diam.}$	percentage of $E_{diam.}$
Cl	42%	20%	38%
H	48%	17%	35%
Me	75%	10%	15%
OMe	> 85%	≈10%	< 5%

In the other PSS (PSS 435 nm), > 95% of $E_{diam.}$ isomer and < 5% of (*Z*)-isomers are present for all four derivatives.[11]

In Table 2 an increase of the percentage of $Z_{param.}$ from the top to the bottom can be observed. This is connected to the electronic properties of the substituents on the 4-position of the pyridine unit. The first moiety, Cl, is an electron-withdrawing group (compared to H), the methyl group and the methoxy group are electron-donating groups, which increase the electron density on the pyridine-N leading to a better intramolecular coordination. Moreover, the photochemical *E/Z* isomerization is also affected, which manifests itself in a decreasing percentage of $E_{diam.}$ isomer.[11]

Usually, azopyridine and azobenzene derivatives are isomerized from (*E*) to (*Z*) when irradiated with a wavelength of 365 nm. For *record player*-type Ni-porphyrins the wavelength to isomerize the internal azo group from (*E*) to (*Z*) is 500 nm, which means that a bathochromic shift of ca 135 nm is observed. This is caused by an interaction between the π,π^* excited state of the porphyrin (Q-band) and the π,π^* state of the azopyridine.[9]

Besides the fully reversible switching of the spin states, the compound also has other benefits. It is very stable under air and ambient temperature.[11] Furthermore, the thermal isomerization from the (*Z*)- to the (*E*)-isomer is not a real issue, as this

process is very slow, and the paramagnetic (*Z*)-isomer is stabilized by the interaction between the pyridine-N and the central Ni^{2+} ion.[9]

These benefits listed here makes the compound interesting for applications as a photo-switchable contrast agent (CA) in MRI. In a future application, the compound might be applied to the patient in the same way as standard contrast agents based on Gd(III) complexes. Small optical fibers might be introduced into the patient and by illuminating the contrast agent, it could be switched “on” or “off”.[11]

A drawback of Ni(II) based CAs is the intrinsically lower longitudinal relaxivity compared to Gd(III) complexes (e.g. gadobutrol) as result of the different numbers of unpaired electrons (2 for Ni(II) and 7 for Gd(III))[11] and the smaller T_{1e} value of Ni(II) (see Section 2.3.3.).

3. Experimental Design

The aim of this thesis is a detailed investigation of the switching efficiency of MeO-RP. During the investigation the following aspects should be examined: kinetics of the switching processes, long-term stability and reversibility of the spin switch, manipulation of the T_1 values during an experiment as well as enhancement of the signal intensity.

At first, the kinetics of both switching processes (from diamagnetic to paramagnetic and the reverse process) has to be established. With these kinetic data the following points can be addressed: how fast these processes proceed and which time is required to switch the compound from one magnetic state to the other.

Another fundamental requirement for the spin switch is the long-term stability and the reversibility of the switching process. As the photo-switchable relaxation agent is repeatedly cycled between the two magnetic states, it is required from the compound to be stable and reversibly switchable over a long time.

Furthermore, it also necessary to demonstrate the real-time manipulation of the longitudinal relaxation time of surrounding nuclei (e.g. protons) during an experiment, in which the recovery of the z-magnetization is studied - e.g. in a modified SR experiment.

Finally, the enhancement of the signal intensity due to the presence of MeO-RP should also be examined with a well-designed experiment.

All the aspects mentioned in the previous paragraphs are studied with different experiments. The idea behind this chapter (apart from describing the aim of this work) is the description of how the experiments are designed. Moreover, a “roadmap” (see Figure 18) is presented, in which an overview over the experiments and their results (see Chapter 5.) is given.

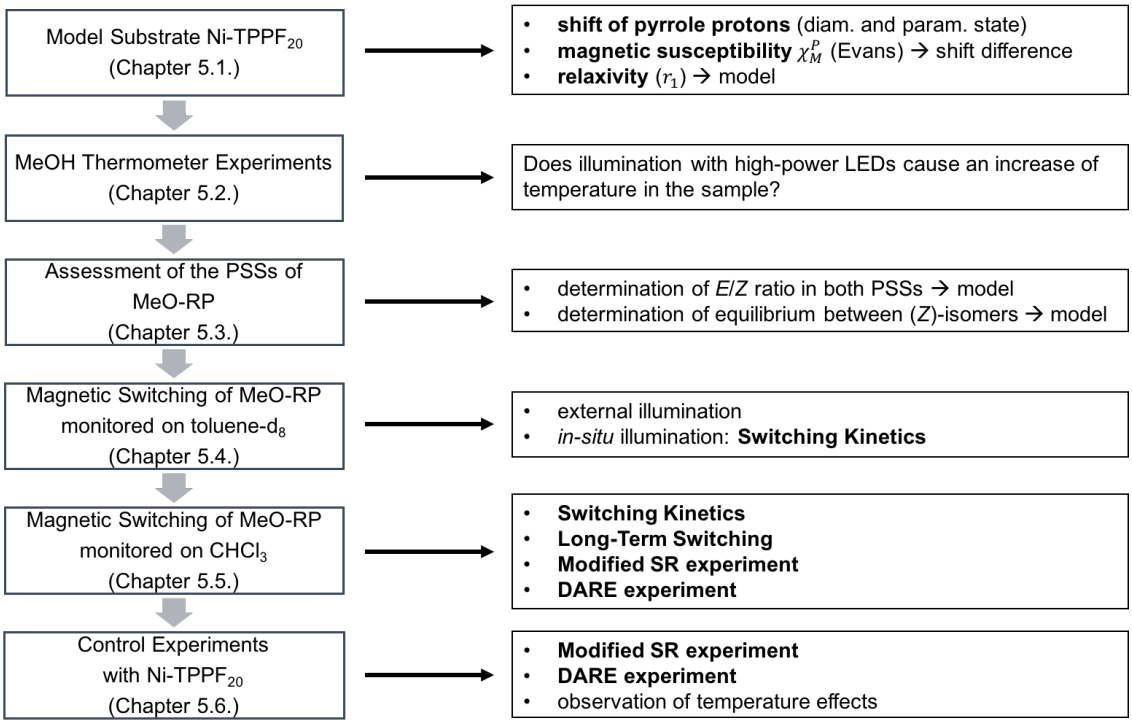

Figure 18. *On the left side of the flow chart the sequence of the subsections of Chapter 5. is depicted. Each subsection is connected to a box on the right side. In these boxes bullet points show the most important experiments or questions in the individual subsection.*

The whole sequence shown in Figure 18 starts with physical-chemical investigations of Ni-TPPF$_{20}$. Owing to the structural similarity between Ni-TPPF$_{20}$ and the methoxy-substituted record player (MeO-RP, see Section 2.4. for structures), Ni-TPPF$_{20}$ serves as model compound.

The data gathered by the experiments with Ni-TPPF$_{20}$ are necessary for theoretical calculations, which are inevitable to estimate the shift difference (see equation (28)) and the relaxation rates in presence of paramagnetic MeO-RP. Knowing the range, in which the experimental values can be expected, is necessary for the design of further experiments in terms of concentration of the agent. This estimation is only valid under the assumption that MeO-RP shows the same paramagnetic susceptibility and the same relaxivity as Ni-TPPF$_{20}$.

Moreover, from the isotropic shift of the *pyrrole* protons (i.e. the difference in chemical shift between protons on the porphyrin ligands in both magnetic states of Ni-TPPF$_{20}$) the ratio of the $Z_{\text{param.}}$ to the $Z_{\text{diam.}}$ isomer of MeO-RP can be assessed (see Chapter 5.3.).

The main question of subsection 5.2. is how the illumination with the high-power LEDs (see Section 4.3.) influences the temperature within an NMR sample. This is of enormous importance in the switching experiments conducted with MeO-RP, as the longitudinal relaxation rate is dependent on the temperature (see Chapter 2.2.4.).

In Section 5.3. the experimental characterization of both PSSs of MeO-RP is described, as the knowledge of the composition of the PSSs is a requirement for the further investigations of the magnetic switching of MeO-RP.

In principle, the first three subsections can be considered as the prerequisite for the subsequent magnetic switching experiments described in the Sections 5.4. and 5.5.

Section 5.4. highlights the magnetic switching experiments of MeO-RP in toluene-d_8. In these experiments, the longitudinal relaxation rate R_1 of the residual solvent protons of toluene-d_8 (measured by a SR experiment) is used to monitor the magnetic state of the spin switch. The switching experiments are carried out in the following modes of operation: external illumination or *in-situ* illumination with the high-power LEDs. With the first mode of operation, a *zigzag* experiment can be conducted, in which the sample is cycled between the green (paramagnetic state) and the blue PSS (diamagnetic state).

When the sample is illuminated within the probe head of the spectrometer (*in-situ* illumination), a *switching kinetics* experiment can be conducted. After a light pulse (up to 5 s) the longitudinal relaxation rate is measured, which allows the tracking the magnetic state of the sample. A PSS of MeO-RP is reached, when the relaxation rate remains constant after an additional pulse of light. The goal of this experiment is the determination of the time required to switch the sample from one magnetic state to another.

In Section 5.5. the magnetic state is monitored by another slowly relaxing compound – $CHCl_3$ with $T_1^0 = 179 \pm 4$ s (10% (v/v) in toluene-d_8). With this compound, another switching kinetics experiment was carried out.

To demonstrate how the longitudinal relaxation rate of a certain solvent signal (e.g. $CHCl_3$) can be manipulated, a *modified SR experiment* is well suited. During the

variable delay, the sample is illuminated with green light and the relaxation agent is switched from the diamagnetic state to the paramagnetic state. This leads to a faster relaxation during the delay, which appears as an improvement in the signal intensity of a certain peak in the NMR spectrum.

The aim of a *long-term switching experiment* is to show the reversibility of the switching process. This type of experiment indeed resembles the zigzag experiment mentioned above, however the number of switchings (i.e. the number of switching processes from one magnetic state to another) is by far larger and the process is carried out *in-situ*. Again, the agent is cycled between the diamagnetic and the paramagnetic state. As the use of SR experiments to determine the current magnetic state of the sample is time-consuming, the shift of the $CHCl_3$ peak (in reference to the methyl group of MeOH-d_4) can also be employed as indicator for the magnetic state. It is shown in Section 5.5. that the shift is only reliable for higher concentrations.

Based on the experimental results in the Sections 5.1. and 5.3., a model for the re-establishment of the z-magnetization in the SR recovery experiment was developed. This said model also includes the effects of paramagnetic substances on the longitudinal relaxation rate. The reason, why this model is presented in this chapter, is that it helped to determine a suitable concentration for the switching experiments described in Sections 5.5.3. and 5.5.4.

As the model should reflect the re-establishment of the z-magnetization of $CHCl_3$, the longitudinal relaxation rate of $CHCl_3$ is required (see above). The relaxivity of the PRE agent MeO-RP was assumed to be equal to the relaxivity of the model compound Ni-$TPPF_{20}$ ($r_1 = 0.087 \pm 0.002$ L mmol^{-1} s^{-1}).

If the PRE agent is switched “off” (completely diamagnetic), the relaxation rate of the $CHCl_3$ proton $R_1 = \frac{1}{T_1^0}$ = 0.006 s^{-1}. For a concentration of e.g. 0.5 mM PRE agent (MeO-RP), which is assumed to contain just the paramagnetic $Z_{param.}$ isomer, the rate R_1 = 0.049 s^{-1} is obtained by using Equation (29).

The z-magnetization curves (normalized to the equilibrium magnetization) can be calculated using Equation (14) for both rates and are displayed in Figure 19.

If R_1 changes within the recovery of the z-magnetization (e.g. in case of switching the PRE agent), Equation (14) has to be modified, as this equation is only valid for constant R_1 values. The solution is simple – instead of calculating the z-magnetization present at a certain delay time, it is calculated from the z-magnetization at a previous delay time and the difference between the delay times.

To do so, the z-magnetization for two different delay times τ_n and τ_{n+1} can be expressed as using Equation (14) (M_{eq} is set to 1):

$$M_z(\tau_n) = 1 - e^{-\tau_n R_1} \text{ and } M_z(\tau_{n+1}) = 1 - e^{-\tau_{n+1} R_1} \tag{39}$$

By defining $\tau_{n+1} = \tau_n + \Delta\tau$, the equation for τ_{n+1} can be written as:

$$M_z(\tau_{n+1}) = 1 - e^{-\tau_n R_1} e^{-\Delta\tau R_1} \tag{40}$$

With $e^{-\tau_n R_1} = 1 - M_z(\tau_n)$ Equation (40) becomes:

$$M_z(\tau_{n+1}) = 1 - \big(1 - M_z(\tau_n)\big) e^{-\Delta\tau R_1} \tag{41}$$

Having this equation in hand, the change in R_1 due to the altering concentration of the PRE agent can be regarded. To every interval $\Delta\tau$ an individual rate constant can be assigned. This equation also allows the calculation of the curve, when no change in R_1 is observed.

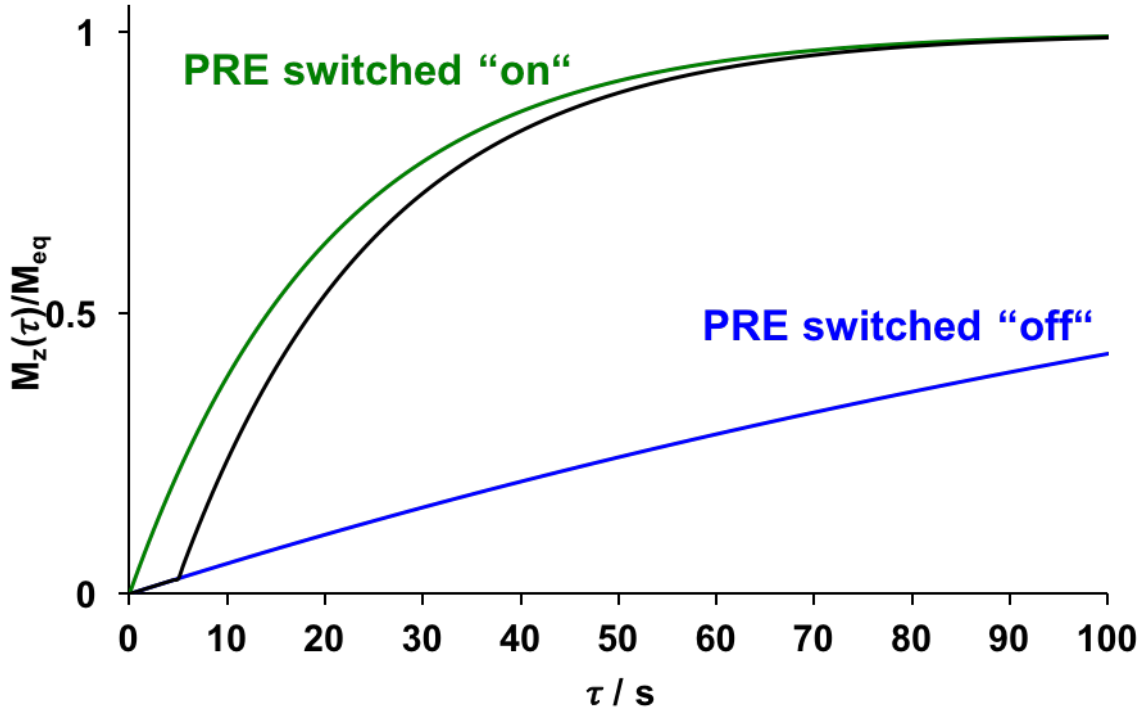

Figure 19. *Plot of the z-magnetization curves (normalized to the equilibrium magnetization) as a function of the delay time τ. The blue curve shows the case, when no PRE agent is present or the agent is completely switched “off” (diamagnetic, R_1 = 0.006 s^{-1}). When the PRE agent is switched “on” (completely paramagnetic), the z-magnetization follows the green curve (R_1 = 0.049 s^{-1}). The black curve shows a case, where the PRE agent is switched “on” after 5 s (i.e. after the acquisition) and is calculated using Equation (41).*

The black curve (obtained by using Equation (41)) in Figure 19 represents a case, in which the PRE agent is switched “off” during acquisition (in the first 5 s) and then switched “on”. It is assumed that the switching process from diamagnetic to paramagnetic is extremely fast (< 1 s). In the paramagnetic regime, the black curve approaches the green curve.

As the signal intensity in NMR spectroscopy is directly proportional to the recovered z-magnetization at the start of the successive scan, an improvement of signal intensity can be expressed as the difference between the blue and the black curve.

In further consequence, the model was more and more refined. The following considerations were integrated into the model at later stages: the percentage of the $Z_{param.}$ isomer at both PSSs (82% in the paramagnetic / green PSS and 21% in the diamagnetic / blue PSS) and the fact, that the switching process is not extremely

fast, as assumed for the first graph. In the end, the model was even adapted to reflect experimental rates instead of the calculated ones by changing some of the parameters.

Finally, the optimal concentration for the switching experiments was determined to be 1.5 mM MeO-RP due to the model (see Section 5.5.3. and 5.5.4.).

The idea to switch the relaxation agent “on” or “off” during the variable delay (relaxation delay) is named *DARE* (= *dynamically accelerated relaxation enhancement*). During the acquisition of the FID, the relaxation agent is in principle in the “off” state, although the paramagnetic isomer is also present in this state (21% $Z_{param.}$ isomer). Then, the agent is switched “on” by illuminating it with green light, which increases the concentration up to 82%. In this state, the longitudinal relaxation of the substrate (e.g. protons) is accelerated. Before the acquisition of the next scan, the agent is switched “off” by irradiating it with blue light. This procedure is presented in Figure 20.

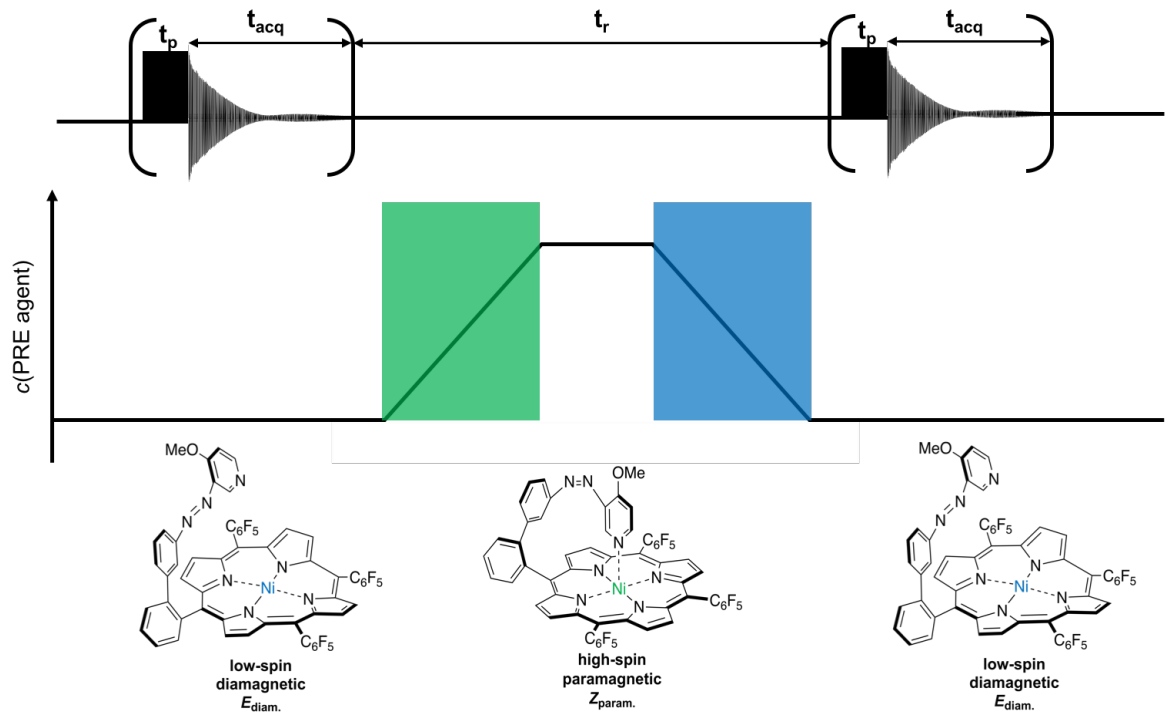

Figure 20. *Paramagnetic relaxation enhancement (PRE) used to increase the longitudinal relaxation during the relaxation delay t_r between two scans. In the first line two scans of an NMR experiment are displayed. The second line shows the concentration trace of the PRE agent MeO-RP. By illuminating the complex with green light (green rectangle), the concentration of paramagnetic MeO-RP is increased. Before the next scan is acquired, the agent is switched back to the diamagnetic state with blue light (blue rectangle). The structures of the main isomers present at the states are presented in the last line.*

Figure 20 also presents the DARE experiment found in Chapter 5.5.4. A faster relaxation during the relaxation delay can easily be quantified by comparing the signal intensity of e.g. a $CHCl_3$ peak acquired during the DARE experiment and the same experiment without the DARE. For the peaks recorded during the DARE experiment, an increase in integral can be expected.

Control experiments (see Section 5.6.) are conducted to distinguish the effects caused by the presence of paramagnetic agent (DARE) from those provoked by an increase in temperature (due to the illumination with high power LEDs).

4. Experimental Section

4.1. Materials

Toluene-d_8 (99.5 atom% D) was purchased from Euriso-top, acetone-d_6 (99.9 atom% D) from Sigma-Aldrich and pyridine-d_5 (> 99.95 atom% D) from Ciba-Geigy. Chloroform was bought from Carl Roth GmbH + Co. KG. Tetramethylsilane (TMS, purity 99.9%) was purchased from Alfa-Aesar. Methyl orange was obtained from Mallinckrodt Chemical Works. Methanol was purchased from Fluka. All chemicals listed here were used without further purification. Both nickel complexes, Ni-$TPPF_{20}$ and MeO-RP, were synthesized in the group of Prof. Herges at the University of Kiel, Germany.[11,12]

4.2. NMR and Spectral Processing

NMR measurements were conducted on a 200 MHz Bruker AVANCE or a 200 MHz Bruker AVANCE DPX spectrometer equipped with a probe head including a quartz rod (intended for CIDNP measurements) to guide the light of the LEDs, which are located under the bottom end of the quartz rod, to the sample. A detailed description of the NMR equipment can be found elsewhere.[41]

Optical couplant (F1-0001V, obtained from Fiber Instrument Sales, NY, USA) was applied in the space between the LEDs and the end of the quartz rod to avoid light losses by reflection. The probe head of the NMR spectrometer was modified with a 3D printed insert holding an elliptic piece of optical Teflon to reflect scattered light back onto the sample. The improvements to the setup described here were only applied for the for the switching experiments with MeO-RP in toluene-d_8 and $CHCl_3$ as well as the control experiments with Ni-$TPPF_{20}$.

For the determination of the longitudinal relaxation times, a saturation recovery (SR) experiment utilizing a Waltz16 pulse train for decoupling was used. Pulse sequences of the experiments are displayed and described in the appendix of this work.

Recorded NMR spectra were processed with the software MestreNova (MestreLab). In all spectra a baseline correction (Whittaker Smoother) and automatic phase correction were applied. Additionally, some spectra were manipulated by a manual phase correction. If necessary, line broadening up to 2 Hz (apodization with an exponential function) was also applied. Chemical shifts are reported in ppm relative to TMS using the residual deuterated solvent signals as internal reference. Prior to measurements pulse lengths and power levels were calibrated.

4.3. High-Power Illumination

High-power illumination was achieved by a module consisting of in total four light emitting diodes (LEDs): two blue LEDs (NCSC219B-V1; peak wavelength: 442 nm, FWHM: 21 nm; optical output power: 2380 mW at 1500 mA) and two green LEDs (NCSE119A; peak wavelength: 502 nm; FWHM: 30 nm; optical output power: 1100 mW at 700 mA). All four LEDs are arranged in a square (10 x 10 mm) with the two LEDs of each wavelength located on a diagonal of the square. The LEDs are operated by a control unit for each pair of LEDs, which are connected to separate outputs of the TCU unit of the NMR spectrometer. Thus, both control units can be triggered during an experiment with separate commands in the pulse sequence permitting the timing of the illumination during an experiment. The equipment was obtained from Sahlmann Photochemical Solutions in Bad Segeberg, Germany.

4.4. UV-Vis

UV-Vis spectra were recorded on a UV-Vis spectrometer equipped with fiber optics and a 1024 pixel diode array detector (J&M Analytik AG, Essingen, Germany).

4.5. Sample Preparation

NMR measurements were performed either in conventional NMR tubes in case of relaxivity measurements of Ni-$TPPF_{20}$ or in the double tube setup (DTS, see reference for details[41]) in case of Evans measurements of Ni-$TPPF_{20}$ and switching experiments with MeO-RP. The DTS consists of an EPR tube filled with a deuterated solvent such as acetone-d_6 and MeOH-d_4 (for susceptibility measurements and temperature monitoring), which is put into a conventional NMR tube. The resulting thin layer (thickness 0.05 mm) is filled with solutions of Ni-$TPPF_{20}$ or MeO-RP (usually about 150 µL).

***Table 3**. Diameters of the tubes used in the double tube setup.*

tube	inner diameter [mm]	outer diameter [mm]
EPR tube (inner tube)	2.80	3.90
NMR tube (outer tube)	4.00	4.95

Additionally, a commercially available double tube setup from Wilmad (517-Complete set) was used for the NMR thermometer experiments and the first switching experiment with MeO-RP. The thickness of the layer between both tubes is 0.45 mm.

***Table 4**. Diameters of the tubes obtained from Wilmad.*

tube	inner diameter [mm]	outer diameter [mm]
inner tube	2.34	3.30
outer tube	4.20	4.97

The solutions of Ni-$TPPF_{20}$ were prepared from a 7 mM stock solution in toluene-d_8. To each solution a small amount of TMS as reference substance and about 10% (v/v) pyridine-d_5 was added to render the complex paramagnetic.

For the preparation of samples stock solutions of MeO-RP were prepared and the concentration was checked with UV-Vis spectroscopy. To each solution 5% or 10% (v/v) chloroform was added.

Before performing NMR experiments all samples were degassed by bubbling argon or nitrogen through the solutions via a cannula for ca. 5 minutes. In case of the MeO-RP solutions in the DTS the inner tube as well as the outer tube were sealed with a UV curable epoxy resin.

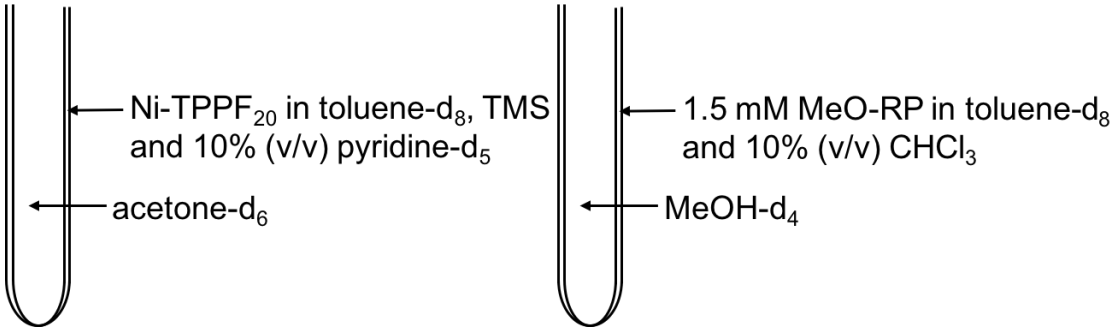

Figure 21. *Schematic representation of both setups used for the NMR experiments. On the left side the DTS (consisting of an NMR and EPR tube) for Evans measurements of Ni-TPPF$_{20}$ is displayed, on the right side the DTS employed in some switching experiments is shown. The thickness of the layer between both tubes is 0.05 mm or 50 µm.*

Figure 21 shows the general scheme for the DTS used in the experiments. Detailed information about the solvents, sample composition and geometry is given in the Section 5.

5. Results and Discussion

5.1. Ni-TPPF$_{20}$ as Model Compound

5.1.1. ^{1}H-NMR Spectra of Ni-TPPF$_{20}$ and Ni-TPPF$_{20}$ · 2 py

In the following two figures, the structures of diamagnetic Ni-TPPF$_{20}$ and paramagnetic Ni-TPPF$_{20}$ · 2 py (py = pyridine-d$_5$) and details of their ^{1}H-NMR spectra are displayed (for theoretical background see Section 2.4.1.).

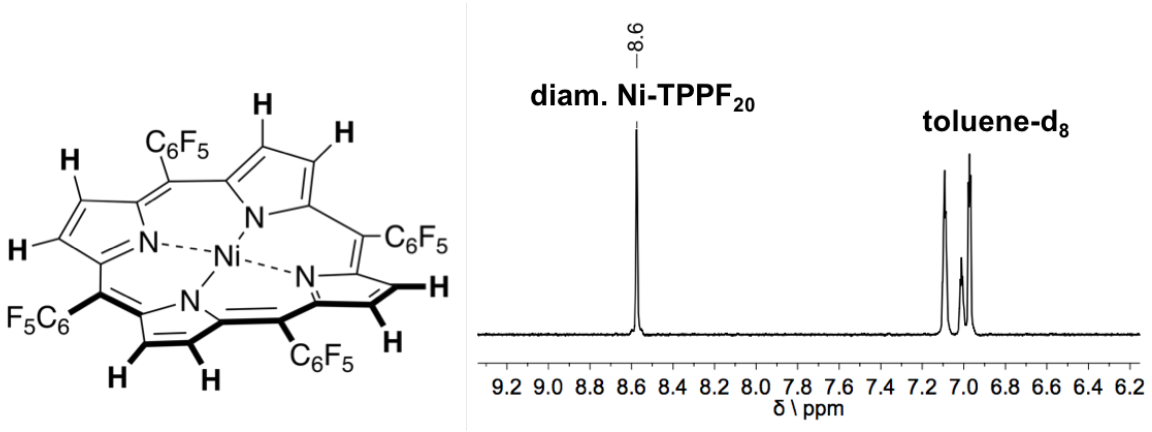

Figure 22. *Left: Structure of diamagnetic Ni-TPPF$_{20}$. Right: Detail of the ^{1}H-NMR spectrum (200 MHz, ns = 16) of diamagnetic Ni-TPPF$_{20}$ (7 mM in toluene-d$_8$ and TMS). The "pyrrole" protons of the ligand (marked in bold) give a singlet at 8.6 ppm.*

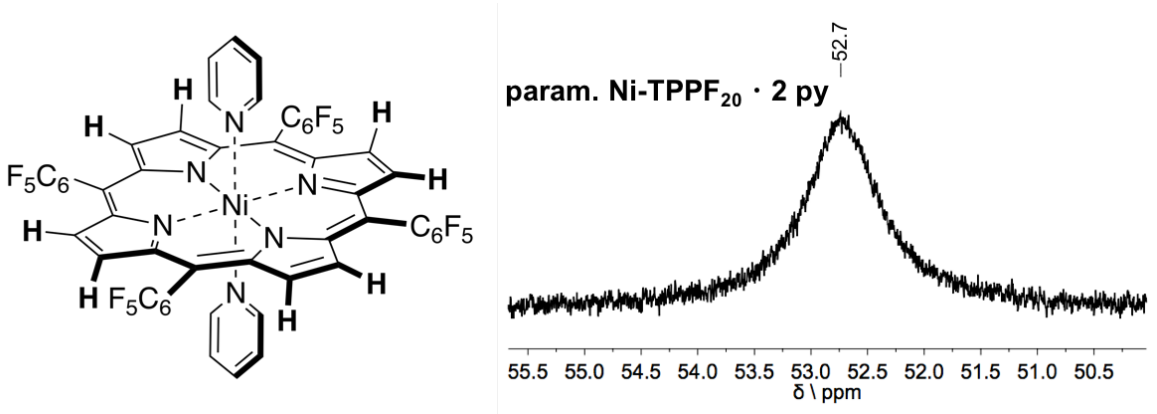

Figure 23. *Right: Structure of paramagnetic Ni-TPPF$_{20}$ · 2 py (py = pyridine-d$_5$, the deuterium atoms are not shown for reasons of clarity). Left: Detail of the ^{1}H-NMR spectrum (200 MHz, ns = 64) of paramagnetic Ni-TPPF$_{20}$ · 2 py (7 mM in toluene-d$_8$ with 5% (v/v) pyridine-d$_5$ and TMS).*

Compared to the pyrrole protons of the diamagnetic Ni-TPPF$_{20}$, the protons of the paramagnetic counterpart are found at much lower field – at 52.7 ppm (compared to 8.6 ppm in the diamagnetic state). The difference between these shifts is known as the isotropic shift (see Section 2.3.1.) and has a value of 44.1 ppm. Moreover, the observed singlet of the protons in the paramagnetic complex is very broad (W = 155 Hz), whereas the pyrrole singlet in the diamagnetic complex has a linewidth of 1.7 Hz. These findings match the expectations from a theoretical point of view.

5.1.2. Paramagnetic Susceptibility of Ni-TPPF$_{20}$ · 2 py

The magnetic susceptibility of Ni-TPPF$_{20}$ · 2 py ("paramagnetic Ni-TPPF$_{20}$") was measured according to the Evans method (see Chapter 2.3.2.).[27] Solutions with various concentrations (1.0 mM, 2.0 mM, 3.0 mM, 4.0 mM, 6.8 mM) of Ni-TPPF$_{20}$ were prepared in toluene-d$_8$ with a small amount of TMS as reference substance and about 10% (v/v) pyridine-d$_5$. Another sample was prepared containing just a small amount of TMS and about 10% (v/v) pyridine-d$_5$ in toluene-d$_8$ and served as reference.

Acetone-d$_6$ was used as reference solvent in the inner tube, whereas the outer tubes were filled with the different solutions which are described above. The signal of the methyl group of acetone-d$_6$ was used to reference the NMR spectra.

In the following table the measured shifts are shown. Each sample was measured in triplicate and the shift difference was calculated in reference to the average TMS shift of the "solvent".

***Table 5**. Calculated shift differences ($\delta\nu^P$(TMS) = ν(TMS in solution of Ni-TPPF$_{20}$) - $\bar{\nu}$(TMS in "solvent")) for each sample.*

sample	ν(TMS) [Hz]	$\delta\nu^P$(TMS) [Hz]
10% (v/v) pyridine-d_5 in toluene-d_8 and TMS ("solvent")	-196.05 ± 0.01	0
1 mM Ni-TPPF$_{20}$ in "solvent"	-190.76 ± 0.12	5.3
2 mM Ni-TPPF$_{20}$ in "solvent"	-186.65 ± 0.01	9.4
3 mM Ni-TPPF$_{20}$ in "solvent"	-184.18 ± 0.01	11.9
4 mM Ni-TPPF$_{20}$ in "solvent"	-180.79 ± 0.04	15.3
6.8 mM Ni-TPPF$_{20}$ in "solvent"	-170.08 ± 0.01	26.0

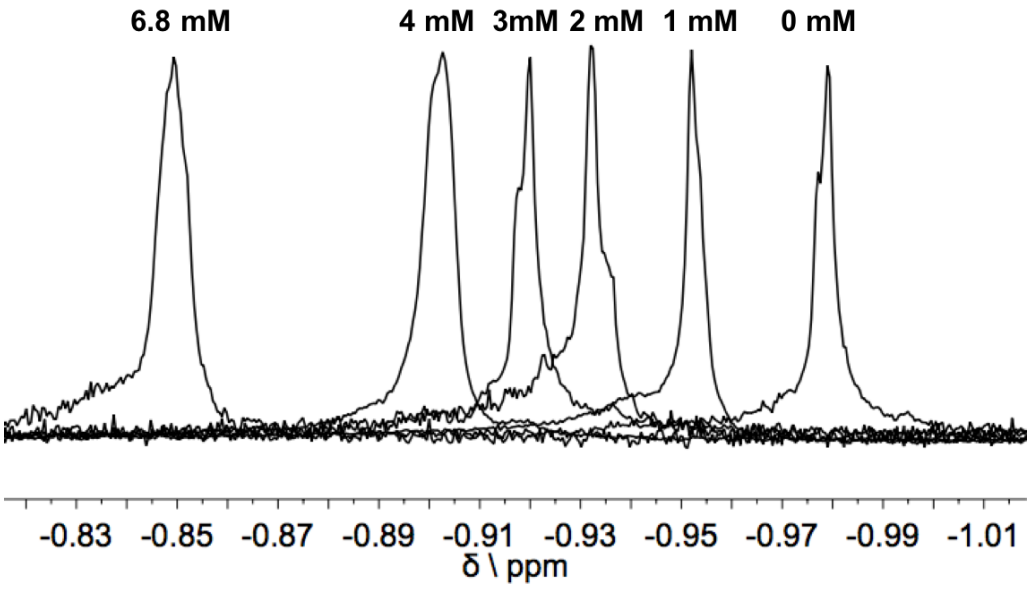

***Figure 24.** Combined ^{1}H-NMR spectra (200 MHz, ns = 32) of the TMS peak in the different solutions (see Table 5) with acetone-d_6 in the inner tube used as reference. With increasing concentration of the paramagnetic nickel complex (from 0 mM to 6.8 mM) a downfield shift of the peak can be observed, which is directly proportional to the concentration of the paramagnetic species.*

A few assumptions were made to simplify Equation (28) found in Chapter 2.3.2. First the density of the solution was assumed to be equal to the "pure" solvent, as a result the third term of Equation (28) becomes zero. Second, the diamagnetic susceptibility is also neglected[27,28] giving the following equation:

$$\chi_M^P = \frac{3\delta\nu^P M^P}{4\pi\nu_0 m^P} + \chi_0 M^P \qquad (42)$$

Table 6. *Parameters used in Equation (42) to calculate the magnetic susceptibility χ_M^P of paramagnetic Ni-TPPF$_{20}$.*

parameter	value
observed shift in frequency $\delta\nu^P$	see Table 5
molar mass of param. Ni-TPPF$_{20}$ M^P	1199.50 g mol^{-1}
frequency of the spectrometer ν_0	2·10^8 Hz
mass concentration of param. Ni-TPPF$_{20}$ m^P	-
mass susceptibility of the solvent χ_0	- 6.60·10^{-7} cm^3 g^{-1} for toluene-d$_8$ [i]

[i] The mass susceptibility of the solvent was calculated from the volume susceptibility, which was obtained from https://www.wilmad-labglass.com/Support/NMR-and-EPR-Technical-Reports/Sample-Devices-and-Magnetic-Susceptibility/; retrieved Jan 3, 2017.

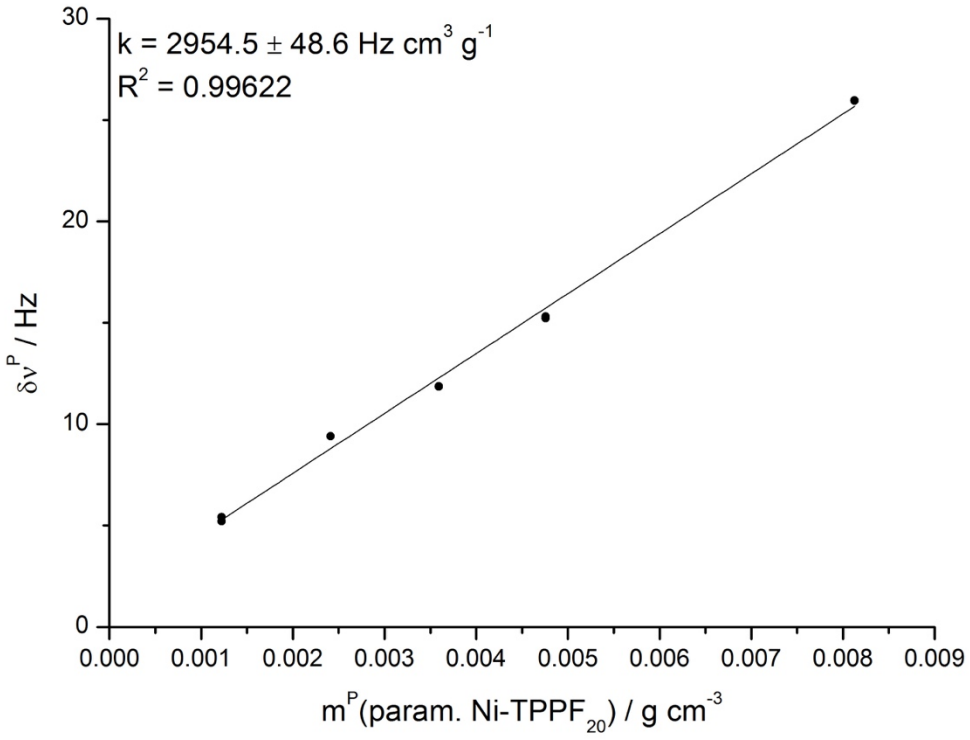

Figure 25. *Linear dependence of the shift difference of the TMS peak in Hz on the mass concentration of Ni-TPPF$_{20}$ · 2 py in g/cm^3. Each concentration level was measured in triplicate.*

The shift difference $\delta\nu^P$ is plotted against the mass concentration of the paramagnetic nickel complex m^P (see Figure 25). Linear regression gives the slope k = 2954.5 ± 48.6 Hz cm^3 g^{-1} leading to χ_M^P = (3.44 ± 0.07)·10^{-3} cm^3 mol^{-1}, which is in good agreement with the paramagnetic molar susceptibility found for the same compound in pure pyridine (χ_M^P = 3.66·10^{-3} cm^3 mol^{-1}).[12]

Equation 3[12] describes the dependence of the magnetic moment resulting from the unpaired electrons (S = 1) in the d-orbitals of the Ni^{2+} ion.

$$\mu = 2.828\sqrt{T\chi_M^P} \tag{43}$$

Inserting T = 298 K (25 °C) and χ_M^P = (3.44 ± 0.07)·10^{-3} cm^3 mol^{-1} into Equation (43) gives μ = 2.86 ± 0.03 BM (Bohr magnetons). In pure pyridine the paramagnetic complex shows a magnetic moment of 2.9 BM.[12] This agrees with the literature, where values between 2.9 and 3.3 BM can be found for Ni^{2+} ions in octahedral complexes.[42]

5.1.3. Longitudinal Relaxivity of Ni-TPPF$_{20}$ · 2 py

Longitudinal relaxation times (T_1) of the same solutions prepared for the Evans experiments were measured in triplicate by using the SR experiment (200 MHz; ns = 2; time delays: 0, 1, 2, 3.5, 5, 7.5, 10, 15, 20, 30 s). By plotting the measured longitudinal relaxation rates ($R_1 = \frac{1}{T_1}$) against the concentration of the paramagnetic Ni-TPPF$_{20}$ complex, the relaxivity (r_1) is obtained as slope (see Equation (29)).

Table 7. *Longitudinal relaxation times T_1 for different concentrations of paramagnetic Ni-TPPF$_{20}$ in "solvent" (10% (v/v) pyridine-d$_5$ in toluene-d$_8$ and TMS).*

sample	T_1 [s]	$R_1 = 1/T_1$ [s^{-1}]
1 mM Ni-TPPF$_{20}$ in "solvent"	8.78 ± 0.32	0.114 ± 0.004
2 mM Ni-TPPF$_{20}$ in "solvent"	5.46 ± 0.02	0.183 ± 0.001
3 mM Ni-TPPF$_{20}$ in "solvent"	3.82 ± 0.02	0.261 ± 0.002
4 mM Ni-TPPF$_{20}$ in "solvent"	2.87 ± 0.04	0.348 ± 0.004
6.8 mM Ni-TPPF$_{20}$ in "solvent"	1.65 ± 0.02	0.608 ± 0.006

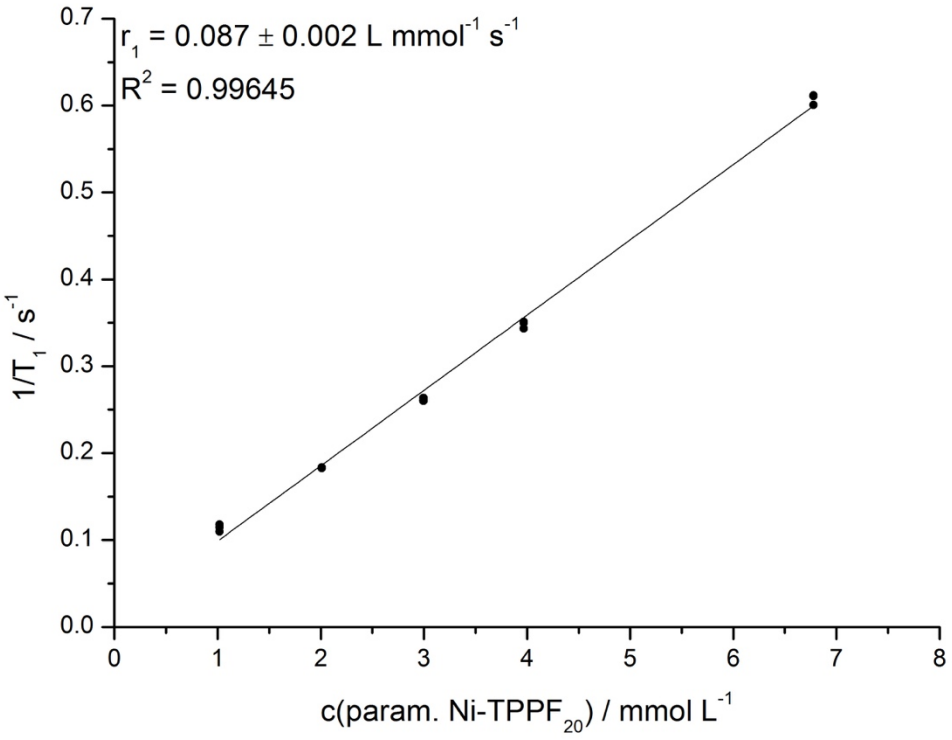

Figure 26. *Linear plot of the longitudinal relaxation rates ($1/T_1$) in s^{-1} against the concentration of the nickel complex in mmol L^{-1}. Each concentration level was measured in triplicate.*

The longitudinal relaxivity (r_1) which is equivalent to the slope of the linear regression is r_1 = 0.087 ± 0.002 L mmol^{-1} s^{-1}.

5.2. NMR Thermometer Experiments

A methanol thermometer was used in order to examine heating effects due to the illumination of the sample with high-power LEDs. The temperature within the NMR tube is monitored simply by recording ^{1}H-NMR spectra of MeOH, to which a light-absorbing compound such as methyl orange is added. The temperature in K within the sample is a function of the shift difference $\Delta\delta$ between the methyl and the hydroxyl group of MeOH in ppm[43]:

$$T = 409.0 - 36.54\,\Delta\delta - 21.85(\Delta\delta)^2 \qquad (44)$$

For the thermometer experiments a double tube setup consisting of commercially available NMR tubes obtained from Wilmad were used (see Section 4.5.). The outer tube was filled with a solution of 4.3 g/L methyl orange in MeOH, whereas toluene-d_8 was used as reference and lock solvent in the inner tube. To ensure complete absorption, an UV-Vis spectrum of the sample in the NMR tube was recorded. For both wavelengths (blue and green light, see Section 4.3.) absorption was ~3, i.e. absorption of 99.9% of the incident light.

^{1}H-NMR spectra (200 MHz; ns = 1) were recorded every two minutes, while the LED was switched on for 24 min (green LED) or 22 min (blue LED). After illumination the cooling process was also monitored.

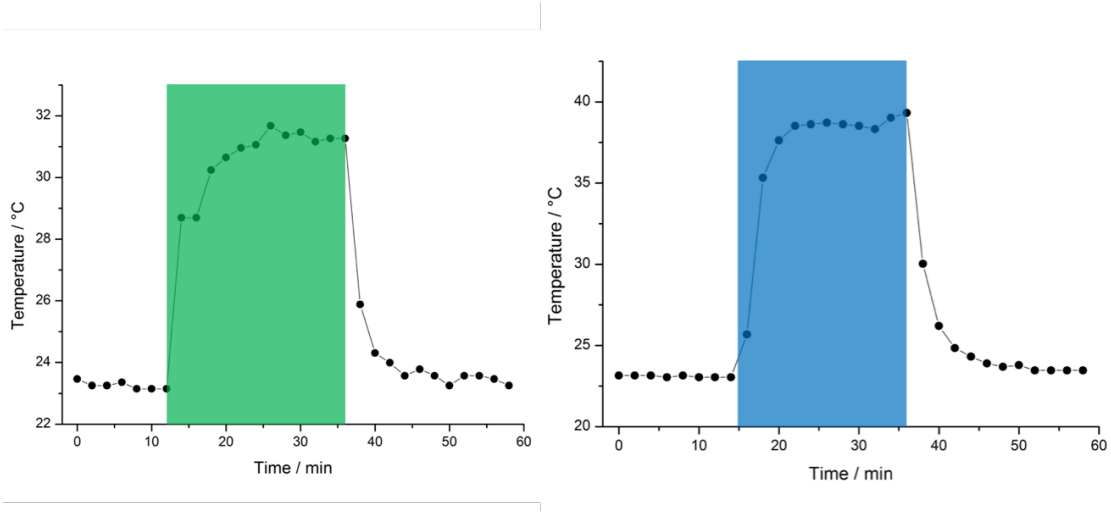

Figure 27. *Left: Development of temperature within the sample upon irradiation with green light emitted from LEDs. After 12 min the LEDs were switched on for 24 min (indicated by the green rectangular box). Right: Development of temperature within the sample upon irradiation with blue light emitted from LEDs. After 14 min the LEDs were switched on for 22 min (indicated by the blue rectangular box).*

Both experiments show that the temperature increases after the LEDs were switched on. Illumination with the blue LED (power 100 %) causes to the sample to heat up from 23 °C to 39 °C (ΔT = 16 °C), whereas illumination with the green LED (power 70%) increases the temperature from 23 °C to 31 °C (ΔT = 8 °C). Therefore, in further experiments involving the illumination of the sample a temperature gradient has to be considered in the interpretation of the results.

5.3. Spectroscopic Characterization of MeO-RP

To make the subsequent chapters more readable, the photostationary states (PSSs) are named in the following way: the PSS, which is reached by illumination with the blue high-power LED is called *blue PSS*, the *green PSS* is obtained, when the sample is irradiated with the green high-power LED.

For the determination of the *E*/*Z* ratios ^{1}H-NMR spectra of the complex in both PSSs have to be recorded. The ratio can then be determined by integration of suitable proton signals (see Figure 28). Even though the protons in the paramagnetic complex exhibit smaller relaxation times, the validity of this method was checked by using solvent signals as reference.[11]

To reach the PSSs a solution of MeO-RP in toluene-d_8 was irradiated with light of the corresponding wavelength from a short distance over night prior to the measurement.

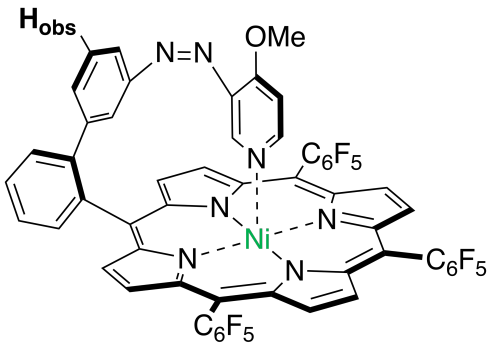

(*Z*)-MeO-RP
$Z_{param.}$

Figure 28. *Position of the observed proton for the determination of the E/Z ratio in the (Z)-isomer. The proton gives a signal for each isomer – $Z_{param.}$ and $E_{diam.}$.*[11]

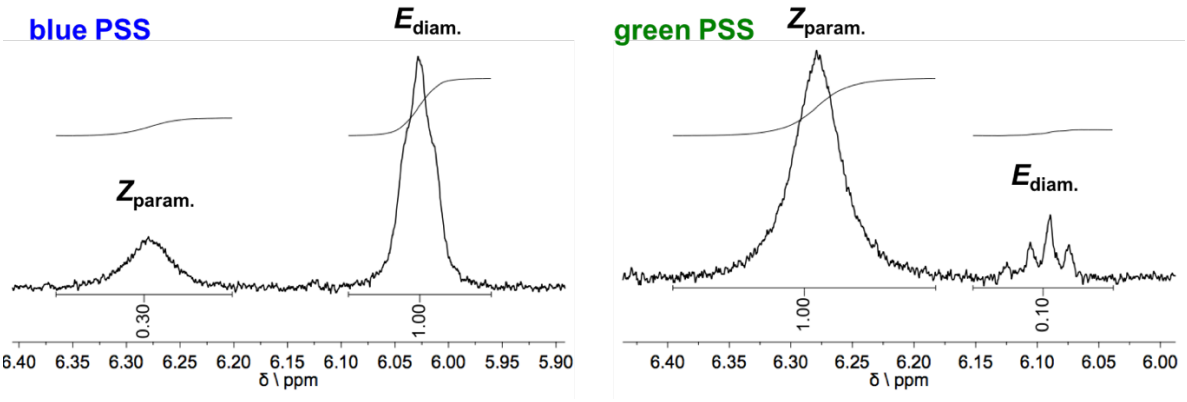

Figure 29. *Details of the ^{1}H-NMR spectra (500 MHz; ns = 128) of MeO-RP in toluene-d_8 in the blue PSS (left) and the green PSS (right). The broad signals at 6.28 ppm featured in both spectra can be assigned to the $Z_{param.}$ isomer, whereas the peak of $E_{diam.}$ is found at 6.03 in the left spectrum or at 6.09 ppm in the right spectrum.*[ii]

The integrals in both PSSs translate to the *E/Z* ratios shown in Table 8.

Table 8. *E/Z ratios and the percentage of (Z)-isomer in both PSSs.*

PSS	blue PSS	green PSS
***E/Z* ratio**	10:3	1:10
percentage of $Z_{param.}$	23%	91%
mole fraction χ_Z	0.23	0.91

Not all (*Z*)-isomers are paramagnetic, actually there is an equilibrium between a coordinated (paramagnetic) and a non-coordinated conformer (diamagnetic) of the (*Z*)-isomer (see Figure 17) in Chapter 2.4.2.[11]

The mole fraction χ_{para} of the coordinated paramagnetic form can be calculated using the shifts of the pyrrole protons of Ni-TPPF$_{20}$ (see Section 5.1.) and of MeO-RP in ppm[10]:

$$\chi_{para} = \frac{\delta - \delta_{dia}}{\delta_{para} - \delta_{dia}} \tag{45}$$

The shift of the pyrrole protons in diamagnetic Ni-TPPF$_{20}$ (δ_{dia}) is 8.6 ppm and in paramagnetic state the pyrrole protons (δ_{para}) can be found at 52.7 ppm. For

[ii] The ^{1}H-NMR spectra were recorded by Eduard Stadler.

MeO-RP the pyrrole protons can be observed at an average shift of 48.4 ppm. χ_{para} gives 0.9, which means that 90% of all (*Z*)-isomers are indeed paramagnetic.

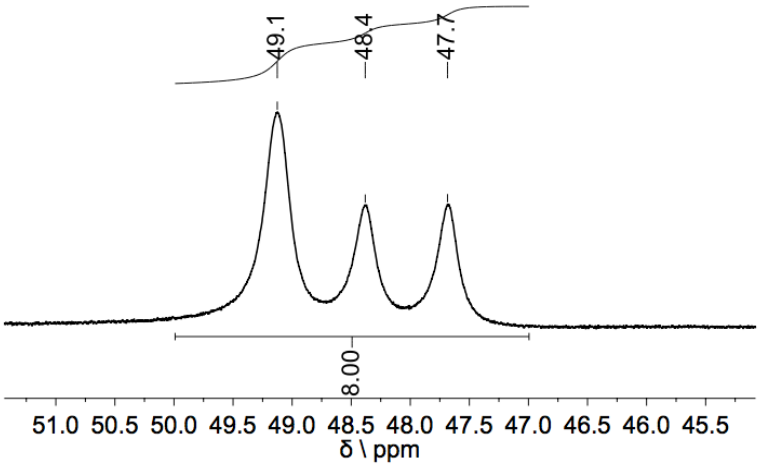

Figure 30. *High shift region of the ^{1}H-NMR spectrum (500 MHz; ns = 160) of MeO-RP in toluene-d_8 in the green PSS.*[iii]

The focus of this work lies on NMR spectroscopic investigations of MeO-RP, however UV-Vis spectroscopy also provides insight in the physical properties of this compound and is necessary for a comprehensive analysis and discussion of the results.

[iii] The ^{1}H-NMR spectrum was recorded by Eduard Stadler.

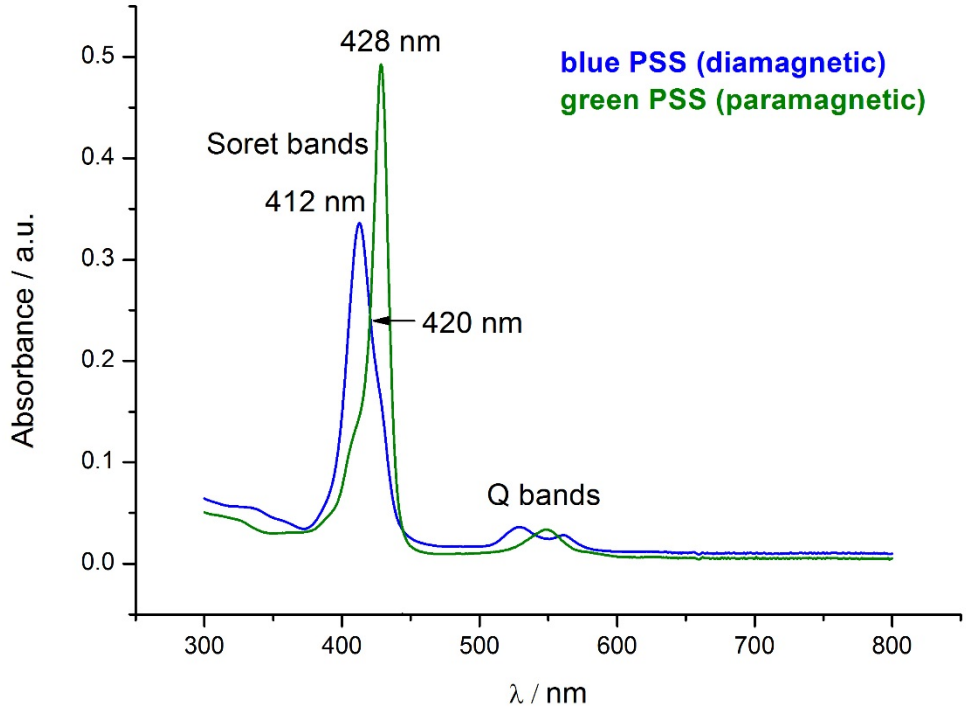

Figure 31. *UV-Vis spectra of MeO-RP ($1.7 \cdot 10^{-6}$ M in toluene) in both PSSs (blue and green).*[iv]

The Soret band is responsible for the red to violet color of the Ni-porphyrin complex MeO-RP. When MeO-RP is in the blue PSS, the maximum of the Soret band is found at 412 nm and two small bands are observed in the range of 500 to 600 nm – the Q bands. If MeO-RP is switched to the green PSS the maximum is shifted to 428 nm (bathochromic shift) and the Q bands are replaced by a new band with its maximum at ca. 550 nm. At 420 nm the isosbestic point is found.[9]

[iv] The UV-Vis spectra were recorded by Eduard Stadler.

5.4. Switching Experiments with MeO-RP in Toluene-d_8

In preliminary experiments, the longitudinal relaxation times of the residual solvent protons of toluene-d_8 were measured by a SR experiment. To calculate the R_1 values of these protons in presence of MeO-RP in both PSSs, Equation (29) can be employed considering that only the $Z_{param.}$ isomer of MeO-RP is acting as relaxation agent. Its concentration is the product of the concentration of all MeO-RP isomers (c), the mole fraction of (*Z*)-isomer (χ_Z) in the PSS (0.23 in the blue PSS or 0.91 in the green PSS) and the mole of fraction of coordinated (*Z*)-isomer (χ_{para} = 0.9). This leads to Equation (46):

$$R_1 = \frac{1}{T_1} = \frac{1}{T_1^0} + c \cdot \chi_Z \cdot \chi_{para} \cdot r_1 \qquad (46)$$

Table 9. *Measured longitudinal relaxation times of different solvent residual protons of toluene-d_8 and calculated longitudinal relaxation rates in both PSSs for a concentration of 0.5 mM MeO-RP in toluene-d_8 using Equation (46).*

signal	T_1^0 [s] [v]	$1/T_1$ in blue PSS [s^{-1}]	$1/T_1$ in green PSS [s^{-1}]
H_{Ar} at 7.1 ppm	149 ± 3	0.016	0.042
H_{Ar} at 7.02 ppm	157 ± 5	0.015	0.042
H_{Ar} at 6.98 ppm	140 ± 5	0.016	0.043
-CH_3 at 2.09 ppm	44 ± 4	0.032	0.058

As a matter of fact, the difference between the rates in the PSSs is a function of the concentration of $Z_{param.}$ in both PSSs and the relaxivity of the complex and is therefore constant (= 0.027 s^{-1}).

[v] Longitudinal relaxation rates of the residual solvent protons of toluene-d_8 were measured by Eduard Stadler.

For the first switching experiment (*zigzag experiment*, see Chapter 3.) a sample in the commercially available DTS (Wilmad) was prepared. The inner tube was filled with D_2O and outer tube with 0.5 mM MeO-RP in toluene-d_8. To the solution in the outer tube TMS was added as reference substance. After degassing as described in Chapter 4.5. the sample was then illuminated externally for 5 min with the LED setup (blue or green light). To avoid potential temperature effects the sample was cooled down to room temperature in a water bath for 3 min. Afterwards R_1 was determined by a standard SR experiment (200 MHz, ns = 2, delays: 0, 2, 4, 8, 16, 32, 64, 128 s; duration: 12 min). This procedure was repeated five times.

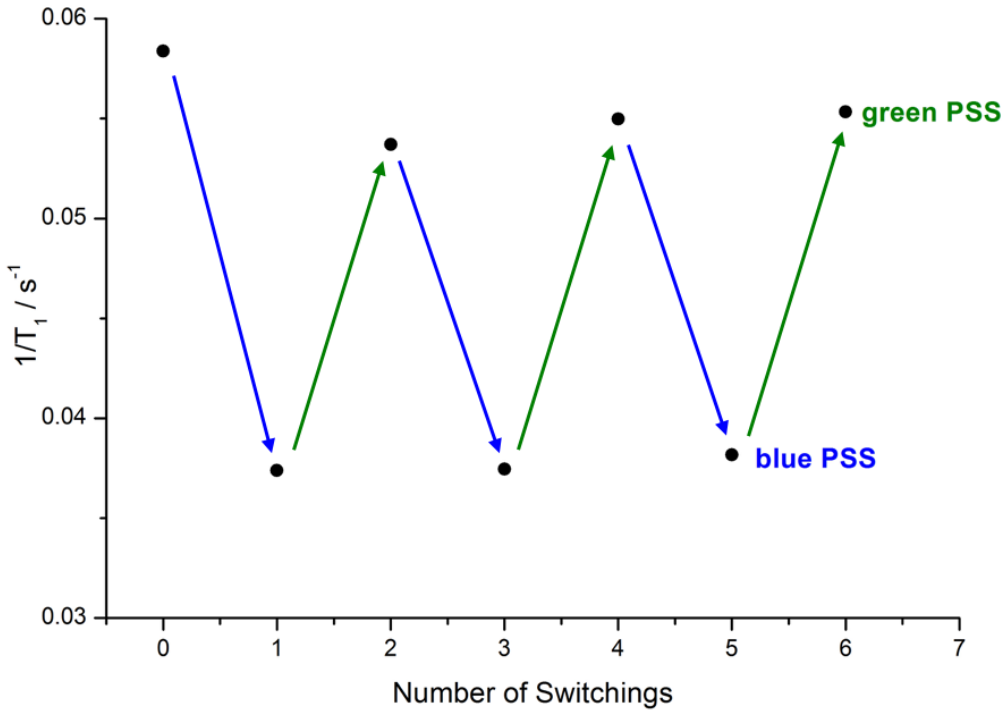

Figure 32. *The $1/T_1$ values of the methyl group of toluene-d_8 (determined by a SR experiment) are plotted as function of the number of switchings. The bigger relaxation rates belong to the green PSS ("paramagnetic state", fast relaxation) and the smaller relaxation rates to the blue PSS ("diamagnetic state", slower relaxation). Colored arrows indicate the switching processes from one PSS to the other with blue or green light. Similar graphs can also be found for the residual aromatic protons (see Figures A1 to A3 in the appendix).*

The average values for R_1 are 0.038 ± 0.001 s^{-1} (blue PSS) and 0.056 ± 0.002 s^{-1} (green PSS), which are in good agreement to the rates calculated for the methyl group above (see Table 9). The small differences might be a result of remaining oxygen, which shifts both rates to higher values, or incomplete switching, which means that the corresponding PSS is not fully reached.

In the previous experiment the sample was irradiated for 5 min before cooling and performing the SR experiment. The illumination times chosen for this experiment are without doubt long enough to switch MeO-RP from one PSS to another, however this experiment does not provide any information about how fast the switching processes (in both directions) are.

The kinetics of these switching processes are monitored in another experiment, which is called *switching kinetics experiment* for convenience. The idea behind this type of experiment is the illumination for a fixed time interval (5 s in this case) and the measurement of the longitudinal relaxation rate of a residual solvent proton such as a methyl proton of toluene-d_8. A schematic representation of this type of experiment is shown in Figure 33 and the pulse program is described in 8.2.1.

Thus, a sample with the same composition was prepared (0.5 mM MeO-RP in toluene-d_8), however the commercial DTS was replaced by the DTS consisting of an EPR and an NMR tube. Again, the inner tube was filled with D_2O.

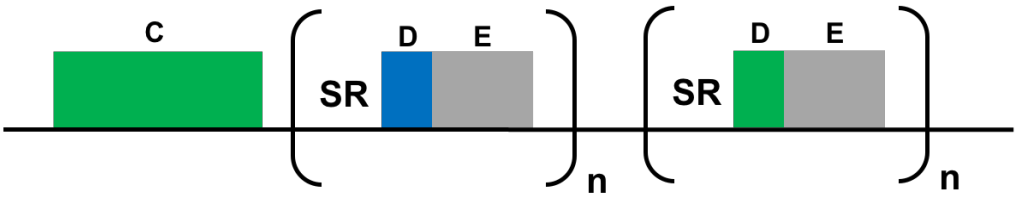

Figure 33. *Schematic representation of the switching experiment leading to the results presented in Figure 34. A long illumination with green light (C = a few minutes) switches MeO-RP to the green PSS. The block with the blue box indicates the switching process from the green PSS to the blue PSS with blue light, whereas the second block depicts the back-switching process. In both cases the illumination interval D is equal to 5 s. After illumination, the sample is allowed to cool down in the cooling delay (grey rectangles, duration E = 10 s). Both blocks were executed twelve times (n = 12).*

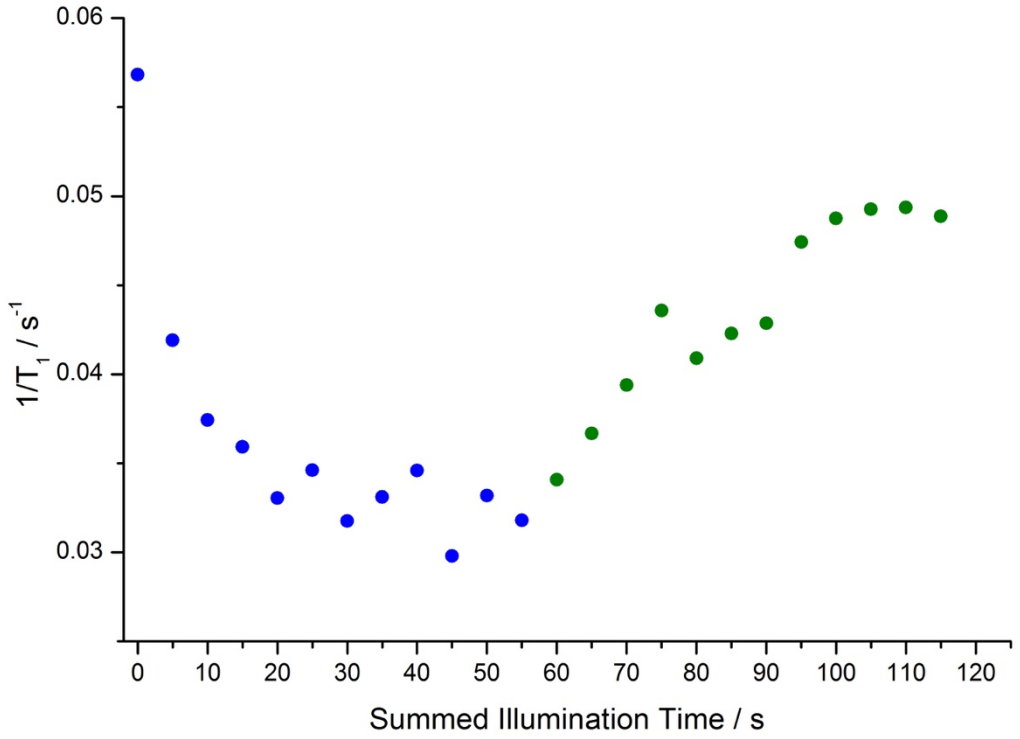

Figure 34. *Plot of the $1/T_1$ values of the methyl group of toluene-d_8 versus the summed illumination time. Each point represents 5 s illumination with the corresponding high-power LED (blue points = blue LED, green points = green LED) and a SR experiment to measure T_1 (200 MHz; ns = 4; delays: 0, 2, 4, 8, 16, 32, 64, 128 s; duration 24 min).*

An interesting feature of Figure 34 is that the initial value in the graph (0.057 s^{-1}) is not reached in the back-switching process (green points), which stops at values around 0.05 s^{-1}.

Due to the drastic reduction of the sample volume located in the coil region the number of scans had to be increased to four to obtain interpretable spectra. Together with the diminished volume the root of this problem is the low concentration of isotopomers of toluene-d_8 carrying one proton and therefore the low S/N ratio. 24 minutes, which it takes to complete a single SR experiment under these conditions and parameters, is way too long to be used meaningfully e.g. in long-term switching experiments to check the stability of the spin switch.

5.5. Switching Experiments with MeO-RP in Toluene-d_8 and $CHCl_3$

To circumvent the problem of long measurement time caused by the low concentration of isotopomers of toluene-d_8 carrying one proton, another slowly relaxing compound such as $CHCl_3$ (T_1 = 179 ± 4 s, 10% (v/v) in toluene-d_8) can be added to the solutions. Besides higher achievable proton concentration another advantage of the use of chloroform is its simple NMR spectrum giving an isolated singlet, which is beneficial for signal intensity and integration. On the contrary, the residual aromatic protons of toluene-d_8 overlap with each other making the determination of the longitudinal relaxation times very tedious and error-prone.

For the further switching experiments, another probe head, which features just one coil, was used. On the contrary, the probe head utilized in the previous experiments comprises two coils holding off more light from the sample.

To further improve the switching process for the subsequent experiments the NMR probe head was equipped with highly reflective optical Teflon and optical couplant was applied between the bottom end of the quartz rod and the high-power LEDs as described in Chapter 4.2.

5.5.1. 0.5 mM MeO-RP

As a starting point, the same concentration, which was previously used in the switching experiments, was chosen. To this 0.5 mM solution of MeO-RP in toluene-d_8, 5% (v/v) $CHCl_3$ was added.

At first, a switching kinetics experiment was conducted to determine the length of the illumination block required to switch the sample from one magnetic state to the other. A schematic representation of the experiment (Figure 35) illustrates the experiment.

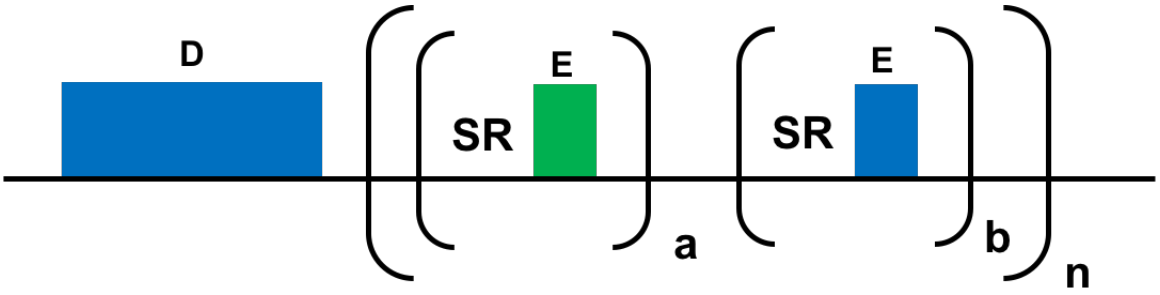

Figure 35. *Schematic representation of the switching experiment leading to the results presented in Figure 36. The sequence starts with irradiation with blue light (length D = a few minutes), then two switching blocks (in small brackets) are conducted (a = number of data points in the switching process from the blue to the green PSS; b = number of data points in the back-switching process). These two blocks are executed n times. In both cases the illumination interval E is equal to 1 s.*

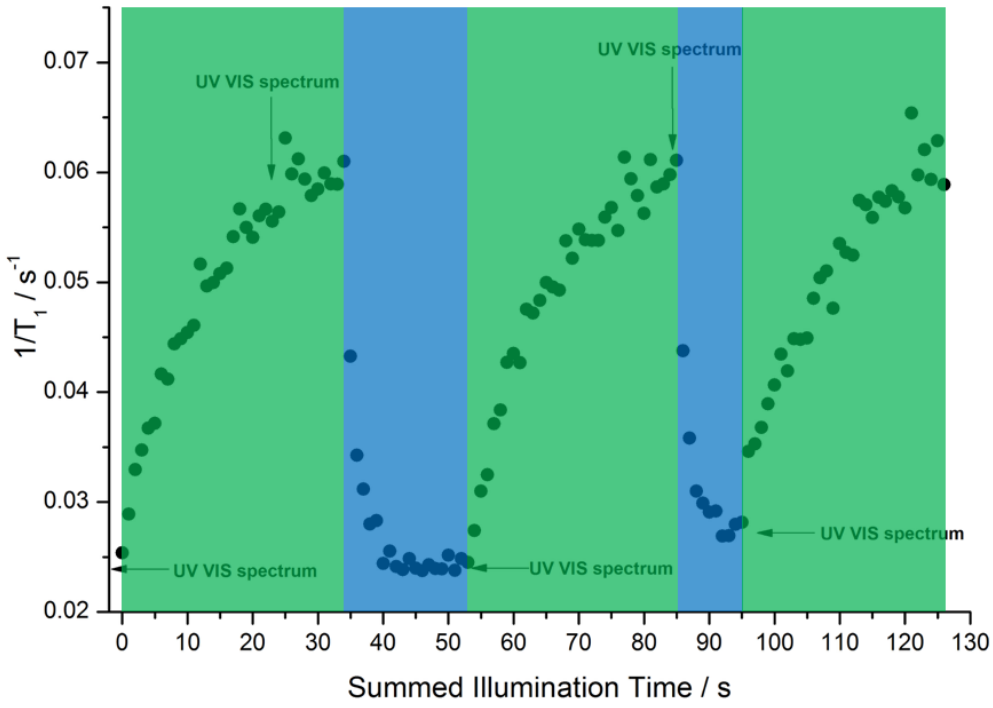

Figure 36. *Two and a half cycles of the switching experiment with 0.5 mM MeO-RP in toluene-d_8 and 10% (v/v) $CHCl_3$. The longitudinal relaxation rate of $CHCl_3$ (measured by a SR experiment: 200 MHz; ns = 1; delays: 0, 2, 4, 8, 16, 32, 64, 128, 200 s; duration: 9 min) is monitored as a measure for the magnetic state of MeO-RP. Green boxes indicate illumination with the green LED and blue boxes with the blue LED. To check for fatigue products or degradation, the UV-Vis spectra of the sample within the NMR tube were recorded (see Figure 38), as indicated in the graph. Data points found in the first blue and second green box are also displayed in Figure 37 in more detail.*

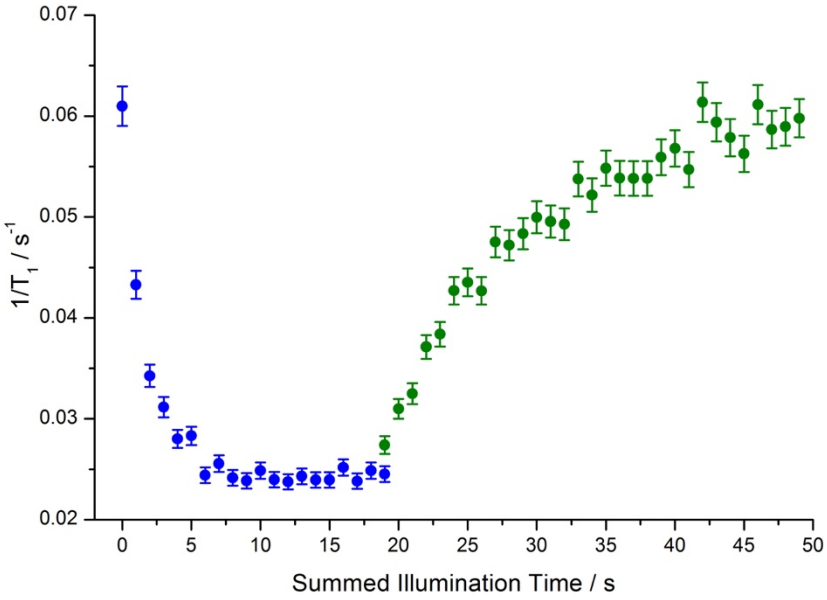

Figure 37. *Plot of the $1/T_1$ values of $CHCl_3$ versus the summed illumination time for the 0.5 mM MeO-RP sample. The blue points belong to the switching process from the green PSS (fast relaxation rates of $CHCl_3$) to the blue PSS (slow relaxation rates of $CHCl_3$). Back-switching from the blue PSS to the green PSS is displayed in the right part of the graph (green points). The error bars indicated in each graph were obtained by measuring the relative standard deviation of the SR experiment (n = 5) after reaching the corresponding PSS.*

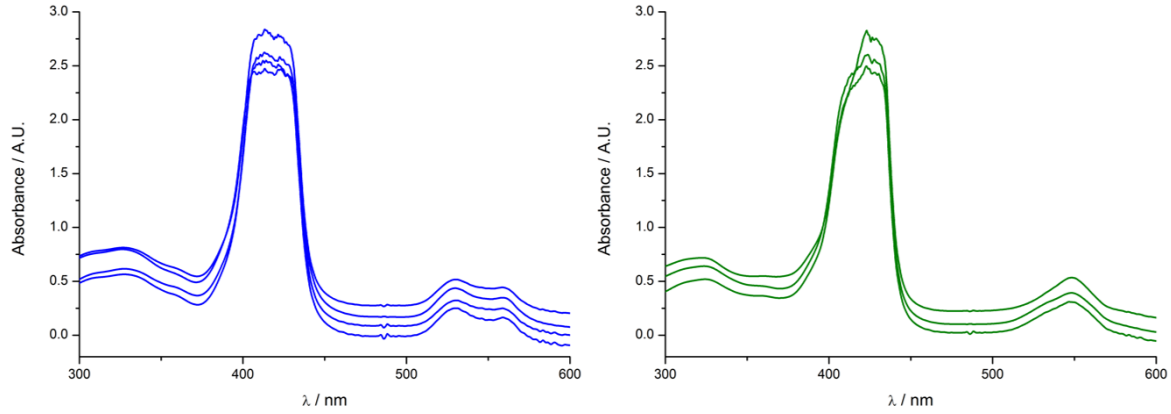

Figure 38. *UV-Vis spectra of MeO-RP in the blue PSS (left) resp. the green PSS (right). All spectra were recorded in the NMR tubes and referenced with a similar DTS filled with the pure (not deuterated) solvents.*

From Figure 36, which presents two and a half switching “cycles”, and Figure 37, which displays two switching processes in more detail, two conclusions can be drawn. First, the switching process with blue light is much more efficient. It takes

about 6 seconds to switch the record player from paramagnetic (green PSS) to diamagnetic (blue PSS), whereas the back-switching process takes about 25 seconds to complete.

Both switching times obtained from this experiment are much smaller than those which were determined in the experiment shown in Figure 34 (30 seconds for switching from the green to the blue PSS, 60 seconds for the reverse process), even though the sample contained the same concentration of the relaxation agent MeO-RP. The reasons for these findings are the improved optical setup as well as the altered probe head (see Chapter 5.5.).

Second, it appears that the relaxation rates found in the first cycle for the blue PSS cannot be reached within the second cycle. As an increase of rates can be observed, diffusion of oxygen (remaining in the sample despite sealing it) into the active volume can be a reason. However, this effect does not emerge in the paramagnetic states, whose rates are found the be the same within a small error.

To rule the formation of fatigue products out and to check the stability of MeO-RP, UV-Vis spectra were also recorded, as indicated in Figure 36. All UV-Vis spectra, which were recorded while the sample was still in the NMR tubes, are displayed in Figure 38. For each PSS the spectrum remains the same except for slightly different baselines. As reference a similar DTS filled with the pure and non-deuterated solvents (toluene in the outer tube and methanol in the inner tube) was used.

Having the switching times in hand, a modified SR experiment (see Figure 39) showing how the relaxation times can be manipulated in real-time was conducted. During the variable delay a switching block with green light (green rectangle) is executed accelerating the relaxation during the delay. After the acquisition the sample is switched back to the diamagnetic state with blue light (blue rectangle). To avoid potential temperature effects a cooling delay is introduced after the back-switching block before another data point is acquired.

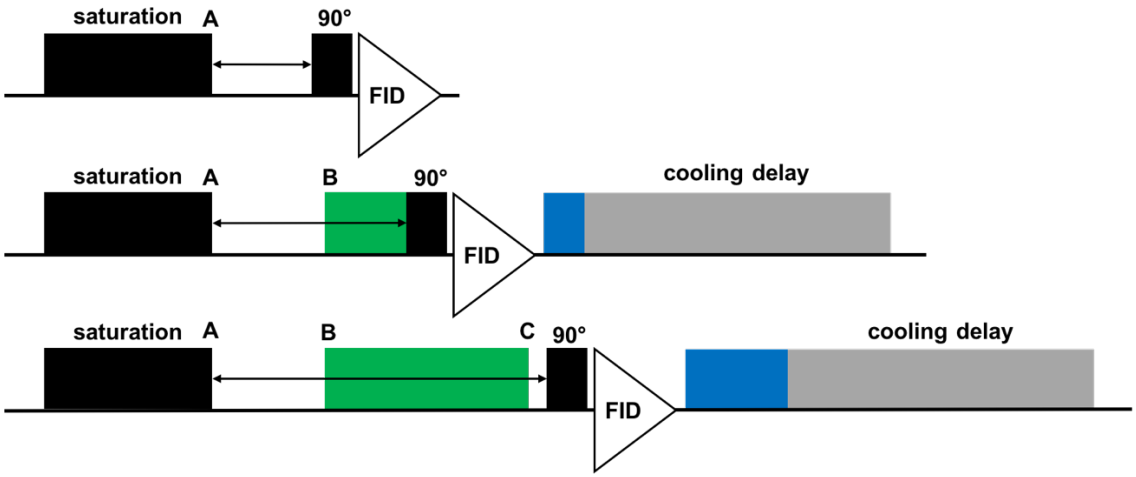

Figure 39. *In the first line of this scheme a standard SR experiment consisting of a saturation block, a variable delay (represented as double-headed arrow), a 90° pulse and the acquisition of the FID is depicted, which is conducted when the delays are shorter than 5 s. The second line shows the sequence for delays with a duration below 25 s, where the illumination with green light (green rectangle) cannot be executed to its full extent. In the third line the delays are long enough to allow the full execution of the switching block. The duration of the blue block is 0.5 times the length of the green illumination block. The cooling delay has a duration of 30 s.*

Table 10. *Parameters for the acquisition of the modified SR experiment.*

parameter	
sample composition	0.5 mM MeO-RP in toluene-d_8 and 5% (v/v) $CHCl_3$
solvent in inner tube	MeOH-d_4
saturation block	5 s
A-B	5 s (11 data points)
B-C	20 s (15 data points)
longer than C	8 data points
ns	1
cycles between PSSs	15 + 8 = 23 (B-C + longer than C)
power blue LED	100 %
power green LED	70 %

To avoid accumulation of paramagnetic MeO-RP and to demonstrate that the spin switch was cycled for every single delay, the delays were not sampled in chronological order, e.g. in ascending order, but in a mixed fashion.

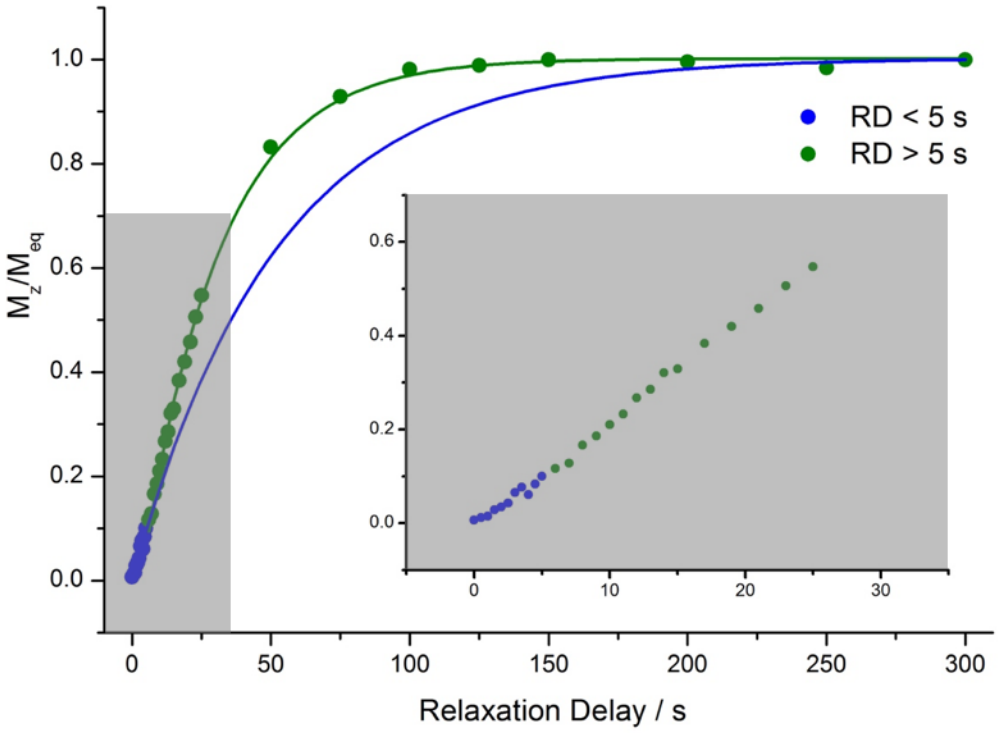

Figure 40. *Relaxation of the z-magnetization (M_z/M_{eq}) in the modified SR experiment with switching from slow to fast relaxation during the relaxation delay. The spin switch is in the diamagnetic state (T_1 = 52 s, blue points) unless the relaxation delay (RD) is longer than 5 s. For RD > 5 s the illumination block with green light is executed switching MeO-RP paramagnetic (T_1 = 28 s, green points), which manifests itself in a small increase in the slope of the relaxation curve (green curve). The blue curve shows the estimated course of the z-magnetization, if MeO-RP is not switched paramagnetic. An insert shows the z-magnetization in the first 35 seconds.*

For relaxation delays between 5 s and 25 s there is no cooling delay between the end of the illumination block and the acquisition of the FID. Actually, the sample is heated up during irradiation with the green light, which can be proven with the peak of the OH-group of MeOH-d_4 in the inner tube of the used DTS (see right part of Figure 41). In the left part of this figure the superimposed $CHCl_3$ peaks are displayed, of which some are probably deteriorated by temperature gradients in the

sample. The $CHCl_3$ peak also shows spinning sidebands as a result of inhomogeneity of the magnetic field.

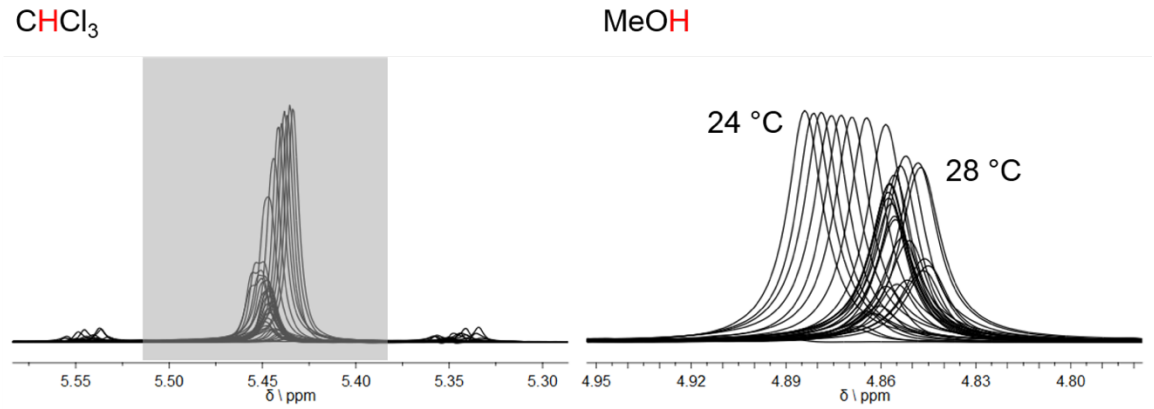

Figure 41. *$CHCl_3$ signals integrated for experiment shown in Figure 40 (left) and temperature development in the inner tube during the experiment (right). In both spectra 1 Hz line broadening was applied.*

The same experiment can also be done the other way round, which means switching from fast to slow relaxation during the delays giving the graph shown in Figure 42.

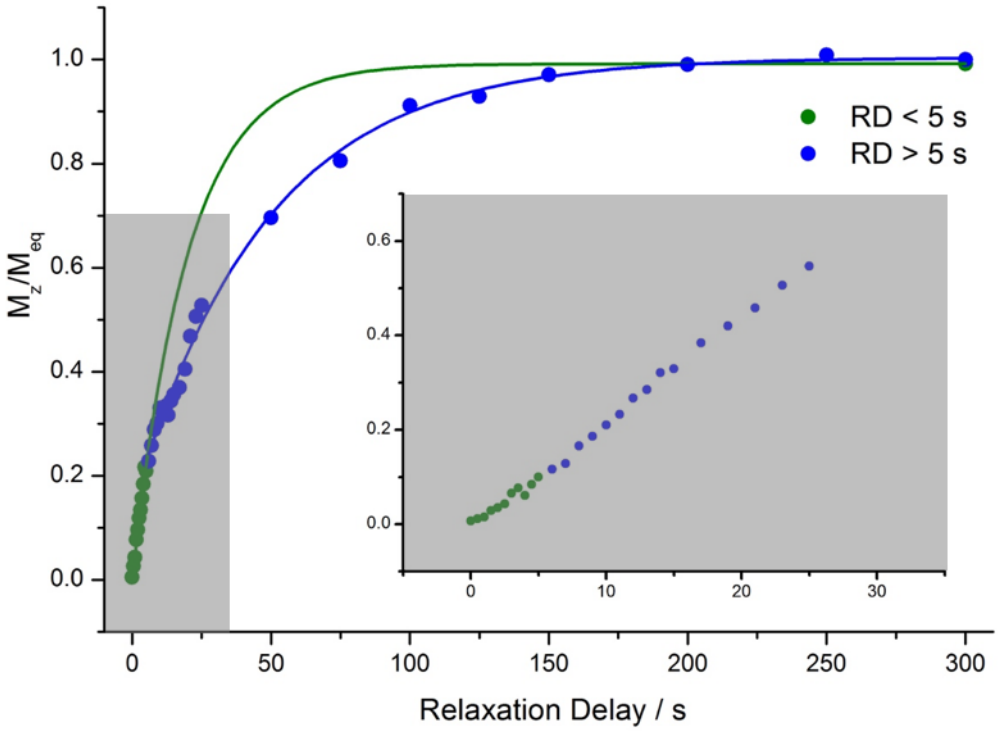

Figure 42. *Relaxation of the z-magnetization (M_z/M_{eq}) in the modified SR experiment with switching from fast to slow relaxation during the relaxation delay. The spin switch is in the paramagnetic state (T_1 = 20 s, green points) unless the relaxation delay (RD) is longer than 5 s. For RD > 5 s the illumination block with blue light is executed switching MeO-RP diamagnetic (T_1 = 48 s, blue points), which manifests itself in a less steep slope of the relaxation curve (blue curve). The green curve shows the estimated course of the z-magnetization, if MeO-RP is not switched diamagnetic. An insert shows the relaxation in the first 35 seconds.*

5.5.2. 5 mM MeO-RP

Although the expected bend in the magnetization curve can be observed for 0.5 mM MeO-RP as previously shown, the effect is rather small and can only be seen when fitting an exponential curve to the data points. It is anticipated that this bend should be better observable for higher concentrations of MeO-RP. Therefore, a more concentrated sample was prepared to examine the effects at higher concentrations consisting of 5 mM MeO-RP in toluene-d_8 and 10% (v/v) $CHCl_3$.

Again, the first experiment conducted with the sample was to determine which time it takes to switch the sample from one magnetic state to another. The pulse

sequence for this experiment is very similar to the one presented in Figure 33, even though the illumination lasts for 2 s (for both LEDs). Not surprisingly, the switching process with green light (switching time around 40 s) is much slower than the reverse process, which takes approximately 12 s to complete (see Figure 43).

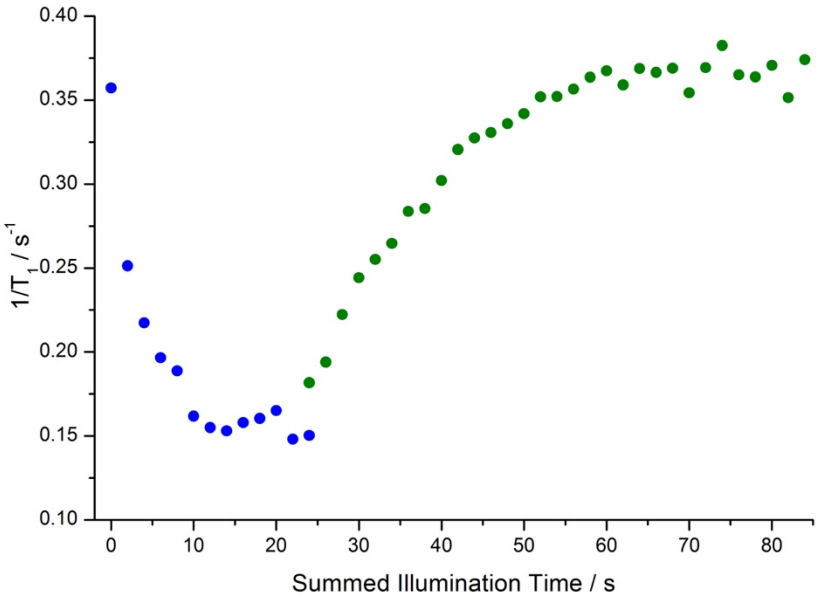

Figure 43. *Plot of the $1/T_1$ values of $CHCl_3$ versus the summed illumination time for the 5 mM sample. The blue points belong to the switching process from the green PSS (fast relaxation rates of $CHCl_3$) to the blue PSS (slow relaxation rates of $CHCl_3$). Back-switching from the blue PSS to the green PSS is displayed in the right part of the graph (green points). Each point represents a SR experiment (200 MHz; ns = 1; delays: 0, 0.5, 1, 2, 3, 4, 5, 6, 7, 8, 9, 10, 11, 12, 13, 14, 15, 20 s; duration: 5 min).*

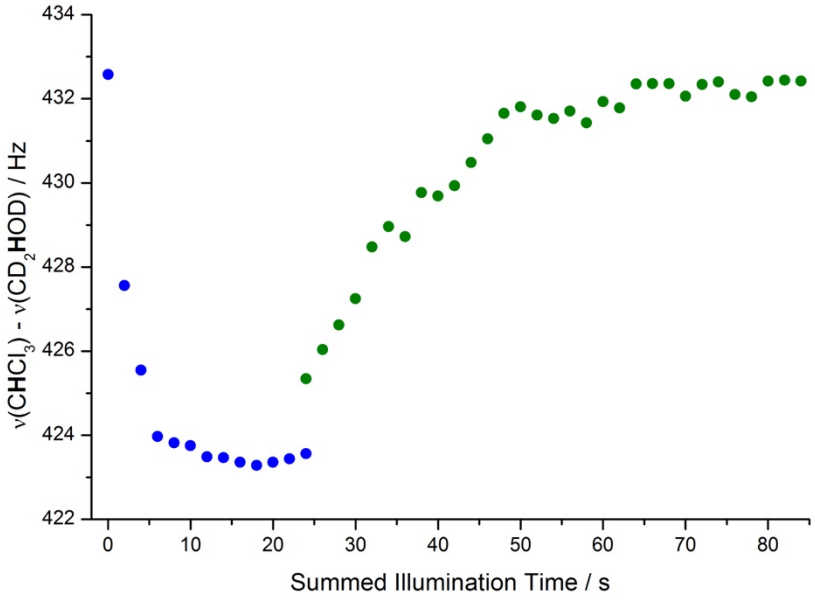

Figure 44. *Plot of the shift difference between the $CHCl_3$ peak and the methyl peak of MeOH-d_4 ($\nu(C\boldsymbol{H}Cl_3) - \nu(CD_2\boldsymbol{H}OH)$) versus the summed illumination time for the 5 mM sample. The blue points belong to the switching process from the green PSS (fast relaxation rates of $CHCl_3$) to the blue PSS (slow relaxation rates of $CHCl_3$). Back-switching from the blue PSS to the green PSS is displayed in the right part of the graph (green points).*

A main advantage of this high concentration is the possibility to observe the shift of the $CHCl_3$ peak as a measure of the current magnetic state of the sample. At the low concentration of 0.5 mM MeO-RP the shift difference is much more susceptible to temperature fluctuations due to illumination with the high-power LEDs and therefore not a very reliable measure for the magnetic state of MeO-RP.

Using the magnetic susceptibility of the paramagnetic Ni-$TPPF_{20}$ · 2 py complex determined in Chapter 5.1.2., the formula proposed by Evans[27] allows the calculation of the theoretical shift difference. Furthermore, for this calculation it has to be taken into account that both paramagnetic and diamagnetic isomers are present at both PSSs (see Chapter 5.3.). The theoretical shift difference of the $CHCl_3$ peak between both PSSs is 2.2 Hz/mM MeO-RP giving a shift difference of 11 Hz for 5 mM MeO-RP. However, a smaller shift difference as expected (approx. 9 Hz) is measured in the experiments.

The shift of the $CHCl_3$ peak (in reference to the methyl group of MeOH-d_4, = $\nu(\mathrm{C\mathbf{H}Cl_3}) - \nu(\mathrm{CD_2\mathbf{H}OH})$) and the longitudinal relaxation rate of the $CHCl_3$ proton show similar dependencies on the summed illumination time. Accordingly, the plot of the shift difference $(\nu(\mathrm{C\mathbf{H}Cl_3}) - \nu(\mathrm{CD_2\mathbf{H}OH}))$ versus $1/T_1$ of $CHCl_3$ (see Figure 45) underpins the linear dependency (cf. Equations (28) and (29)).

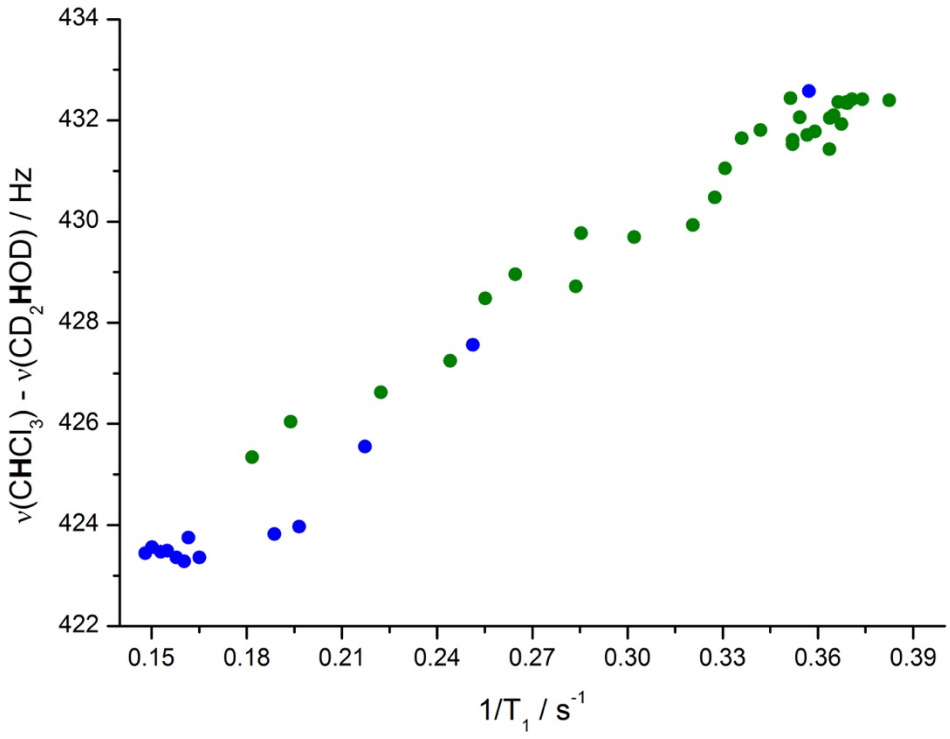

Figure 45. *Linear plot of the shift difference* $(\nu(C\boldsymbol{H}Cl_3) - \nu(CD_2\boldsymbol{H}OH))$ *versus* $1/T_1$ *of the* $CHCl_3$ *peak for both switching processes. Blue points: switching from the green PSS to the blue PSS with the blue LED. Green points: back-switching from the blue PSS to the green PSS with the green LED.*

A higher concentration of the switchable relaxation agent MeO-RP goes in hand with an increase of remaining paramagnetic complex in the blue PSS which results in a fast relaxation in this state. For the further experiments a lower concentration of MeO-RP was used.

5.5.3. 1.5 mM MeO-RP

According to the model describing the re-establishment of the z-magnetization in presence of paramagnetic substances in Section 3., it was found that 1.5 mM MeO-RP is the optimal concentration to observe the desired effect (DARE).

Using a sample of 1.5 mM MeO-RP in toluene-d_8 and 10% (v/v) $CHCl_3$ the switching times were determined (for a pulse sequence see Figure 33). The illumination interval prior to the SR experiments is 1 s for the blue LED (switching from the green to the blue PSS) and 2 s for the green LED (reverse process).

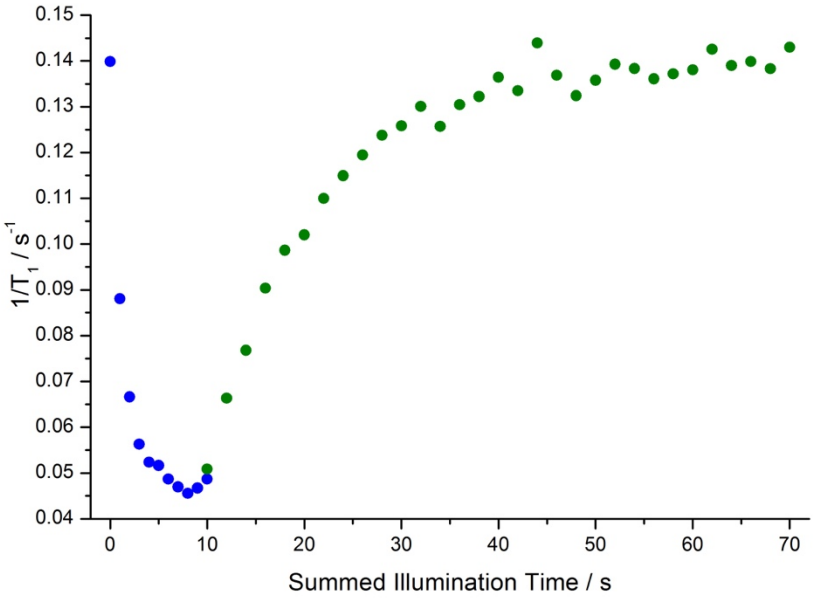

Figure 46. *Plot of the $1/T_1$ values of $CHCl_3$ versus the summed illumination time for the 1.5 mM sample. The blue points belong to the switching process from the green PSS (fast relaxation rates of $CHCl_3$) to the blue PSS (slow relaxation rates of $CHCl_3$). Back-switching from the blue PSS to the green PSS is displayed in the right part of the graph (green points). Each point represents a SR experiment (200 MHz; ns = 1; delays: 0, 1, 2, 4, 6, 8, 10, 12, 14, 20, 40, 60 s; duration: 5 min).*

Figure 46 shows that it takes about 6 seconds to reach the blue PSS when starting in the green PSS. The back-switching process takes ca. 40 seconds. As shown with the 5 mM sample it is convenient to observe the shift of the chloroform peak (Figure 47) instead of the time-consuming SR experiments. What was previously mentioned about the dependency of the shift and the relaxation rate is also true for

the less concentrated sample discussed at this point (see Figure 48). The shift difference between both PSSs is about 4 Hz (theoretical value 3.2 Hz).

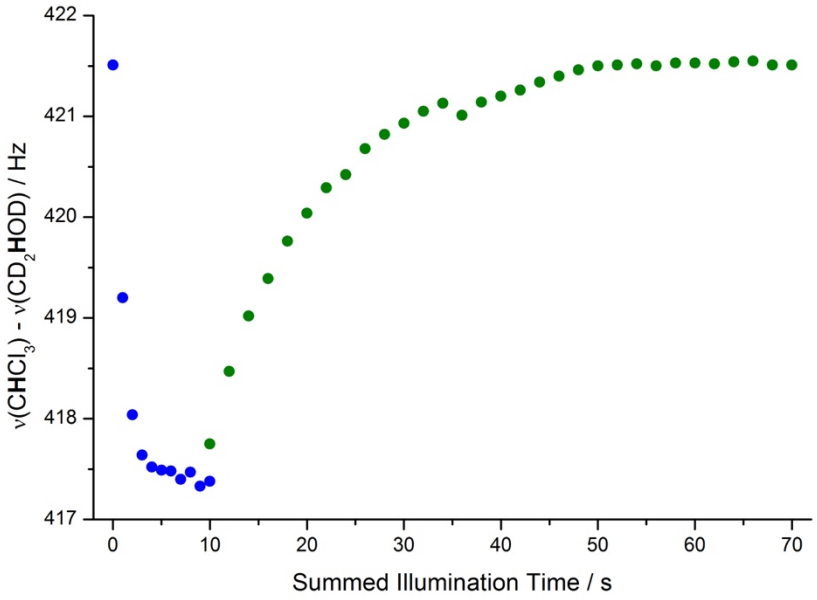

Figure 47. *Plot of the shift difference* $(\nu(C\boldsymbol{H}Cl_3) - \nu(CD_2\boldsymbol{H}OH))$ *versus the summed illumination time for the 1.5 mM sample. The blue points belong to the switching process from the green PSS (fast relaxation rates of* $CHCl_3$*) to the blue PSS (slow relaxation rates of* $CHCl_3$*). Back-switching from the blue PSS to the green PSS is displayed in the right part of the graph (green points).*

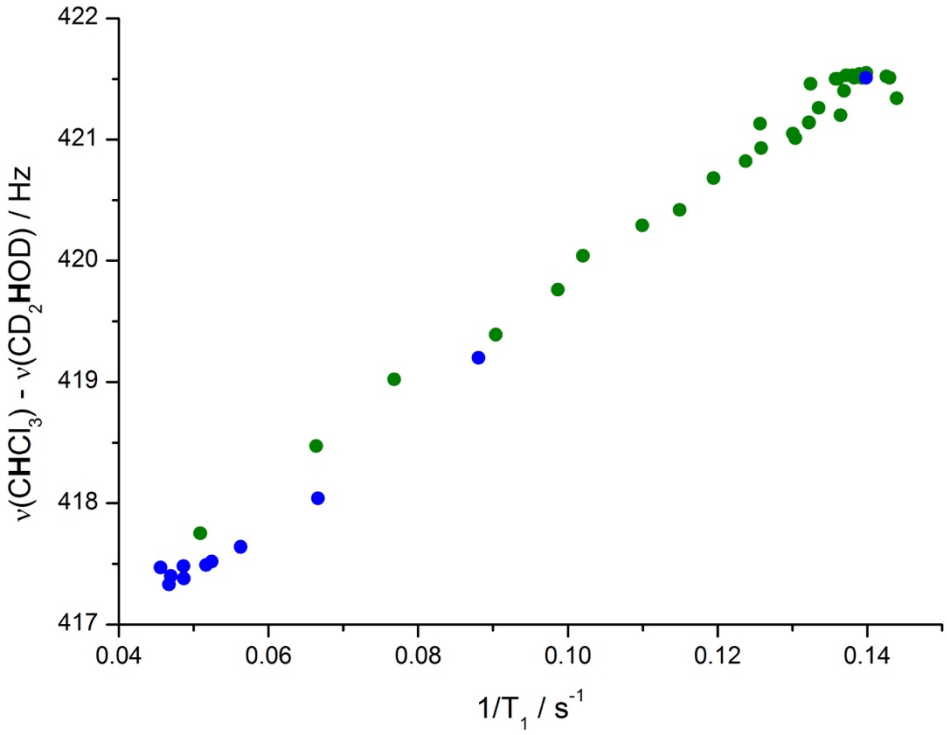

Figure 48. *Linear plot of the shift difference* $(\nu(C\boldsymbol{H}Cl_3) - \nu(CD_2\boldsymbol{H}OH))$ *versus* $1/T_1$ *of the* $CHCl_3$ *peak for both switching processes. Blue points: switching from the green PSS to the blue PSS with the blue LED. Green points: back-switching from the blue PSS to green the PSS with the green LED.*

Long-term switching experiments are necessary to show the stability of the relaxation reagent when cycling it repeatedly. The magnetic state of the spin switch can be monitored by either measuring the longitudinal relaxation rate of the $CHCl_3$ peak or determining the shift difference $(\nu(\mathrm{C\mathbf{H}Cl_3}) - \nu(\mathrm{CD_2\mathbf{H}OH}))$. The sequence for both experiments is depicted in Figure 49 and the pulse program is displayed in Section 8.2.2.

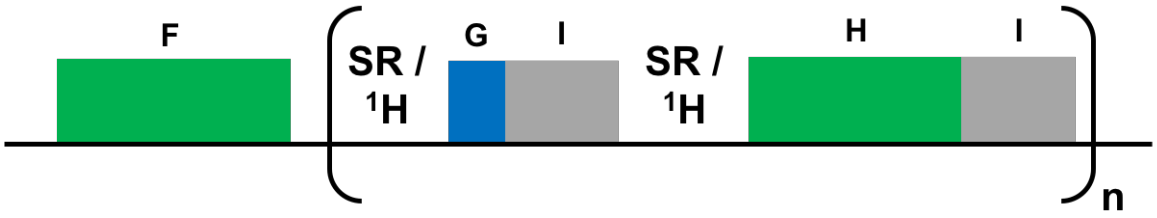

Figure 49. *Schematic representation of a long-term switching experiment, where the magnetic state and stability of the spin switch is monitored by the longitudinal relaxation rate of $CHCl_3$ (measured by a SR experiment) or by the shift of the same peak (measured by a simple ^{1}H-NMR experiment). It starts in the green PSS (F = a few minutes). The switching block (in brackets) consists of two SR experiments or ^{1}H-NMR experiments separated by an illumination block with blue light (G = 4 s) and a cooling delay (I = 2 min) and is completed with a green switching block (H = 15 s) and the same cooling delay.*

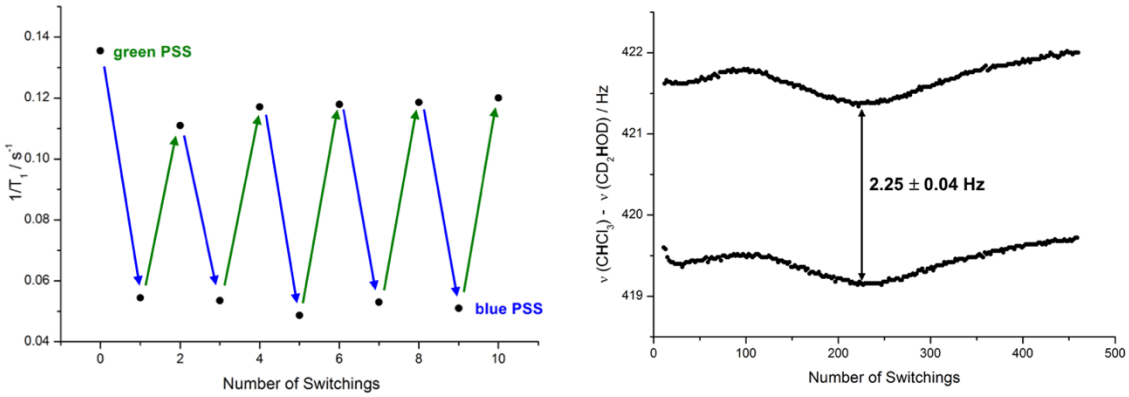

Figure 50. *Left: The $1/T_1$ values of $CHCl_3$ (determined by a SR experiment: 200 MHz; ns = 1; delays: 0, 1, 2, 4, 6, 8, 10, 12, 14, 20, 40, 60 s; duration: 5 min) are plotted as function of the number of switchings. The bigger relaxation rates belong to the green PSS ("paramagnetic state", fast relaxation) and the smaller relaxation rates to the blue PSS ("diamagnetic state", slower relaxation). Colored arrows indicate the switching processes from one PSS to the other with blue or green light. Right: The shift differences $(\nu(C\boldsymbol{H}Cl_3) - \nu(CD_2\boldsymbol{H}OH))$ are plotted as function of the number of switchings. The points in the upper parts of both graphs were acquired after the sample was illuminated with green light for 15 s, whereas the points in the lower part were acquired after illumination with blue light for 4 s. After each irradiation step the sample was allowed to cool for 2 min prior to measurement.*

It can be clearly seen in the left graph of Figure 50 that the first $1/T_1$ value is higher than the other values in the green PSS. The length of the green illumination block is too short to switch MeO-RP back to the (original) green PSS, which has a longitudinal relaxation rate of 0.135 s^{-1}. The blue PSS however is reached every

time, as the irradiation with blue light for 4 seconds is long enough to switch it back completely.

With a duration of 4 min for every single SR experiment together with the cooling delays and the illumination intervals this type of experiment would be very time-consuming, when addressing the long-term stability of MeO-RP. As highlighted in Figure 45 and Figure 48, the shift difference $(\nu(\mathrm{C}\mathbf{H}\mathrm{Cl}_3) - \nu(\mathrm{CD}_2\mathbf{H}\mathrm{OH}))$ is also suited to indicate the present magnetic state. Therefore, the remaining part of the switching experiment was monitored by the shift of the $CHCl_3$ peak.

It could be shown that the relaxation agent is stable for at least 460 switchings. The upper curve in the right part of Figure 50 belongs to the state with a higher concentration of $Z_{\text{param.}}$ MeO-RP, whereas the lower curve represents the state with a lower concentration of the active relaxation agent. The shift difference between those two states is 2.25 $\pm$ 0.04 Hz. Slight fluctuations in temperature cause both curves to migrate up and down for the same amount (see Figure A4 in appendix).

Again, the modified SR recovery experiment was conducted, whose sequence is depicted and explained in Figure 39. The pulse program is displayed in Chapter 8.2.3. For the experiment the length of the cooling delay was optimized – it was adjusted to twice the length of the green illumination block. The parameters of this experiment can be found in Table 11. Rather than fitting exponential curves through the data points as done in Figure 40 and Figure 42, two additional SR experiments were conducted. In the first one the relaxation agent remained in the blue PSS (“off”) during the whole SR experiment. Accordingly, the second one was conducted while the relaxation agent was in the green PSS (“on”). The results are displayed in Figure 51.

Table 11. *Parameters for the acquisition of the SR experiment.*

parameter	
sample composition	1.5 mM MeO-RP in toluene-d_8 and 10% (v/v) $CHCl_3$
solvent in inner tube	MeOH-d_4
A-B	2 s, 21 data points
B-C	30 s, 22 data points
longer than C	7 data points
ns	1
cycles between PSSs	22 + 7 = 29 (B-C + longer than C)
power blue LED	100%
power green LED	100%

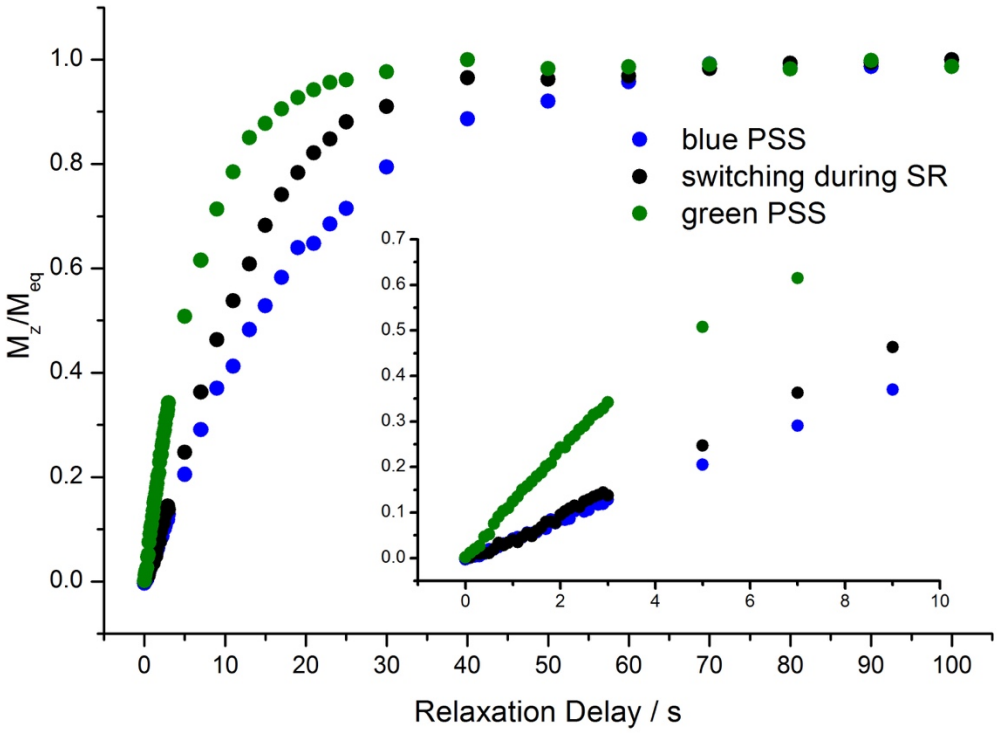

Figure 51. *Relaxation of z-magnetization (M_z/M_{eq}) in the blue and the green PSS compared to the relaxation curve obtained with the modified SR experiment. An insert shows the z-magnetization in the first 10 seconds. Both blue and black curves start with the same slope until the green LED is switched on after 2 seconds leading to faster relaxation.*

The most distinct feature of Figure 51 is without doubt the course of the three curves, of which the “switching” curve is enclosed by the relaxation curves in both PSSs, as expected from a theoretical point of view. Additionally, this figure serves to determine the optimal parameters for the DARE experiment described on the next pages.

Due to the illumination in the relaxation delay the $CHCl_3$ peaks corresponding to relaxation delays in the range of 5 to 80 seconds are probably deteriorated as a result of the induced temperature increase. Furthermore, because of inhomogeneity of the magnetic field spinning sidebands of the $CHCl_3$ also occurred (see Figure 52).

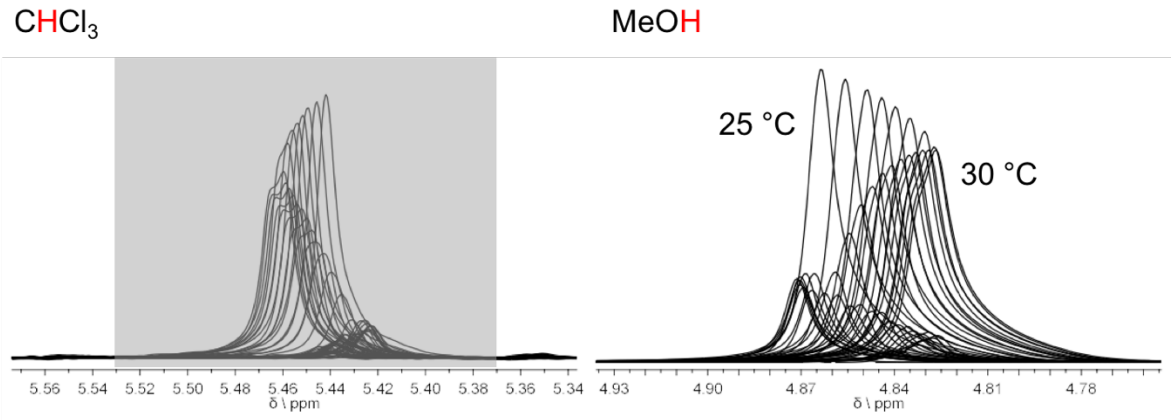

Figure 52. *$CHCl_3$ signals integrated for experiment shown in Figure 51 (left) and temperature development in the inner tube during the experiment (right). In both spectra 1 Hz line broadening was applied.*

5.5.4. DARE Experiment

When comparing the z-magnetization curve of the switching experiment (black dots in Figure 51) and the curve obtained when the relaxation agent is in the blue PSS (blue dots), the highest signal enhancement (up to 30%) can be found in the range of 7 s to 25 s of the illumination block. With this information, the DARE experiment was planned (see Figure 53, for pulse program see Section 8.2.4.). It is composed of a standard 1D-NMR sequence – 90° pulse, acquisition and delay. During the delay, which has a total length of 22 s, two illumination blocks are executed – the first one (duration 15 s) switches the relaxation agent “on”, which is then switched

"off" with blue light (duration 4 s). The remaining time (3 s) is set as cooling delay to attenuate the effects of temperature gradients induced by the irradiation on the observed peak of $CHCl_3$.

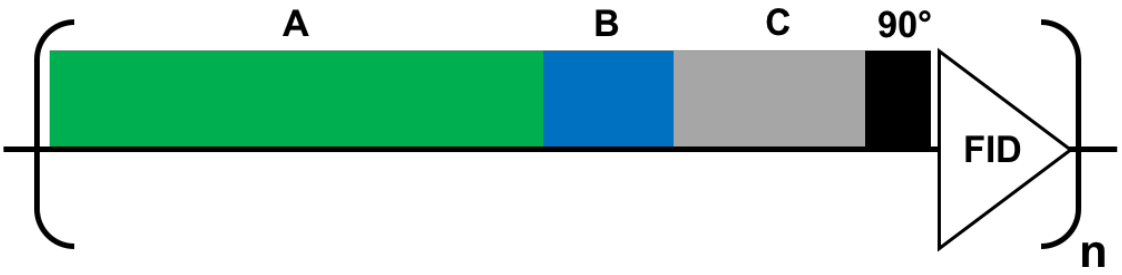

Figure 53. *Schematic representation of a conventional 1D-NMR experiment with DARE enhancement. It starts with green illumination (duration A = 15 s) to switch the relaxation agent "on". The agent is switched "off" with blue light (B = 4 s). A cooling delay (C = 3 s) separates the illumination blocks from the 90° pulse and the acquisition of the FID.*

A total of 16 scans (n = 16) was acquired during the experiment, of which the first 8 scans served as "dummy scans" to allow the sample to equilibrate its temperature and were not included in the manual addition of the remaining 8 scans.

To interpret the results of the DARE experiment, the experiment has to be repeated when the relaxation agent is in either of both PSSs (i.e. switched "on" or "off"). To do so, the agent was switched "on" and "off" by irradiating with green and blue light for at least 30 seconds, respectively before starting the experiment. During the experiment the high-power LEDs were not switched on.

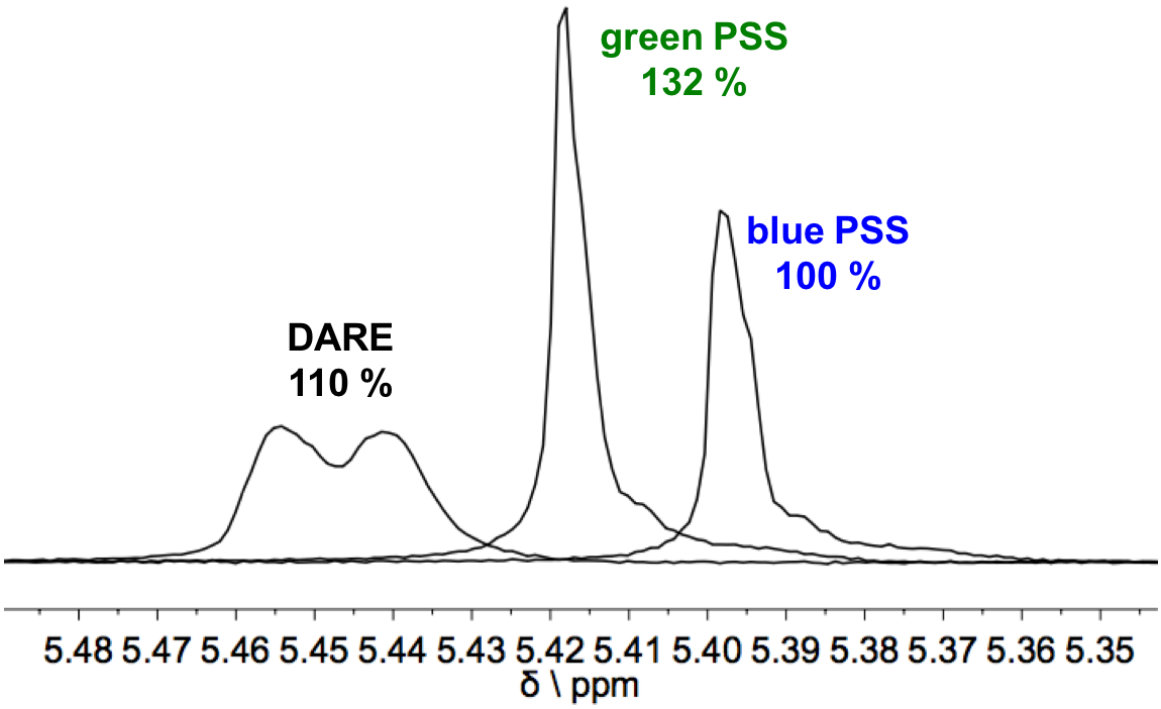

Figure 54. *Superimposed ^{1}H-NMR spectra of the $CHCl_3$ peaks in different PSSs and DARE. Each peak shown in here is a sum of the last 8 spectra. The integral of the $CHCl_3$ peak in the blue PSS was set to 100 %. The DARE peak is deteriorated, probably due to temperature gradients in the sample (33 °C in the inner tube).*

5.6. Control Experiments with Ni-TPPF$_{20}$

The use of methanol in the inner tube showed that the temperature of the sample was effected by the illumination with the high-power LEDs.

To distinguish the temperature effects from the effects due to the switching of the relaxation agent such as DARE (see Figure 54) or the influence on the equilibration of the z-magnetization (see Figure 51), control experiments with diamagnetic Ni-TPPF$_{20}$ were conducted. Diamagnetic Ni-TPPF$_{20}$ can only be switched to a paramagnetic state upon addition of axial ligands such as pyridine.[12] Therefore illumination of a solution of Ni-TPPF$_{20}$ does not impact the magnetic state of the central nickel ion. The main advantage of this compound is its similar structure and hence, optical properties.

A sample of 1.5 mM Ni-TPPF$_{20}$ in toluene-d$_8$ and 10% (v/v) $CHCl_3$ was prepared in the same manner as the MeO-RP solutions. Again, MeOH-d$_4$ was used to fill the inner tube.

First, the relaxation of the z-magnetization with and without illumination was monitored. The pulse sequence shown in Figure 39 was simplified by exchanging the illumination block with green light by a block with blue light, which was adjusted to a power of 70% on the control unit. The relaxation delays and the order of the delays were the same as those used in the modified SR experiment described in Chapter 5.5.3.

Because no axial ligand such as pyridine was added to the solution of the Ni-TPPF$_{20}$, the complex remained in its diamagnetic state resulting in a slow equilibration of the z-magnetization after the saturation block (i.e. a small relaxation rate of the $CHCl_3$ proton). The integral of the $CHCl_3$ plotted in Figure 55 corresponds to the observed z-magnetization.

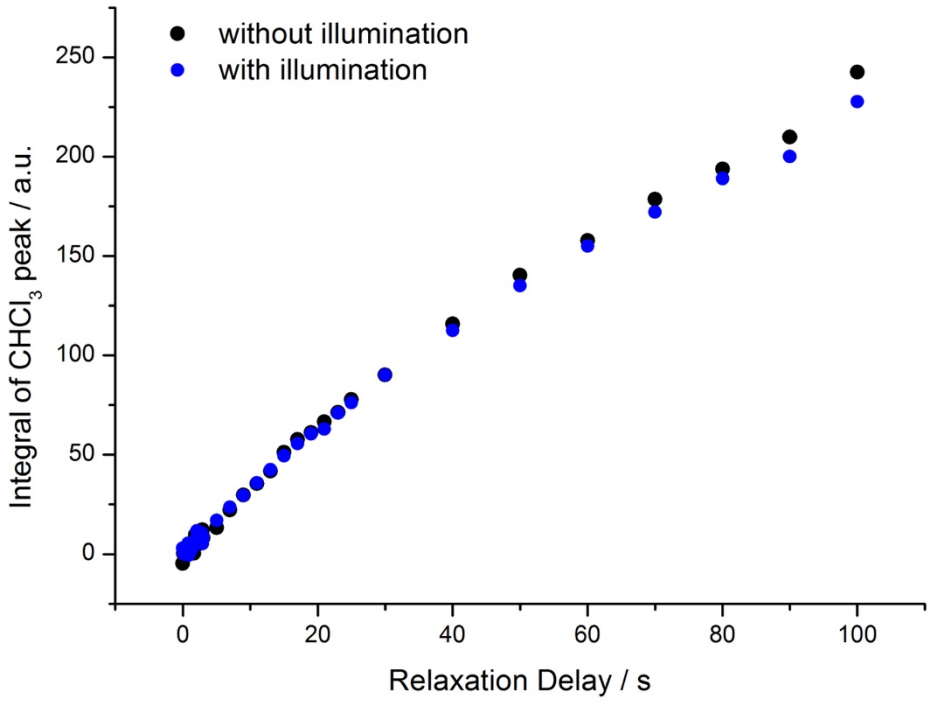

Figure 55. *Plot of the integral of the $CHCl_3$ peak (corresponds to the z-magnetization) as function of the relaxation delay. The same experiment was conducted with illumination with blue light (blue dots) and without illumination (black dots).*

By all means, Figure 55 clearly shows that the enhanced relaxation due to magnetic switching of the sample is influenced only to a small extent by the temperature gradients induced by the illumination of the sample. It seems that the irradiation of

the sample slows down the relaxation a little bit leading to smaller integrals (reduction by about 5 % for the longest delay), which can be seen especially in the right part of the figure – at longer relaxation delays. As described in Chapter 2.2.4., the longitudinal relaxation time T_1 should be longer for higher temperatures, which is the probable reason for these findings.

Furthermore, the temperature during the acquisition of the single data points was monitored for both the 1.5 mM MeO-RP and the 1.5 mM Ni-TPPF$_{20}$ sample and is plotted as a function of the relaxation delay in Figure 56.

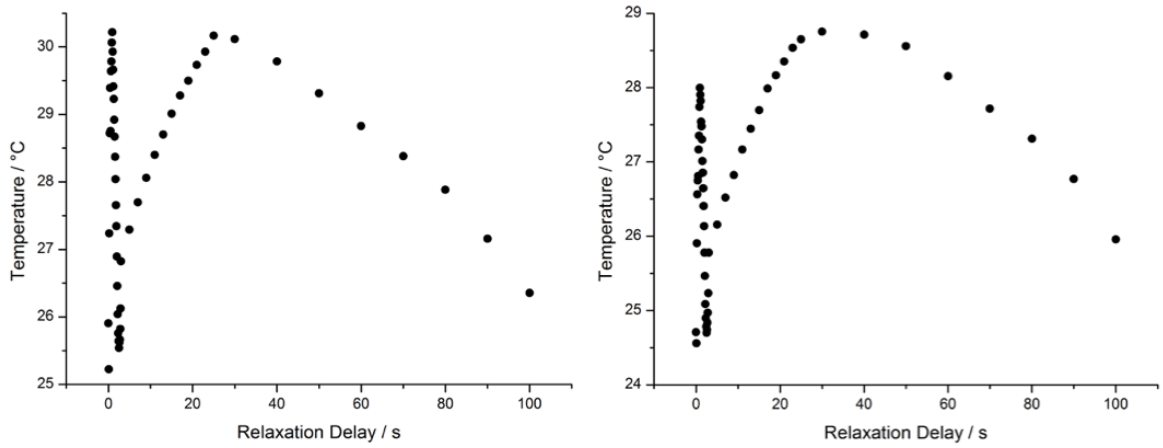

Figure 56. *Temperature during acquisition of the data points for the modified SR experiment as function of the relaxation delay (left: 1.5 mM MeO-RP in toluene-d_8 and 10% (v/v) $CHCl_3$, right: 1.5 mM Ni-TPPF$_{20}$ in toluene-d_8 and 10% (v/v) $CHCl_3$ as control sample). The blue or green light is switched on 2 s after the saturation block resulting in a rise of the temperature from 2 s to 30 s (maximal duration of illumination = 30 s). After 30 s the temperature decreases as there are cooling delays between the end of illumination and the measurement of the temperature. The first "peak" at 0.9 s is caused by mixing the relaxation delays – the delays found in this area are placed between two long relaxation delays.*

The only difference between the functions plotted in Figure 56 is that the temperature is slightly higher for the MeO-RP sample. This allows the comparison of control experiment with the modified SR experiment with MeO-RP.

The other experiment is aimed at the control of the DARE experiment. In order to conduct this experiment the sequence (see Figure 53) was also simplified – instead of illumination with green light for 15 s and blue light for 4 s (100% power for both), the sample was irradiated for 19 s at a power of 70%.

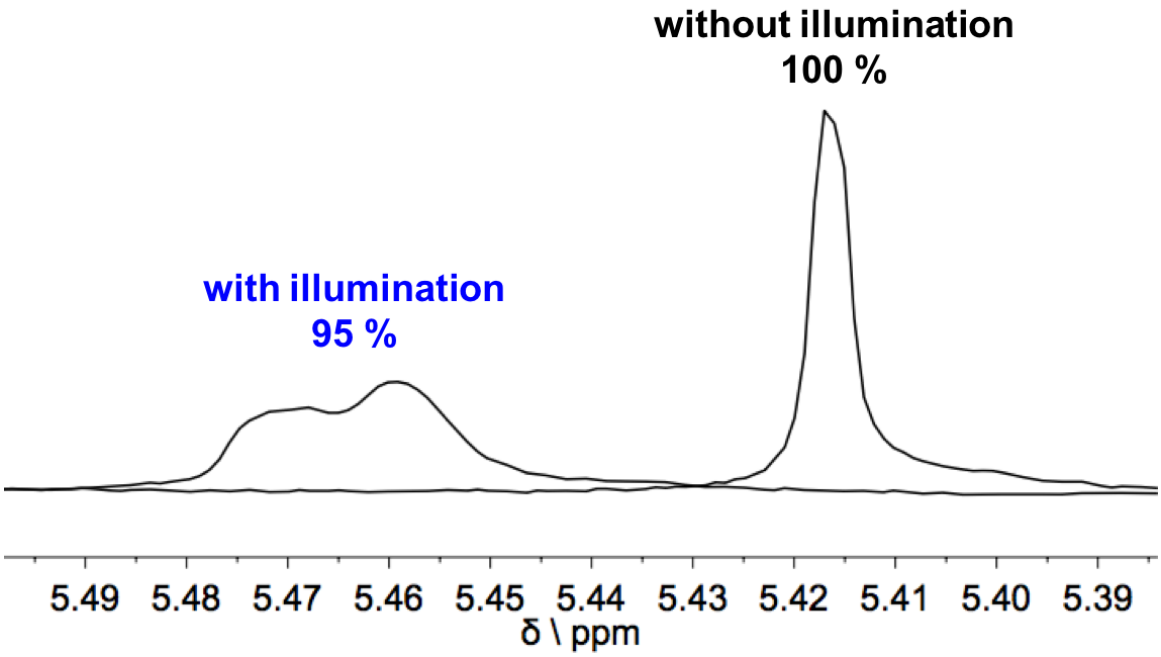

Figure 57. *Superimposed ^{1}H-NMR spectra of the $CHCl_3$ peaks with and without illumination during the experiment. Each peak shown in here is a sum of the last 8 spectra. The integral of the $CHCl_3$ peak obtained by the experiment without illumination was set to 100 %. The downfield shift observed for the peak as well as the shape of the peak on the right is a result of the temperature increase in the sample (38.5 °C).*

By setting the integral of the $CHCl_3$ peak obtained by the experiment without illumination to 100% it can be seen that the other peak (with illumination) has an integral, which is by 5% smaller. This was also noticed in the other control experiment (see Figure 55). Moreover, the experiment shows that the source of the deteriorated shape of the $CHCl_3$ peak and its shift to lower field are very likely temperature gradients in the sample.

The conclusion which can be drawn from the control experiments is that both the relaxation enhancement and the intensity enhancement (DARE) are induced by the magnetic switching of the used relaxation agent. The temperature, however, plays only a minor role. Moreover, both experiments suggest that increasing the temperature slows down the relaxation a little bit leading to a smaller integral in both experiments compared to the ones obtained by the respective experiments without illumination. This observation is consistent with the theory. At elevated temperatures an increase of the rotational correlation time for small molecules (such as $CHCl_3$) is expected. This in turn reduces the longitudinal relaxation rate (see Section 2.2.4.).

Additionally, the effect of the temperature on the shift of the $CHCl_3$ peak is actually not a problem, if the sample can be subjected to a cooling delay prior to the measurement of the shift. The shift of the $CHCl_3$ peak is not a qualified measure of the present magnetic state of the sample if there is no or a too small cooling delay between the end of the illumination and the measurement.

5.7. Comprehensive Analysis of the Switching Kinetics Experiments

As the switching kinetics experiments were conducted for each concentration of MeO-RP discussed above, a comprehensive analysis makes sense at this point. In the paragraphs above it was only stated that the switching process from paramagnetic to diamagnetic MeO-RP is much faster than the back-switching process, although it was not clarified why there is a discrepancy between those two processes.

Figure 58 shows the normalized relaxation rates (obtained by dividing all rates belonging to one concentration by the highest one for this concentration) as a function of the summed illumination time for both switching processes. Interestingly, it takes longer to reach the blue PSS when the concentration is increased from 0.5 to 1.5 and 5 mM (left part of Figure 58). In contrast to that the reverse process is not influenced by the concentration, as the same curve is obtained for each concentration (right part of Figure 58). The reasons for this behavior can be found in the optical properties of the relaxation agent.

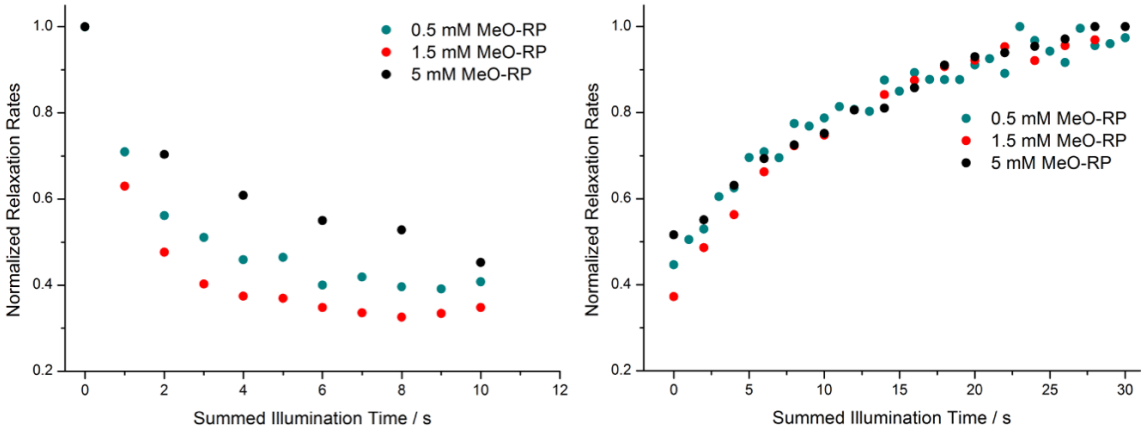

Figure 58. *Normalized longitudinal relaxation rates of $CHCl_3$ as a function of the summed illumination time obtained by dividing the longitudinal relaxation rates by the highest relaxation rate. Left: Switching processes from the green PSS to the blue PSS with blue light for different concentrations of MeO-RP. Right: Switching processes from the blue PSS to the green PSS with green light for different concentrations of MeO-RP.*

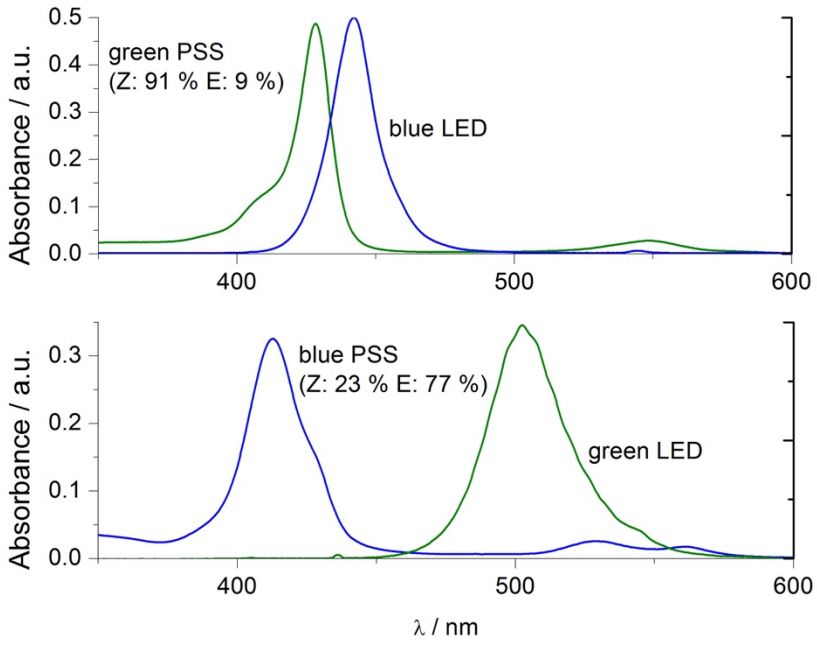

Figure 59. *Overlay of the emission spectra of both LEDs and absorbance spectra of the two PSSs. Top: Blue LED emission spectrum and absorbance spectrum of the green PSS. Bottom: Green LED emission spectrum and absorbance spectrum of the blue PSS.*[vi]

[vi] The spectra shown in this graph were recorded by Eduard Stadler.

An overlay of the absorbance spectrum of MeO-RP in the green PSS and the emission spectrum of the blue LED which is used for the switching process from the paramagnetic PSS to the diamagnetic PSS shows that there is a notable overlap of both curves (see Figure 58). A much smaller overlap is observed in the opposite case (blue PSS and green LED).

Another criterion for the different "switching times" are the quantum yields of the processes. The quantum yield for the E → Z switching process with green light is 1.4%, whereas the reverse process (Z → E) with green light has just a quantum yield of 0.4%. For the Z → E switching process using blue light a quantum yield of 8% is found (reverse process 6%).[vii]

However, increasing concentrations of MeO-RP slow down the switching process from the green to the blue PSS due to higher absorbance of the blue light. This effect is more pronounced at a concentration of 5 mM MeO-RP indicating that the penetration depth might be a limiting factor. Limiting factors for the reverse process might be the intensity of used light and the low quantum yields at the used wavelength.

[vii] The quantum yields presented here were measured by Eduard Stadler.

6. Conclusion and Outlook

In contrast to the traditional PRE agents, the recently developed Ni(II)-porphyrin MeO-RP is photo-switchable between a paramagnetic and a diamagnetic state. This allows overcoming the inherent drawback of PRE agents – the cause of line broadening – by switching the compound diamagnetic during the acquisition of the FID. Hence, no or only slight line broadening should be observable in the recorded NMR spectra.

In fact, the switching process is not 100% efficient for the used compound MeO-RP. Both PSSs comprise the diamagnetic as well as the paramagnetic isomer of the complex. At the blue PSS, a percentage of 21% $Z_{param.}$ isomer remains, whereas in the green PSS, 82% of $Z_{param.}$ is present. Fortunately, Ni(II) has a low electron relaxation time, which in turn leads to only small effects on both relaxation times. Thus, the line broadening induced by in the paramagnetic state of MeO-RP is kept within limits.

Nevertheless, it could be demonstrated that the photo-switchable contrast agent MeO-RP can govern the relaxation rate of surrounding (solvent) protons. This is impressively shown in the switching kinetics experiment – by choosing the length of the illumination interval, the relaxation rate can be adjusted between the rates exhibited in both PSSs. Furthermore, the switching kinetics experiment also indicates that the switching process with blue light, in which the complex is switched to the diamagnetic state, is four to five times faster than the reverse process. This behavior has its roots in the optical properties of the complex.

In the first place, the experiments were monitored by using the relaxation rates of the residual solvent protons of toluene-d_8, however, the small concentration of the isotopomers carrying one proton makes this approach time-consuming. To get interpretable NMR spectra, at least four scans were needed, which took about 24 minutes.

For that reason, $CHCl_3$ was used for the further experiments. The switching process was also improved by changing the spectrometer featuring another probe head and by applying an optical gel between the quartz rod and the high-power LEDs. Furthermore, more light was reflected onto the sample by inserting optical Teflon into the probe head.

With the new samples containing $CHCl_3$ it was possible to carry out the modified SR experiment, in which an illumination block with green light enhances the relaxation rate during the relaxation delay. After the acquisition of the FID, the agent is switched back to its diamagnetic state with blue light. At the low concentration of 0.5 mM the expected bend in the relaxation curve was hardly detectable.

Going to higher concentrations allows using the shift of the $CHCl_3$ peak as a measure for the present magnetic state of MeO-RP. Thus, the time-consuming SR experiment could be replaced by a simple ^{1}H-NMR experiment, which was used to monitor the switching kinetics. Furthermore, this also allowed to conduct a long-term switching experiment, in which it could be shown that the switching process is completely reversible even after 225 cycles. What should be kept in mind, is that the shift is extremely susceptible to temperature gradients within sample and it is simply not feasible to use the shift as indicator at a concentration level of 0.5 mM MeO-RP.

Experiments showed that the concentration of 5 mM MeO-RP is too high, as in the blue state about 1 mM paramagnetic $Z_{\text{param.}}$ isomer is always present. Therefore, the relaxation is by far too fast to conduct reasonable switching experiments, when the agent is in the blue PSS.

By using predictions based on the theoretical calculations on the rate constants, it was possible to determine the optimal concentration for the switching experiments, which is 1.5 mM MeO-RP.

As the signal intensity of a certain peak is directly proportional to the z-magnetization of the nucleus, a faster re-establishment of the equilibrium magnetization should lead to an increased signal intensity. Indeed, the DARE experiment shows that a faster relaxation during the recycle delay or relaxation delay indeed enhances the signal intensity.

All these effects described and discussed in the experimental section really arise from the change in concentration of MeO-RP induced by the illumination with the high-power LEDs. This could be proven by the control experiments performed with Ni-TPPF$_{20.}$ This diamagnetic Ni(II)-porphyrin complex is not photo-switchable and has similar optical properties. Thus, the complex only absorbs light and leads to an increase of the temperature in the sample without becoming paramagnetic.

The control experiments have shown that heating up the sample actually reduces the longitudinal relaxation rate of the $CHCl_3$ protons. At elevated temperatures small molecules such as $CHCl_3$ tend to tumble faster in the solution, which leads to reduction of the rotational correlation time and hence reduces the longitudinal relaxation rate, as mentioned in Section 2.2.4.

The enhanced relaxation rate in presence of PRE agents such as MeO-RP leads to a significant reduction in NMR instrumental time when running numerous scans. As the z-magnetization recovers faster after the acquisition of the previous scan, the recycle delay can be diminished without causing loss of signal intensity. It is also possible to run more scans in the same amount of time needed for an experiment without paramagnetic additives. This in turn results in an augmented S/N ratio.

For the future, an improvement relating to the composition of the PSSs might be worth considering. As mentioned above, both diamagnetic and paramagnetic isomers are present in the two PSSs. In an ideal photo-switchable system, only one isomer would be present at either of the two different PSSs, e.g. the paramagnetic state would only comprise paramagnetic isomers.

This problem can actually be attenuated, when using a different wavelength for the switching process from the green to the blue PSS. Replacing the blue LED (peak wavelength 442 nm) by a LED with a peak wavelength of 435 nm, it might be possible to reduce the share of remaining $Z_{\text{param.}}$ isomer in the blue PSS from 21% to less than 5%.[11]

For future applications, a photo-switchable system based on high-spin Fe(III) might be of interest. In contrast to the current system, HS Fe(III) has a higher electron relaxation time and even 5 unpaired electrons and thus the longitudinal relaxation of nuclei in vicinity should be even faster than with Ni(II). A negative side-effect is

the stronger impact on the line-width, however it is possible to overcome the drawback by switching the HS Fe(III) to LS Fe(III). Low-spin Fe(III) has a smaller T_{1e} value than Ni(II) does, therefore the effect on the linewidths caused by a paramagnetic LS Fe(III) complex should be even less distinct (see Chapter 2.3.3.). This hypothetical spin switch should work in the same manner as depicted in Figure 20.

Another promising application in the future would be the replacement of traditional contrast agents based on Gd(III) chelates used in MRI. Instead of the precious and toxic lanthanide metal[7] contrast agents containing cheaper transition metals such as iron or nickel could come to operation. Moreover, the possibility to design photo-switchable contrast agents (such as MeO-RP[11]) is also beneficial for targeted contrast enhancement effects.

7. Bibliography

(1) Hore, P. J. *Nuclear Magnetic Resonance*, 2nd ed.; Oxford University Press: Oxford, 2015.

(2) Keeler, J. *Understanding NMR Spectroscopy*, 2nd ed.; John Wiley & Sons Ltd: Chichester, 2010.

(3) Markley, J. L.; Horsley, W. J.; Klein, M. P. *J. Chem. Phys.* **1971**, *55* (7), 3604.

(4) Cai, S.; Seu, C.; Kovacs, Z.; Sherry, A. D.; Chen, Y. *J. Am. Chem. Soc.* **2006**, *128* (41), 13474.

(5) Theillet, F.-X.; Binolfi, A.; Liokatis, S.; Verzini, S.; Selenko, P. *J. Biomol. NMR* **2011**, *51* (4), 487.

(6) Caravan, P. *Acc. Chem. Res.* **2009**, *42* (7), 851.

(7) Caravan, P.; Ellison, J. J.; McMurry, T. J.; Lauffer, R. B. *Chem. Rev.* **1999**, *99* (9), 2293.

(8) Oktaviani, N. A.; Risør, M. W.; Lee, Y.-H.; Megens, R. P.; de Jong, D. H.; Otten, R.; Scheek, R. M.; Enghild, J. J.; Nielsen, N. C.; Ikegami, T.; Mulder, F. A. A. *J. Biomol. NMR* **2015**, *62* (2), 129.

(9) Venkataramani, S.; Jana, U.; Dommaschk, M.; Sönnichsen, F. D.; Tuczek, F.; Herges, R. *Science* **2011**, *331* (6016), 445.

(10) Dommaschk, M.; Schütt, C.; Venkataramani, S.; Jana, U.; Näther, C.; Sönnichsen, F. D.; Herges, R. *Dalt. Trans.* **2014**, *43* (46), 17395.

(11) Dommaschk, M.; Peters, M.; Gutzeit, F.; Schütt, C.; Näther, C.; Sönnichsen, F. D.; Tiwari, S.; Riedel, C.; Boretius, S.; Herges, R. *J. Am. Chem. Soc.* **2015**, *137* (24), 7552.

(12) Thies, S.; Bornholdt, C.; Köhler, F.; Sönnichsen, F. D.; Näther, C.; Tuczek, F.; Herges, R. *Chem. Eur. J.* **2010**, *16* (33), 10074.

(13) Hore, P. J.; Jones, J. A.; Wimperis, S. *NMR: The Toolkit - How Pulse Sequences Work*, 2nd ed.; Oxford University Press: Oxford, 2015.

(14) Bloch, F. *Phys. Rev.* **1946**, *70* (7–8), 460.

(15) Kowalewski, J.; Mäler, L. *Nuclear Spin Relaxation in Liquids: Theory, Experiments, and Applications*; Moore, J. H., Spencer, N. D., Eds.; Series in Chemical Physics; Taylor & Francis: Boca Raton, 2006; Vol. 2.

(16) McDonald, G. G.; Leigh, J. S. *J. Magn. Reson.* **1973**, *9* (3), 358.

(17) Slichter, C. P. *Principles of Magnetic Resonance*, 3rd ed.; Cardona, M., Fulde, P., von Klitzing, K., Queisser, H.-J., Eds.; Springer Series in Solid-State Sciences; Springer-Verlag: Berlin, Heidelberg, New York, 1990; Vol. 1.

(18) Satterlee, J. D. *Concepts Magn. Reson.* **1990**, *2* (2), 69.

(19) Satterlee, J. D. *Concepts Magn. Reson.* **1990**, *2* (3), 119.

(20) Drago, R. S.; Zink, J. I.; Richman, R. M.; Perry, W. D. *J. Chem. Educ.* **1974**, *51* (6), 371.

(21) McConnell, H. M.; Holm, C. H. *J. Chem. Phys.* **1957**, *27* (1), 314.

(22) McConnell, H. M.; Robertson, R. E. *J. Chem. Phys.* **1958**, *29* (6), 1361.

(23) Bloembergen, N. *J. Chem. Phys.* **1957**, *27* (2), 572.

(24) Cockerill, A. F.; Davies, G. L. O.; Harden, R. C.; Rackham, D. M. *Chem. Rev.* **1973**, *73* (6), 553.

(25) Lehmann, J.; Kleinpeter, E. *Magn. Reson. Chem.* **1993**, *31* (1), 68.

(26) Gonçalves, P. F. B.; Axt, M.; Emílio, V.; Costa, U.; Livotto, P. R. *Comput. Chem.* **1998**, *22* (5), 399.

(27) Evans, D. F. *J. Chem. Soc.* **1959**, 2003.

(28) Deutsch, J. L.; Poling, S. M. *J. Chem. Educ.* **1969**, *46* (3), 167.

(29) Piguet, C. *J. Chem. Educ.* **1997**, *74* (7), 815.

(30) Solomon, I. *Phys. Rev.* **1955**, *99* (2), 559.

(31) Peters, J. A.; Huskens, J.; Raber, D. J. *Prog. Nucl. Magn. Reson. Spectrosc.* **1996**, *28* (3–4), 283.

(32) Bertini, I.; Luchinat, C.; Parigi, G.; Pierattelli, R. *ChemBioChem* **2005**, *6* (9), 1536.

(33) Levy, G. C.; Cargioli, J. D. *J. Magn. Reson.* **1973**, *10* (2), 231.

(34) Zhou, Z.; He, Y.; Qiu, X.; Redwine, D.; Potter, J.; Cong, R.; Miller, M. *Macromol. Symp.* **2013**, *330* (1), 115.

(35) Gansow, O. A.; Burke, A. R.; Vernon, W. D. *J. Am. Chem. Soc.* **1972**, *94* (7), 2550.

(36) Levy, G. C.; Edlund, U.; Hexem, J. G. *J. Magn. Reson.* **1975**, *19* (2), 259.

(37) Le Bihan, D.; Johansen-Berg, H. *Neuroimage* **2012**, *61* (2), 324.

(38) Gütlich, P.; Gaspar, A. B.; Garcia, Y. *Beilstein J. Org. Chem.* **2013**, *9*, 342.

(39) Thies, S.; Sell, H.; Bornholdt, C.; Schütt, C.; Köhler, F.; Tuczek, F.; Herges, R. *Chem. Eur. J.* **2012**, *18* (51), 16358.

(40) Walker, F. A.; Hui, E.; Walker, J. M. *J. Am. Chem. Soc.* **1975**, *97* (9), 2390.

(41) Stadler, E.; Eibel, A.; Neshchadin, D.; Gescheidt, G. *Z. Phys. Chem.* **2017**, *231* (3), 625.

(42) Lever, A. B. P. *Inorg. Chem.* **1965**, *4* (5), 763.

(43) Ammann, C.; Meier, P.; Merbach, A. E. *J. Magn. Reson.* **1982**, *46* (2), 319.

8. Appendix

8.1. Additional Figures

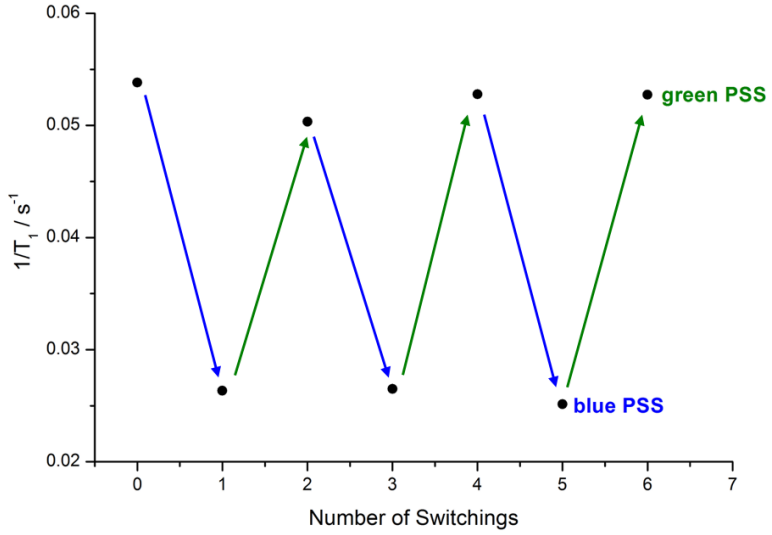

Figure A1. *The $1/T_1$ values of the aromatic group at 6.98 ppm of toluene-d_8 (determined by a SR experiment) are plotted as function of the number of switchings. The bigger relaxation rates belong to the green PSS ("paramagnetic state", fast relaxation) and the smaller relaxation rates to the blue PSS ("diamagnetic state", slower relaxation). Colored arrows indicate the switching processes from one PSS to the other with blue or green light.*

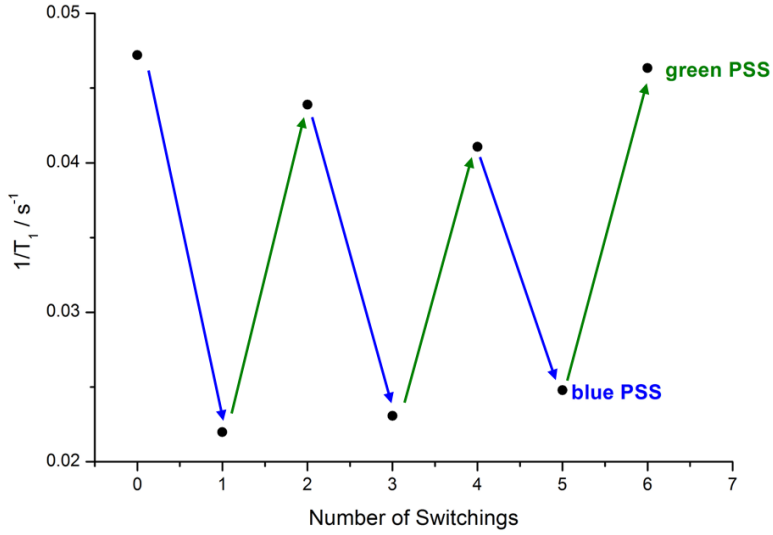

Figure A2. *The $1/T_1$ values of the aromatic group at 7.02 ppm of toluene-d_8 (determined by a SR experiment) are plotted as function of the number of switchings. For further information see Figure A1.*

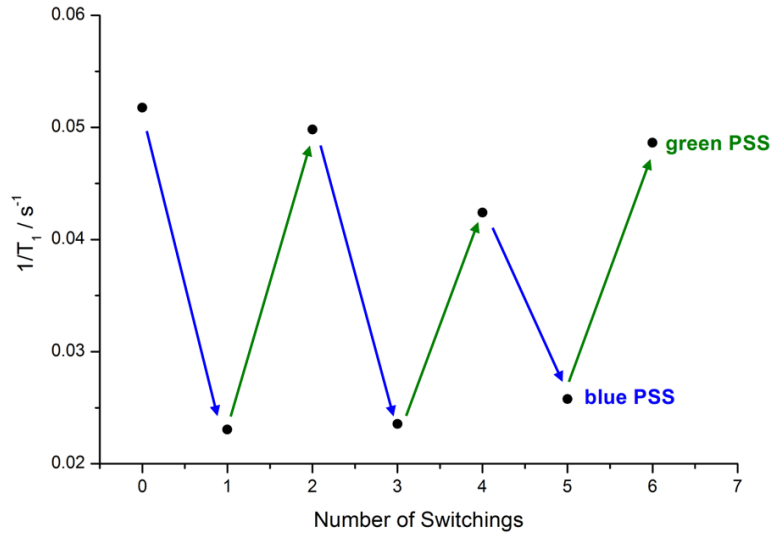

Figure A3. *The $1/T_1$ values of the aromatic group at 7.1 ppm of toluene-d_8 (determined by a SR experiment) are plotted as function of the number of switchings. For further information see Figure A1.*

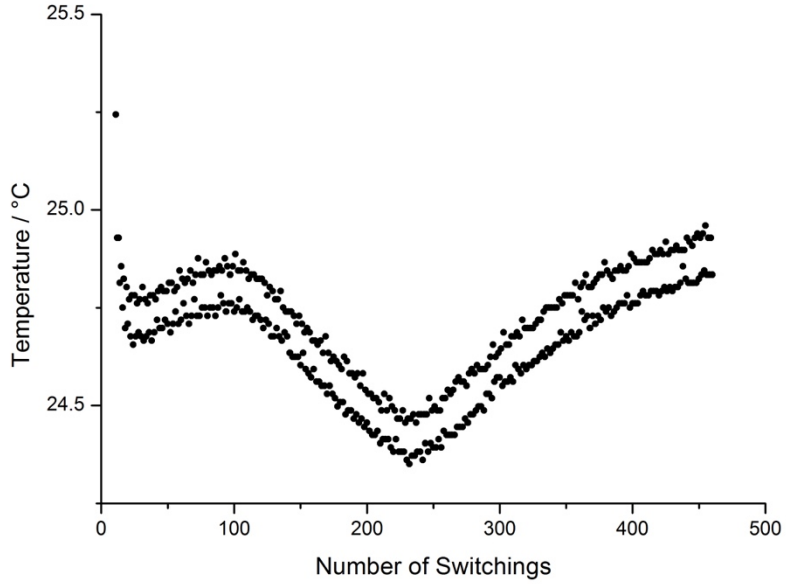

Figure A4. *Profile of sample temperature during the long-term switching experiment shown in the right part of Figure 50.*

8.2. Pulse Programs of selected NMR Experiments

8.2.1. Switching Kinetics Experiments

The switching kinetics experiment consists of a series of single experiments comprising a SR sequence followed by short light pulse (1 or 2 s). These individual experiments are repeated unless a PSS is reached. The following pulse program belongs to a single experiment in the series to monitor the switching process from the blue PSS to the green PSS with green light.

```
#include <Avance.incl>
;Switching Kinetics Experiment (saturation recovery sequence using
     waltz16 decoupling; illumination with green light)

"d11=50u"

1 ze
2 d1
  d11 pl1:f1          ;power level for observing pulse
  d11 pl12:f2         ;power level used for the decoupling

  d11 cpd2:f2         ;decoupling switched on
  d12                 ;time for decoupling, use 5 or 10 seconds
  d11 do:f2           ;decoupling switched off

  vd                  ;delay for recovery experiment

  p1:f1 ph2           ;radiofrequency pulse
  go=2 ph31           ;data acquisition

  d11 wr #0 if #0 ivd ;writing data to file and moving list pointer to
                      next delay in vd-list
  lo to 1 times td1   ;loop statement (td1=number of delays)

3 setnmr8|8           ;switching the green LED on
  2s
  setnmr8^8           ;switching the green LED off

exit

ph2=0 1 2 3           ;phase program for pulse
ph31=0 1 2 3          ;phase program for the receiver

;pl1 : f1 channel - power level for pulse (default)
;p1 : f1 channel -  90 degree high power pulse
;pl12 : power level for decoupling pulse, around 30dB for 100 us as
     determined with a xau paropt.
;pcpd2 : 100 us as determined with paropt.
;o2p: carrier frequency used for decoupling, place in the center of the
     spectrum.
;d1 : relaxation delay, can be short, e.g. 1s
;d11: delay for disk I/O
;vd : variable delay, taken from vd-list
;td1: number of experiments = number of delays in vd-list
;this pulse program produces a ser-file (PARMOD = 2D)
;$Id: t1ir,v 1.8 2002/06/12 09:05:15 ber Exp $
```

The following pulse program belongs to a single experiment in the series to monitor the switching process from the green PSS to the blue PSS with blue light.

```
#include <Avance.incl>
;Switching Kinetics Experiment (saturation recovery sequence using
     waltz16 decoupling; illumination with blue light)

"d11=50u"

1 ze
2 d1
  d11 pl1:f1          ;power level for observing pulse
  d11 pl12:f2         ;power level used for the decoupling

  d11 cpd2:f2         ;decoupling switched on
  d12                 ;time for decoupling, use 5 or 10 seconds
  d11 do:f2           ;decoupling switched off

  vd                  ;delay for recovery experiment

  p1:f1 ph2           ;radiofrequency pulse
  go=2 ph31           ;data acquisition

  d11 wr #0 if #0 ivd ;writing data to file and moving list pointer to
                       next delay in vd-list
  lo to 1 times td1   ;loop statement (td1=number of delays)

3 setnmr8|7           ;switching the blue LED on
  1s
  setnmr8^7           ;switching the blue LED off

exit

ph2=0 1 2 3           ;phase program for pulse
ph31=0 1 2 3          ;phase program for the receiver

;pl1 : f1 channel - power level for pulse (default)
;p1 : f1 channel -  90 degree high power pulse
;pl12 : power level for decoupling pulse, around 30dB for 100 us as
     determined with a xau paropt.
;pcpd2 : 100 us as determined with paropt.
;o2p: carrier frequency used for decoupling, place in the center of the
     spectrum.
;d1 : relaxation delay, can be short, e.g. 1s
;d11: delay for disk I/O
;vd : variable delay, taken from vd-list
;td1: number of experiments = number of delays in vd-list
;this pulse program produces a ser-file (PARMOD = 2D)
;$Id: t1ir,v 1.8 2002/06/12 09:05:15 ber Exp $
```

8.2.2. Long-Term Switching Experiment

```
#include <Avance.incl>
;Long-Term Switching Experiment (series of 1H-NMR experiments, pseudo-2D
experiment)


"d11=50u"
"p2=0.33*p1"        ;use of 30° pulse instead of 90° pulse
"l1=250“            ;loop counter

1 ze

2 d1                ;relaxation/recycle delay
  p2:f1 ph2         ;radiofrequency pulse
  go=2 ph31         ;data acquisition

  d11 wr #0 if #0   ;writing data to file

  setnmr8|8         ;switching the green LED on
  15s
  setnmr8^8         ;switching the green LED off
  120s              ;cooling delay

3 d1                ;relaxation/recycle delay
  p2:f1 ph2         ;radiofrequency pulse
  go=3 ph31         ;data acquisition

  d11 wr #0 if #0   ;writing data to file

  setnmr8|7         ;switching the blue LED on
  4s
  setnmr8^7         ;switching the blue LED off
  120s              ;cooling delay

  lo to 1 times l1  ;loop statement, determines how often the sequence is
                     executed

exit

ph2=0 1 2 3         ;phase program for pulse
ph31=0 1 2 3        ;phase program for the receiver


;pl1 : f1 channel - power level for pulse (default)
;p1 : f1 channel -  90 degree high power pulse
;d1 : relaxation delay, can be short, e.g. 1s
;d11: delay for disk I/O
;this pulse program produces a ser-file (PARMOD = 2D)
;$Id: t1ir,v 1.8 2002/06/12 09:05:15 ber Exp $
```

8.2.3. Modified Saturation Recovery Experiment

```
#include <Avance.incl>
;Modified Saturation Recovery Experiment (switching during delay; waltz16
decoupling)


"d11=50u"

1 ze
2 d1
  d11 pl1:f1            ;power level for observing pulse
  d11 pl12:f2           ;power level used for the decoupling

3 d11 cpd2:f2           ;decoupling switched on
  d12                   ;time for decoupling, use 5 or 10 seconds
  d11 do:f2             ;decoupling switched off


if "vd<=d13"            ;if the delay is too short, there is no
                        switching, d13=2s
{
vd
}
else
{
if "vd<d14"             ;if vd is between the illumination period,
                        d14=32s
{
 "d16=vd-d13"           ;calculation of the illumination period
 d13
 setnmr8|8              ;switching the green LED on
 d16
 setnmr8^8              ;switching the green LED off
}
else
{                       ;if vd is longer than pre-illumination and
                        illumination
 "d17=vd-d13-d15+10u"   ;calculation of the remaining time after
                        illumination
 "d16=vd-d17-d13"       ;calculation of the illumination period
                        (necessary for back-switching)
 "d15=d14-d13"          ;calculation of the maximal illumination period
                        (d15=30s)
 d13
 setnmr8|8              ;switching the green LED on
 d15
 setnmr8^8              ;switching the green LED off
 d17
}
}

  p1:f1 ph2             ;radiofrequency pulse
  go=2 ph31             ;data acquisition

  if "vd<=d13" goto 5   ;no back-switching needed in this case
```

```
6 setnmr8|7             ;switching the blue LED on ;back-switching block
  d16*0.5               ;back-switching block = 0.5*switching block
  setnmr8^7             ;switching the blue LED off

  d15
  d15                  ;cooling delay (=2*d15)

5 d11 wr #0 if #0 ivd   ;writing data to file and moving list pointer to
                        next delay in vd-list
  lo to 1 times td1     ;loop statement (td1=number of delays)

exit

ph2=0 1 2 3             ;phase program for pulse
ph31=0 1 2 3            ;phase program for the receiver


;pl1 : f1 channel - power level for pulse (default)
;p1 : f1 channel -  90 degree high power pulse
;pl12 : power level for decoupling pulse, around 30dB for 100 us as
determined with a xau paropt.
;pcpd2 : 100 us as determined with paropt.
;o2p: carrier frequency used for decoupling, place in the center of the
spectrum.
;d1 : relaxation delay, can be short, e.g. 1s
;d11: delay for disk I/O
;vd : variable delay, taken from vd-list
;td1: number of experiments = number of delays in vd-list

;define VDLIST
;this pulse program produces a ser-file (PARMOD = 2D)
;$Id: t1ir,v 1.8 2002/06/12 09:05:15 ber Exp $
```

8.2.4. DARE Experiment

```
#include <Avance.incl>
;DARE Experiment (pseudo-2D experiment)


"d11=50u"

1 ze
2 setnmr8|8          ;switching the green LED on
  15s
  setnmr8^8          ;switching the green LED off
  setnmr8|7          ;switching the blue LED on
  4s
  setnmr8^7          ;switching the blue LED off
  3s                 ;cooling delay

  p1:f1 ph2          ;radiofrequency pulse
  go=2 ph31          ;data acquisition

  d11 wr #0 if #0    ;writing data to file
  lo to 1 times td1  ;loop statement, determines how often the sequence
                     is executed

exit

ph2=0 1 2 3         ;phase program for pulse
ph31=0 1 2 3        ;phase program for the receiver


;pl1 : f1 channel - power level for pulse (default)
;p1 : f1 channel -  90 degree high power pulse
;d1 : relaxation delay, can be short, e.g. 1s
;d11: delay for disk I/O
;td1: number of experiments
;this pulse program produces a ser-file (PARMOD = 2D)
;$Id: t1ir,v 1.8 2002/06/12 09:05:15 ber Exp $
```